MEASUREMENT AND ANALYSIS OF LIGO VACUUM SYSTEM SHOCK VIBRATION, AND ACOUSTIC NOISE

(Rev. 2)

Prepared by:

Kyle Martini, Klaus Kleinschmidt, Carina Ting, Joel Garrelick

January 10, 1997

LIGO-C970091-00-V
Report U-2379-2041

Prepared for:

Process Systems International, Inc.
20 Walkup Drive
Westborough, MA 01581-5003
PSI Purchase Order 554386-00

Cambridge Acoustical Associates, Inc.
200 Boston Avenue, Suite 2500
Medford, MA 02155-4243

TABLE OF CONTENTS

I. INTRODUCTION AND SUMMARY

The LIGO specification places special operational constraints on the functioning of a number of devices that make up the interferometer vacuum system. Consideration has been given to these devices as sources of noise, vibration, and shock and their effect on the sensitivity and alignment of the interferometer. In conjunction with Process Systems International, Inc. a plan was proposed[1] to reduce the risks associated with these issues. The plan included selecting the proper equipment, measuring the noise, vibration and shock of the equipment, designing the first order mitigation treatments and analyzing performance with the treatments in place to determine the degree of compliance with the LIGO specification.

Source measurements were performed on a short cryo-pump, a turbomolecular pump, a turbomolecular backing pump, both the ion pumps and their controllers, a purge and vent compressor and several valves. The following are general observations concerning these measurements:

1. The vibration from the cryo-pump is broadband with peaks corresponding to resonances of the structure. Levels below 10 Hz were higher than expected, possibly due to a mounting resonance.

2. Narrow band spikes above 450 Hz due to rotor unbalance and power line frequencies characterize the turbomolecular pump. The pump's controller produces vibrations in the 50-450 Hz range. Although not part of the design, isolating the pump controller and building an enclosure around the pump and controller will reduce both the vibration and noise levels.

3. No discernible vibration or noise was measured from the ion pumps. The small ion pump controller located in the vacuum equipment will be isolated to attenuate its vibration. Locating the large ion pump controller in the mechanical equipment room will attenuate its noise and vibration.

4. The turbomolecular backing pump and the vent and purge system have levels that are 20-40 dB higher than the other equipment with significant low frequency energy. They will be located in the mechanical room on isolation pads.

5. The motor operated gate valves meet the shock specification, .01 g peak-to-peak. The pneumatically operated gate valves' peak shock level is 1.9 g. The valves are located a large distance from the chambers. Estimated level at the chamber is 0.02 g. The 10" and 14" manual valves, located near the chambers, have peak levels of 10g and 0.3 g, respectively.

The vibration and shock path analyses utilize three different models to predict the receiver response over the entire frequency range. One is a low frequency finite element beam and plate model. This model is extended large distances to capture the primarily low frequency influence of the boundaries. In the frequency range where the influence of the boundaries is negligible, but the response of the structure still exhibits distinct modal peaks, a mid frequency finite element shell model is used. In the high frequency region, where modal overlap is strong, a statistical energy analysis is performed. Room acoustics and sound transmission methods are used for the acoustic noise analyses. The following are general observations concerning the transmission paths:

1. Transmission at the lower frequencies is governed by the mode shapes of structural resonances. The body of the equipment and the manifolds behave as rigid masses on the flexibility of the supports and bellows. The lower natural frequencies occur in the lateral direction where the supports are weakest. These resonances will be excited by any ambient floor vibration as well as the source listed above.

2. Displacements near the beam splitter are lower than those near a ham or large gate valve because of the beam splitter's mass and its stiffer support structure.

3. Above approximately 50 Hz, transverse shell and axial modes develop, associated with flexibility at changes in the diameter of the beam manifold. These are captured in the mid frequency model.

4. With increasing frequency, structural discontinuities (bellows, changes in diameter, flanges, etc.) increase the transmission loss. Mass and distance are strong factors in the computed transmission loss.

5. The ham bellows is less compliant and less effective than the beam manifold bellows.

6. The sound transmission models were based on construction details as described within.

The models and sources are combined using Norton's Equivalent Source Theorem. Vibration treatments, bellows, springs or isolation pads, separate the sources from the transmission paths. These are low impedance elements that reduce the complexity of the interaction besides providing attenuation. Each source is represented by a force vector in three orthogonal directions. Similarly, the translational response at each receiver is calculated along three orthoganal directions. The resulting nine response components are assumed incoherent and summed accordingly. The following are general observations concerning our results:

1. Most receiver vibration response levels do not meet the LIGO specification.

2. Levels are lower when there is a bellows between the source and the receiver.

3. Levels at the stiffer, massive beam splitter are significantly lower than those at the hams, gate valves and beam manifold.

4. Each cryopump has at least one bellows and several supports between it and a chamber, and only exceeds specifications at the chambers below 10 Hz, to any significant extent.

5. Vibration response levels due to the turbomolecular pump/controller have significant mid frequency content.

6. In the corner station mode cleaner tubes, the vibration levels are high because of the light mass of the 30" tube, the small mass and flexibility of the ham, and the stiffer ham bellows.

7. Acoustic levels from the vacuum pumps and auxiliary equipment are expected to meet the project noise criterion of NC-20 during operational conditions, except during intermittent operations of the turbo pump carts and, in the case of the corner station, during vent and purge compressor operations.

8. Structureborne flanking paths such as pipes, ducts etc. have not been analyzed in detail. Isolation treatments have been designed for these paths and are expected to attenuate any vibration.

II. LIGO SPECIFICATIONS

A. Vibration

The LIGO vibration specification[2] for the spectral density of the allowable displacement δ on the walls of any vacuum chamber or on the floor within 1 meter of any chamber is shown in Fig. 1a. This spectral density represents the allowable level of a tone having a bandwidth of 1 Hz at any frequency between 0.1 Hz and 10 kHz. Because accelerometers are used more commonly than displacement sensors to measure equipment vibrations, it is useful to recast the specification of Fig. 1a in terms of acceleration. This is accomplished by multiplying by ω^2, where ω is radian frequency, and expressing the result in $\mu g/\sqrt{Hz}$ as shown in Fig. 1b.

B. Noise

The specified acoustic noise limit from all simultaneously operating vacuum equipment in normal operation at any location within the LIGO vacuum equipment and laser areas is NC-20.[2] This noise criterion, shown in Fig. 2, is defined in terms of octave band levels from 63 Hz to 8 kHz center frequencies.

C. Shock

Valve actuation or other intermittent device operations shall induce no more than 0.01 g peak-to-peak acceleration at any point within 1 meter of any vacuum chamber.

III. APPROACH TO SPECIFICATION COMPLIANCE

A. Overall Plan

A comprehensive plan was put in place to identify all potential sources of significant noise, vibration, and shock, from the vacuum equipment, to determine the degree of compliance with specifications, to design and evaluate control measures proposed in PSI's proposal,[1] and to test installed vacuum equipment in the LIGO facility. The objective was to achieve the lowest possible impact on the gravity wave instrumentation. The plan consisted of the following four parts:

1. Evaluation of vacuum system equipment with respect to vendors' stated vibration, noise, and shock performance and the inherent equipment design features that impact these characteristics.

2. Testing of selected equipment to verify vendor claims and to supplement vendor data with detailed measurements to cover the full range of the LIGO specifications. To accommadate the extremely low levels, low noise instrumentation and specialized equipment mountings were used to enhance the measurement capability.

3. Implemetation of vibration, noise, and shock mitigation requirements as defined by Ref. 1. Constraints imposed by the LIGO facility were incorporated into the treatment design.

4. Analysis of the transmission of shock, vibration, and sound from the identified sources to the vacuum chambers and to the laboratory floor. Comparison of estimated levels (with first order treatments in place) with LIGO specifications. Regions where compliance with specifications is not achievable have been identified for further review and assessment.

B. Sources of Equipment Vibration, Noise, and Shock

1. Mechanical Roughing Pumps

First stage roughing pumps are not subject to vibration specifications.

2. Turbomolecular Roughing Pumps

Turbomolecular roughing pumps achieve their pumping capability with multi-stage vanes rotating at high speed (approx. 27,000 RPM). Pump shafts are driven by brushless motors. Shaft bearing designs include ceramic ball and magnetic.

The principal vibration source of these pumps is the unbalance in the rotor. This produces a spectrum with a line at the rotational speed and its harmonics. Vibrations at the power line frequency, typically around 1 kHz, and its harmonics result from magnetostrictive effects in the stator pole structure. Finally, with non-magnetically levitated bearings, broadband noise, (e.g., due to the interaction of the balls with the lubricant) is generated.

3. Ion Pumps

Ion pumps operate without moving parts. They are energized by high voltage DC from an AC powered controller. Ion pump vibration and noise is primarily associated with the high voltage power supply and controller, which incorporate cooling fans and transformers.

4. Cryogenic 80K Pumps

These pumps consist of exposed surfaces refrigerated to a cryogenic temperature upon which gases are condensed. The proposed pumps use liquid nitrogen that boils at atmospheric pressure at a temperature of 80°K. The boiling action of liquid nitrogen involves cavitation (i.e., vapor bubble formation and collapse) which produces broad spectrum pressure pulses that act on vessel and liquid/air surfaces to produce noise and vibration.

5. Purging and Venting Compressors

Non-reciprocating screw compressors are planned for this purpose and will be located in adjacent Mechanical Equipment Rooms.

6. Gate Valves

Gate valves are subject to the shock specification which limits the peak vibrational amplitude induced by their operation. Primary mechanisms of shock are deceleration and seating. Both electric and pneumatic valve actuators are used at various LIGO locations.

C. Source Level Testing

1. Test Chambers

The background acoustic and vibration levels at the test areas must be equal to or less than equipment levels being measured. A special acoustically treated chamber was built at PSI to test the Turbomolecular pump, its backing pump and the ion pump. A prototype beamsplitter was built to test the short cryopump. The gate valves with actuators, and the vent and purge system, exhibit higher levels of noise and vibration and were tested at the vendors' facilities.

2. Equipment Mounting

Equipment to be tested were supported compliantly for isolation from the test chamber, thus allowing the measurement of the quasi-free vibration levels required for our analyses.

3. Test Instrumentation - Sensors

a. Vibration - When equipment levels were below the measurement capability of general purpose accelerometers, high-sensitivity ultra low-noise accelerometers were used. Two such sensors were available to span the full frequency range of the LIGO specifications. The Wilcoxon Research model 731A accelerometer (10V/g, 600 gm) was used from 0.1-300 Hz and model 916BTO-1 (7.5 V/g, 700 gm) provided low noise capability above 300 Hz. The equivalent acceleration spectral densities corresponding to the electronic noise floors of these sensors are shown in Fig. 1b. Above 10 Hz, the noise floor of model 731A is lower than the specified amplitude. Above 300 Hz, the noise floor of the 916BTO-1 is below the specified amplitude.

Several other accelerometers were also employed. When testing the 80 K cryogenic pump, a special PCB model 351B41 cryogenic accelerometer was used (0.1 V/g, 32 gm). It's average noise floor is approximately $2\,\mu g/\sqrt{Hz}$. In addition, a more sensitive, non-cryogenic, Endevco charge accelerometer was provided by LIGO. It's average noise floor is approximately $0.3\,\mu g/\sqrt{Hz}$. No malfunction due to temperature was noticed. High source levels, or vibrations at difficult mounting locations, were monitored with a general purpose PCB model 321A35 accelerometer (0.1 V/g, 20 gm). It's average noise floor is approximately $10\,\mu g/\sqrt{Hz}$. As required, electronic noise occurring outside the frequency bandwidth of interest was limited using high-order bandpass filters.

b. **Noise** - Operating equipment noise was measured using a Bruel and Kjaer model 2236 Precision Sound Level Meter for assessing the overall sound pressure level in the Laser and Vacuum areas of the LIGO facility.

c. **Shock** - Shock measurements were performed at the gate valve vendor site using small, lower sensitivity accelerometers.

4. Test Instrumentation-Data Analysis and Processing

a. **Vibration** - Vibration signals were acquired on a digital recorder and processed to obtain frequency spectra in the form of spectral densities. Acquisition and processing of these signals were performed using CAA's SIGNAL system.

b. **Noise** - Acoustic measurements were performed using a Bruel and Kjaer type 2236 precision sound level meter. Noise levels in the octave bands between 63 Hz and 8 kHz were recorded. This meter has a noise floor satisfying NC-10.

c. **Shock** - Measurements of shock-induced vibration due to operation of the gate valves were performed by recording the output of accelerometers oriented along three orthogonal directions and mounted on the gate valve fixture. Signals were recorded for the entire duration of the closing event, and the peak acceleration amplitude was obtained.

D. Vibration Mitigation

1. Main Turbomolecular Pumps

Each of the main turbomolecular pumps is separated from its backing pump. The turbopump is placed on its own cart and isolated from the interferometer by a soft bellows. The turbopump/cart is anchored to the floor to prevent the bellows from compressing axially under the external pressure. High frequency isolators in the form of rubber bushings and washers isolate the turbopump from the cart.

The backing pump, which is a much greater source of vibration than the turbopump, is placed on its own cart and located in the Mechanical Equipment Room. The backing pump cart has its own vibration isolators.

2. Ion Pump Power Supplies

The sources of vibration with the ion pumps are the power supplies. For the large ion pumps, the power supplies are located in the Mechanical Equipment Room. The small ion pumps power supplies are located in the Vacuum Equipment Room and rest on vibration isolators. The cable will incorporate "drip loops" to enhance flexibility.

3. Cryogenic Pumps

The 80K pumps produce vibrations from the formation and collapse of bubbles in the liquid nitrogen. An experiment was performed using air and water to simulate the two phase flow of the nitrogen entering the 80K pump. It showed that the generation of large bubbles via the inlet pipe can be reduced by bringing the stratified flow from the inlet above the liquid reservoir. The incoming liquid now flows gently down a chute into the reservoir while the gas escapes without bubbling through the liquid. The bubbles generated from the boiling liquid in the reservoir are smaller and generate higher frequencies. Interferometer vibration resulting from this action are reduced by the introduction of low frequency isolators. Finally, in the supply and return lines, flex lines are used to attenuate vibrations.

4. Purging and Venting Compressors

The vent and purge system will be "skidded" and placed inside the Mechanical Equipment Room. The skid is mounted on vibration isolators. The discharge and suction side of the system in the corner station have mufflers or sound attenuators. The mid and end station's systems are not operated during interferometer operation.

5. Equipment Located in Adjacent Mechanical Equipment Rooms

The turbomolecular backing pumps, vent and purge compressor skids, and the ion pump controllers are located in Mechanical Equipment rooms. These rooms are located adjacent to the vacuum equipment area on separate floor slabs. All lines going from the mechanical room to the vacuum equipment area will have flex connectors.

E. Noise Mitigation

Noise radiated by operating pumps and electronics are mitigated by reducing the vibrations of the external structural surfaces of the equipment. These mitigations methods are described in the previous section. The turbomolecular backing pumps, vent and purge compressor skids, and the ion pump controllers are located in Mechanical Equipment rooms. These units take advantage of the noise control provisions required to adequately isolate auxiliary equipment (e.g., fans, chillers, pumps) located in these rooms from the vacuum equipment areas.

F. Shock Mitigation

The gate valves are located in close proximity to the chambers. With the exception of adding a short flexible bellows, blocking the shock path is not an option. In this regard therefore the valve manufacture was required to reduce the shock at the source. The valves will be compliantly supported from below to isolate them from the facility floor.

IV. SOURCE MEASUREMENTS

Source measurements were performed on a short cryopump, a turbomolecular pump, a turbomolecular backing pump, both the ion pumps and their controllers, a purge and vent compressor and several valves. The equipment used to measure source levels is described in Section III.C.

There is contamination associated with the low level measurements. The contamination is caused by: i) facility background levels; ii) amplification in the frequency region around the mounting resonance, approximately 5 Hz; iii) sensor sensitivity; and, iv) facility line noise, i.e., 60 Hz electrical noise. In describing the measurements below, these contaminations will be noted.

A. Vibration Measurements

1. Cryogenic 80 K Short Pump

A schematic of the cryopump is shown in Figure 3a. The cryopump was supported in the vertical direction by spring hangers connected to a support beam. A beamsplitter was used as the vacuum jacket in which the support beam was attached. The fundamental mount resonance of the cryopump was 5 Hz in the vertical direction, and lower horizontally. A photograph of the cryopump outside the beamsplitter is shown in Figure 3b.

The cryopump was filled with liquid nitrogen. During the measurements there was no nitrogen flow but vapor was allowed to escape. This vapor was monitored to determine the boiling rate. The boiling rate was controlled by adjusting the heat load. The flow rate was varied between 2.8 CFM and 9.5 CFM. (4.1 CFM is approximately the flow rate at the cryopump's frosted condition.)

Two accelerometers were installed on the support mount of the cryopump, the PCB cryogenic accelerometer in the vertical direction and the LIGO Endevco accelerometer laterally. The PCB general purpose accelerometer was attached to the

support beam and the seismic accelerometer was mounted at the base of the beam splitter to monitor the ground motion.

Each set of test data was recorded at 20,000 samples per second for a duration of 2.1 seconds. Using the analysis package SIGNAL, acceleration power spectral densities (PSD) were created with a 4,096 point spectrum (4.88 Hz resolution) and a Hanning window. Ten samples were averaged from the 2.1 seconds of data. For diagnostic purpose 16,384 point spectra were also analyzed, to further resolve the spectra.

Plots of cryopump accelerations at an operating condition of 4.1 CFM are shown in Figures 3c and 3d in the lateral and vertical directions, respectively. The levels are compared to the background measurements made three days later after all of the liquid had boiled off. Except at 60 Hz, there is a good SNR in the lateral direction, less so vertically. The measurements below 10-20 Hz are affected by the mounting resonance. The first shell resonance occurs at approximately 100 Hz. The transfer function and coherence between the vertical and lateral accelerations are shown in Figure 3e (16,384 point spectrum). The levels are comparable in the shell resonance region.

Vibration measurements were recorded at various bubbling rates. The frequency response of these data is plotted in Figure 3f (frequency smoothing was applied to remove narrow band fluctuations). The data show the stiffness and resonance regions of the shell, but no trend with boiling rate. In contrast, based on analysis[6] a 3 dB per doubling of the boiling rate was expected, amounting to a 5 dB increase in level from the lowest to the highest rate.

The low frequency acceleration of the shell, as predicted in Ref. 6 is also plotted in Figure 3f. The comparison is good. It is noted that in the analysis, the rise velocity of a bubble was predicted on the assumption that the bubble is a rigid sphere and Stokes' law applies. However, experiments indicate that Stokes' law applies only to bubbles that are smaller than those in the cryopump.[7] For a single bubble of the size observed in boiling, bubble deformations reduce its terminal velocity by an order of magnitude compared to

predictions based on Stokes' law. But, it is also observed in Ref. 7 that the terminal velocity increases in the presence of other bubbles, and the cryopump produces a bubble swarm.

A possible source of data contamination are the ambient floor or ground vibrations being transmitted to the pump. Measured floor vibration levels are compared with the levels on the pump in Figure 3g. The floor levels are lower except below 10 Hz, and above the background. Accelerometer measurements on the warm side of the cryopump support were inconclusive. The measured levels were below the electronic noise floor of the accelerometer.

The horizontal levels shown in Figure 3c were taken to be the source levels. Those measured in the vertical direction were not used because they were believed to be more contaminated near the support resonance frequency.

2. Turbomolecular Pump

A schematic of the test configuration is shown in Figure 4a and a photograph of the pump is shown in Figure 4b. The turbopump has two sources of noise and vibrations, the pump and it's controller, and two transmission paths. One path is through the pump's flange via a bellows into the beam manifold. The second path is through the support.

Two test configurations were used to measure the levels through the two transmission paths. For the path through the pump's flange, the pump on its cart was resting on the floor and the free vibration of the flange was measured. For the path through the support, the cart was placed on 5 Hz mounts and the free vibration at the base was measured. Acceleration was measured in three orthogonal directions for each case. Because of mounting difficulties, the low frequency accelerometer was used only in the vertical direction on the top of the flange and at the base of the cart. The general purpose accelerometers were used in the other two directions. The high frequency accelerometer was not used.

On the flange the vertical and lateral levels were comparable, and slightly higher than the levels in the axial direction. On the base of the cart, the vertical vibrations dominated. Figures 4c and 4d show the vibration levels in the vertical direction on the flange and the cart respectively. Below 300 Hz the data were obtained from the low frequency accelerometer, above 300 Hz with the general purpose accelerometer.

There is ground vibration contamination below 20 Hz. Below 450 Hz, the vibration is primarily due to the pump's controller. The peaks are higher in this region on the cart than on the flange. The fundamental rotation frequency of the pump, at 450 Hz, and the power line frequency around 1 kHz and harmonics are evident on the plot. The lower level broadband noise is limited by the general purpose accelerometer sensitivity.

3. Large Ion Pump and Controller

The ion pump, photographed in Figure 5a, was tested on a soft mount (approximately 10-15 Hz). Both the low and high frequency sensitive accelerometers were used. No measurable vibration was expected, and as shown in Figure 5b there was no difference in levels with the pump on or off. The ion pump will not be considered as a source in our analyses.

The large ion pump controller is located in the mechanical room and is not considered an important source because of its location.

4. Small Ion Pump and Controller

The small ion pump vibration levels were not measured, but assumed to be comparable to those of the large pump. The controller is located in the vacuum equipment area and is considered an important source. Its vibration levels, measured on soft (approximately 10-15 Hz) mounts, are shown in Figure 6. The controllers will be placed on isolators to attenuate their vibration.

5. Turbomolecular Backing Pump

The backing pump was tested on isolators using the general purpose accelerometers. The "worst direction" vibrations are shown in Figure 7. Levels are

relatively high. However, its location, on a separate foundation in the mechanical room, and isolation pads, will attenuate the levels transmitted to the vacuum equipment area.

6. Vent and Purge System

The LIGO vent and purge system was not available for testing. The vendor identified a similar system, located near PSI, and tests were performed on site. Unfortunately, this was a noisy mechanical equipment room with other sources of vibration. Nevertheless, measurements on a concrete slab adjacent to the system are shown in Figure 8. (The extraneous sources of vibration could not be turned off.) The vent and purge system is located in the mechanical room of the corner station. In our analysis, the measured levels were applied directly to the foundation.

B. Noise Measurements

In the following, the airborne sound levels were measured at a distance of 3 feet and a height of 5 feet from the source.

1. Cryogenic 80K Pumps

The cryogenic 80K pumps are located inside a vacuum chamber and are considered structureborne, rather than noise, sources.

2. Turbomolecular Pumps

A resiliently mounted turbomolecular pump was tested in PSI's acoustic chamber. Measured noise levels with the equipment turned on and off are shown in Figure 9. The peak within the 250 Hz octave band is due to the controller.

3. Large Ion Pump and Controller

The large, resiliently mounted, ion pump was tested in PSI's acoustic chamber. Measured noise levels are shown in Figure 10a. There is no measured difference with the equipment on or off. The controller test was in the same chamber but, because of scheduling, performed during noisy working hours. The data are shown in Figure 10b. Below 125 Hz, there was background noise contamination.

4. Small Ion Pump and Controller

The small ion pump was not tested. The small ion pump controller, resiliently mounted, was tested in PSI's acoustic chamber. Levels are shown in Figure 11. There is no difference in level with the controller on or off.

5. Turbomolecular Backing Pump

The backing pump is noisy and it was not necessary to test it in the acoustic chamber. The levels are shown in Figure 12.

6. Vent and Purge System

The LIGO vent and purge system was not available to test. Measurements were made on a unit of similar capacity in a noisy mechanical room. Levels are shown in Figure 13. Based on more recent manufacturer's overall noise data, 71 dBA, lower levels are anticipated on the purchased unit.

C. Shock Measurements

1. 44 Inch Gate Valve with Motor Actuator

LIGO G44E valve shock levels during opening and closing were measured at the manufacturer's facility (GNB) by the consulting firm of Charles M. Salter Associates, Inc.[8] The valve was mounted and tested in accordance with the requirements of PSI specification #V049-2-005, Rev. 3. Vibration amplitudes were recorded in three orthogonal directions and at two locations during the tests. All readings indicate amplitudes of 0.002 g or less. The maximum allowable shock is 0.01 g. The motor actuator valves are not considered as sources.

2. 44 Inch Gate Valve with Pneumatic Operator

GNB tested a pneumatic valve as described above. Peak levels between 1 and 1.9g were measured.[9] Sample acceleration time histories are shown in Figures 14. The pneumatic valves are located at the far end of the corner station (see GV6 and GV8 on Figure 16c). The effects of the shock on the chambers is discussed in the next section.

3. 10 Inch and 14 Inch Manual Valves

The Varian 10" and 14" manual valve shock levels were measured at PSI.[10] The valves were rigidly mounted to a beam splitter. Peak shock levels of 10 g and 0.3 g were measured on the 10" and 14" valves, respectively. Sample acceleration time histories are shown in Figures 15a and 15b. The manual valves are located near the chambers. The effects of the shock on the chambers is discussed in the next section.

V. TRANSMISSION ANALYSIS

A. Vibration

The modeling of the transmission path between source and receiver is divided into three frequency regions, low, mid and high. In the low frequency, or large structural wavelength, region the vacuum equipment and connecting manifolds are modeled with beam finite elements, the foundation slab is represented by plate elements and lossy springs represent the soil. The model extends large distances and captures the primarily low frequency influence of the boundaries on the transmission.

The transition from the low to mid-frequency region begins when circumferential shell modes in the tubing that comprises the major part of the interferometer vacuum system structure, provides significant contributions to its response. In this region the transmission path is modeled with axisymmetric shell finite elements. The model assumes axisymmetric tubes, but applied loads, boundary conditions and in turn, displacements may be asymmetric. To obtain practical computation times, it was necessary to limit the extent of the structure considered. As a consequence, this model is limited by the influence of the boundaries at which the model is artificially terminated, although this becomes less important with increasing frequency. However, as frequency increases further, the size of the required finite element model approaches the limit of CAA's computer and (Nastran) finite element code.[11] Above this frequency, statistical energy analyses were performed. With this technique the structure is divided into

"global" subsystems with the power flow between subsystems calculated based on coupling loss factors for "canonical" geometries.

Low frequency models of the entire vacuum equipment area in the end, mid and corner stations of the Washington site were created. Selected sections of each station, as shown in Figures 16 a,b,c, were modeled in the mid and high frequency regions. In these figures, turbomolecular pump and cryopump sources along with receiver locations specified by LIGO[12] are also indicated.

The following sections describe the models of the structures, the sources, and our results.

1. Low Frequency Models

Nastran[11] finite element beam representations of the equipment are plotted in Figures 17 a,b,c for the end, mid and corner stations respectively. Beam cross sectional properties were calculated for all equipment and their supports. The mass and stiffness properties of the bellows are derived from data provided by the bellows manufacturer. Stiffeners, flanges and non-structural components are modeled as masses. The model at each station is terminated at the gate valve connecting it to the beam tube, which is not modeled.

The effective loss factor for the manifold and chamber material is assumed to be 0.01(Q=100). The partially welded/bolted construction of the supports creates more damping through friction and air pumping. The effective support material loss factor is assumed to be 0.04(Q=25).

The 30" concrete floor is modeled with plate elements and the soil as a distributed, lossy spring. Soil properties were obtained from Ref. 13. A plot of the end, mid and corner station foundation models is shown in Figure 17 d and e respectively.

The Nastran complex, direct frequency, solution was used to perform the analysis. Harmonic forces from 1-100 Hz were applied at the turbo pump locations, the floor below the turbo cart and at the cryopump in each of three perpendicular directions. Since shell-

like vibration modes and local bending of the neckdown sections cannot be totally neglected above 50 Hz, results computed at the upper frequencies are used primarily for diagnostic purposes. At the lower frequencies, the body of equipment and the manifolds behave as a rigid mass resting on the flexibility of the supports and bellows. Structural detail and not wavelength was the dominant factor in determining the mesh size.

The input listings of the three Nastran models can be found in Appendix A.

2. Mid Frequency Models

The mid-frequency models consist of Nastran[11] axisymmetric conical shell and trapezoidal solid elements. The applied loads and displacements need not be axisymmetric, as the formulation allows for a Fourier expansion about the circumferential coordinate. The conical shell element, used primarily to model the tubing, the most common part of the structure, includes both membrane and bending flexibility. Solid axisymmetric elements are used to model the relatively thick and inflexible flanges.

We have assumed, in choosing to model the vacuum equipment as solely axisymmetric, that the effects of many non-axisymmetric attachments to the shell are negligible. Attachments, such as the turbo pumps and ion pumps are ignored. The supports and slab are also omitted from the model. The beam splitters, horizontal access modules and gate valves, are replaced with cylindrical shells that have the same mass and estimated static stiffness as the actual items. The bellows models consist of equivalent cylindrical shells with membrane stiffnesses set to produce the equivalent axial stiffness reported by the manufacturer; the bending stiffnesses are based on the actual thicknesses and material properties, and the material density is assigned such that the total mass is equal to that of the actual item.

The vibration sources, the turbo pumps and cryo pumps, are simulated by constant frequency point forces applied in three translational directions to the shell. As in the low frequency range, the Nastran direct frequency formulation was used for these

calculations. In the case of the turbo pumps, the loads were applied to the shell at the center point of the location of the ports. The cryo pump excitations were applied at the points where the isolator/supports attach to the inner cryo-pump sleeve of the outer housing. Only the outer portion of the cryo-pump housing is included in the model.

Calculations were performed for driving frequencies between 40 Hz and 1 kHz. The model was meshed such that there were 10 shell elements per infinite plate flexural wavelength at 420 Hz, 8 elements per wavelength at 660 Hz and 6.5 elements per wavelength at 1 kHz. (The latter case slightly violates the general rule of thumb of 8 elements per structural wavelength.)

Four portions of the vacuum tube interferometer structure were modeled. The Right End Station model consists of the tubing assemblies including beam splitter BSC9 to gate valve GV20. Figure 18a is a sketch of the finite element model with the sources and receiver points indicated. It was not possible to obtain all of the listed receiver points from the model; for example, the End Station receiver locations 1a, and 1b on the slab are calculated on the A-7 tubing adjacent to the beam splitter.

The Right Mid Station model consists of the assemblies from BSC5 to gate valve GV16; note that the other side of BSC5 is identical to the Right End Station already modeled. On the Corner Station, HAM5 to HAM6 is analyzed. Lastly, the fourth model consists of the vacuum tubing between BSC7 and BSC4 on the Corner Station. Computer plots of the four finite element models are shown in Figures 18b-e. Nastran inputs for these models are listed in Appendix B.

3. High Frequency Models

a. Introduction - In this section we describe our high frequency analysis of structureborne noise along the LIGO beam manifolds. Although the basic formulation (subsection b) has been implemented for all sections, the discussion below (subsection c) focuses only on the application to an end section from the gate valve to the beam splitter.

For the thin shell and plated box-like structures along this path the predominant high frequency wave motion tends to be flexural. By high frequency we mean frequencies at which the flexural wavelengths are small relative to the structural scales, such as the lengths and diameters of the tubular sections. For thin steel plating the flexural wavelength is given by

$$\lambda_f(m) = 2\pi/k_f \simeq 96.\sqrt{h(m)/f(Hz)} \qquad (1)$$

where h is the plating thickness and f is frequency. To illustrate, with $6.35\,x\,10^{-3}\,m$ (1/4 in.) plating at 1 kHz., $\lambda_f \simeq 0.3\,m$ (12 in.). Structureborne noise levels will attenuate as they propagate from a noise source to a receiver. The overall attenuation is the result of both a spreading of the vibration energy and its dissipation, that is conversion to heat. Along two dimensional plated structures the spreading is cylindrical with acceleration levels decreasing as $r^{-1/2}$ where r is the distance (range) along the plating from source to receiver. Dissipation associated with flexural wave propagation is conveniently expressed in terms of a structural loss factor η. Here the associated attenuation is of the form $\exp(-k_f r\eta/4) = \exp(-\pi\eta r/2\lambda_f)$. Dissipation may also be associated with parallel propagation paths that do not measurably couple to the receiver. For example for the problem of interest, the vibrational energy transmitted to the concrete slabs and in turn the ground via the manifold tube supports is believed to fall into this category.

Statistical energy analysis (SEA) is an analytical formulation that captures the phenomena described above and allows one to estimate absolute levels at receiver locations, e.g., the beam splitter, in terms of the noise source strength (input power). The technique is briefly outlined below and applied to the various stations and excitations in the following section.

b. <u>Statistical Energy Analysis (SEA) Concepts</u> - With this technique the structure to be analyzed is divided into subsystems each "large" in terms of

the characteristic wavelengths. For each subsystem "j" a steady state power balance is imposed

$$\Pi_j^i = \Pi_j^d + \sum \Pi_{j,k}^c \tag{2}$$

where Π_j^i is power input to the subsystem, Π_j^d is the power it dissipates and $\Pi_{j,k}^c$ the power "lost" to neighboring subsystems. A fundamental SEA concept is that the above dissipated and "coupled" powers are proportional to the space-averaged stored energy of the subsystem, <E>. Specifically,[14]

$$\Pi_j^d = \omega \eta_j < E_j > \tag{3}$$

and

$$\Pi_{j,k}^c = \omega [\eta_{j,k} < E_j > - \eta_{k,j} < E_k >] \tag{4}$$

here $\omega = 2\pi f$ and η_j and $\eta_{j,k}$ are defined as dissipation and coupling loss factors. For structureborne noise

$$< \ddot{w}_j^2 > = \omega^2 < E_j > / M_j \tag{5}$$

where $< \ddot{w}_j^2 >$ is the subsystem space-averaged squared acceleration and M_j the subsystem mass. The analysis is executed by defining the appropriate subsystems, using Eq. 4 to formulate a set of simultaneous equations in the unknown stored energies, obtaining the required loss factors,[15, 16] defining the source strength(s), solving the equations, and using Eq. 5 to obtain the desired response. This is described below for the end section structure pictured in Fig. 19.

c. <u>SEA Model of LIGO End Section Structure</u> - The section being analyzed is shown in Fig. 19. There are twelve subsystems in our SEA representation,

each a uniform section of the tubular manifold. Power is coupled among them across structural discontinuities of various types, viz., stiffening ribs modeled by their inertia, bellows characterized by their compliance, and section radius changes. Power may also be transmitted through the supports and lost to the floor slab. In addition it propagates beyond the modeled sections where it is "lost" to the beam splitter on one end and the continuation of the manifold on the other.

As is common practice with this approach, we obtain the required coupling loss factor expressions from the analytical solutions to highly idealized, so called "canonical", problems. For coupling from one manifold section (i) to another (j) we take all such problems to be one-dimensional with a loss factor of the form $\omega \eta_{i,j} = \Pi^c_{i,j} / M_i < v_i^2 >$ where $< v_i^2 >$ is the mean squared velocity of subsystem i. Also manifold curvature is ignored, thus limiting the validity of the analyses to frequencies above the ring frequency ($\Omega = \omega a / c = 1$) of the smallest diameter, (1.1m), manifold section, roughly 1.4 kHz.

Our model for computing subsystem coupling loss factors is sketched in Fig. 20a. A freely propagating flexural wave is partially reflected and transmitted at the discontinuity between tube sections. Assuming a strong discontinuity and hence weak coupling, the incident energy is primarily reflected and the coupling loss factor takes the form

$$\omega \eta_{i,j} = \tau^2 Re\,[Z_j] / m_i \qquad (6)$$

where $Z_j = (1 - i)\,\omega\,\rho\,h / k_f$ is the drive line flexural (semi-infinite) plating impedance of tube j, $k_f = \sqrt{3.46\,\omega / ch}$ is the flexural wavenumber in plating of thickness h and sound speed c, $m_i = M_i / 2\,\pi\,a_i$ the total mass of tube i per unit distance around the circumference, and the transmission coefficient τ is the ratio of the transmitted to incident wave amplitudes.

Ribs and flanges are modeled by their lumped inertia. For coupling at a section radius change the rotational (inertial) impedance of the discontinuity relative to that of the tube plating is taken to be infinite and coupling across the junction is through translation only. In this case we obtain

$$\tau = 2/|2i - (1 - i)Z| \tag{7}$$

with

$$\bar{Z} = (-i\omega m_{rib} + Z_j)/(\omega m_i / k_{f(i)}) \tag{8}$$

For coupling across a rib joining two tube sections of the same radius and plating thickness, we account for transmission from both rotation and translation of the rib. Here we obtain

$$\tau^2 \Rightarrow \tau_t^2 + \tau_r^2 \tag{9}$$

with

$$\tau_t^2 = |2(1 + Z_j/Z_{rib})|^{-2}$$

and

$$\tau_r^2 = |2(1 + Z_j^r/Z_{rib}^r)|^{-2}$$

where the superscript r denotes a rotational impedance.

For coupling across a bellows in this high frequency regime it is assumed that the low frequency spring-like isolation provided by the bellows is short-circuited by flexural waves propagating along the corrugated thin skin as if it were straightened. Here the

discontinuity is the difference in the tube and bellows plating thicknesses. This yields[17]

$$\eta_{i,j} = \sigma \tau^2 / k_{f(j)} L_i \qquad (10)$$

where

$$\tau = (\sigma^{-5/4} + \sigma^{-3/4} + \sigma^{3/4} + \sigma^{5/4}) / (.5\,\sigma^2 + \sigma^{-1/2} + \sigma^{1/2} + .5\,\sigma^{-2})$$

with $\sigma = h_j / h_i$.

Finally, in Fig. 20b we sketch our model for estimating the coupling loss factor from manifold plating into the concrete floor slab via each support and the associated vibration levels of the slab away from the support. Representing each support as a semi-infinite compressional member, the coupling loss factor from section i to the slab is given by

$$\omega \eta_{i,\,slab} = \rho c A_{supt} / \omega M_i \qquad (11)$$

where A_{supt} is the cross-sectional area of the support. The associated force transmitted to the support is

$$|F_{supt}|^2 = (\rho c A_{supt} / \omega)^2 < \ddot{w}_i^2 >$$

To estimate the resulting surface vibration levels of the slab we model it as an elastic half-space and consider (only) the far-field Rayleigh wave contribution to the response[17]

$$|\ddot{w}_{slab}(r)/F| = \omega^2 (K/G) (k_R / 2\pi r)^{1/2} \qquad k_R r >> 1 \qquad (12)$$

with

$$K = (\beta^2/8)\sqrt{1-\alpha^2} / [2 - \beta^2 - (1-\alpha^2)^{1/2} (1-\beta^2)^{1/2} - \gamma]$$

and

$$\gamma = [1 - .5(\alpha^2 + \beta^2)] / \sqrt{(1 - \alpha^2)(1 - \beta^2)}$$

where the shear modulus of concrete $G = 8.9 \times 10^9 N/m^2 (1.3 \times 10^6 psi)$, the Rayleigh wavenumber $k_R = \omega / c_R$ with the Rayleigh wave speed given by $c_R = 0.92\, c_s$, $\alpha = c_R / c_d$ and $\beta = c_R / c_s$ r is range and the dilatational and shear speeds in concrete are taken to be $c_d = 3 \times 10^3 m/\sec\ (1.18 \times 10^5 in/\sec)$ and $c_s = 1.8 \times 10^3 m/\sec\ (7.6 \times 10^4 in/\sec)$, respectively.

For all of our numerical simulations, we let $\eta_d = 0.01$, typical of fabricated metal structures. At any vibration source, the input power is taken to be that for a compact radial force either directly driving the tube plating as if it were of infinite extent, $P_i = |F|^2 Y_{pltg}$ with $Y_{pltg} = (4\rho c h_{pltg}^2 / \sqrt{3})^{-1}$ or, if applied through a rib, driving an infinite beam with $P_i = |F|^2 Re[Y_{beam}]$ and $Re[Y_{beam}] = k_{f(beam)} / 4\omega \rho A_{beam}$.[18]

4. Model of Floor Vibrations from Mechanical Room to Vacuum Equipment Area

To analyze this "flanking" path it is assumed that the 8" mechanical room foundation is connected directly to the 30" vacuum equipment area foundation. The gap between foundations is ignored. Both are supported on lossy springs representing the soil. The mechanical room foundation is 32'x32' and the vacuum equipment foundation is 38'x32'. The source, turbomolecular backing pump or vent and purge system, is located in the mechanical room 10' from the vacuum equipment area. The receiver is located in the vacuum equipment area 25' from the mechanical room. Only vertical excitations and responses are considered.

5. Source-Model Interaction

a. Cryopump - Norton's "equivalent source" theorem, (Figure 21) is

used to convert measured source acceleration levels to model input forces. For the cryopump, the support impedance is much less than that of the cryopump or the cryopump 's vacuum jacket. In this case the force into the vacuum jacket is determined by computing the reaction force of the support when the vibration source is applied to the cryopump end. The resulting force to acceleration transfer function across a single cryopump support is shown in Figure 22a. It is assumed that the applification due to the mount resonance is included in the source measurement (see Section IV-A.)

There are ten such supports connecting the cryopump to its vacuum jacket, four vertical, four lateral and two axial. Each support is excited in three directions. A total of thirty forces are applied to the model. The forces are assumed to be incoherent and responses are combined incoherently, i.e., the square root sum of the squares.

b. <u>Turbomolecular Pump</u> - The turbomolecular pump is connected to the beam manifold through a bellows. The bellows, like the cryopump support, is characterized by a low impedance. The force into the beam manifold is therefore calculated as above and the transfer function is plotted in Figure 22b. Three forces are applied to the model, corresponding to the three principal directions.

For the vibration path through the pump's support, the impedance of the support is much less than that of the massive foundation. Isolation pads under the support are ignored because they are likely short circuited by the required holddown loads. Figure 22c compares the measured drive point acceleration at the base of the suppport with the calculated drive point accelerance of the foundation. From Figure 21, the force into the slab can be calculated from the product of the velocity and the measured drive point impedance at the base of the support. Only the vertical direction is considered. There are four incoherent forces corresponding to the four support legs. This analysis is performed only on the low frequency model.

c. <u>Turbomolecular Backing Pump</u> - The turbomolecular backing pump sits on 20 Hz isolators. Using the impedance of the isolators and the inertial

impedance of the backing pump, the forces into the foundation are computed using the equation in Figure 20.

d. Vent and Purge System - The effective source level of the vent and purge system was measured on the foundation. The force into the foundation was determined by multiplying the measured velocity by the foundation's calculated impedance. Although the system will sit on 20 Hz isolators, they were (conservatively) excluded from our model.

6. Results

Forces are applied to the models as discussed in Section A.5. Responses are calculated along three directions and incoherently summed. Results for each source-receiver pair are presented below as displacement power spectral densities. They are plotted against the LIGO vibration specification (lower dashed line) and the Hanford Corner ground vibration measurement (upper dashed line) for quick comparison.

a. End Station - Results for various source-receiver pairs are plotted in Figures 23a thru 23k. The levels at BSC9 in response to the closer turbomolecular pump (Fig. 23a) are high in the mid frequency range. This is the result of an axial resonance associated with the flexibility of the neckdown region of the beam manifold, high input levels from the turbo-pump controller, and lack of a bellows between the source and receiver. The levels are lower at the second turbo-pump location, due in part to the bellows (Fig. 23b). The chamber response to the cryopump (Fig. 23c) is high at the low frequencies owing to high source levels and the lateral resonance of the cryopump section at 8Hz.

Generally, the levels in close proximity to sources are high (Fig. 23d-g). The high, low frequency response at gate valve WGV20 (Figs. 23h-i) is due to a number of system resonances. However, the modeling of the end valve did not include the stiffness of the beam tube and its natural frequency may be underestimated. Its natural frequency, 2 Hz, is lower than the 8 Hz natural frequency of gate valve WGV29.

The levels on the floor near BSC9 in response to sources exciting the beam manifold are low (Fig. 23j). The levels transmitted through the pump's cart (Fig. 23k) are high in the mid-frequency range because of the controller. Isolation pads located under the cart will be short circuited as a result of the pump's hold down requirements.

b. Mid Station Results - Results for various source-receiver pairs are plotted in Figures 24a and 24b. The mid station is similar to the end station but with an extra turbo pump port and cryopump. Consequently the levels are similar. The beam manifold section is shorter and stiffer, thus increasing some of the natural frequencies.

c. Corner Station Vertex/Mode Cleaner Results - Results for various source-receiver pairs are plotted in Figures 25a and 25b. The chamber responses are highest in this area. The ham support is very flexible resulting in low frequency resonances and higher levels. In addition, the mode cleaner tubing is less massive with fewer structural discontinuities and the ham bellows are stiffer than the others resulting in higher mid and high frequency levels.

d. Corner Station Diagonal Section - Results are plotted in Figures 26a and 26b. These results are similar to those for the turbo-beam splitter with a bellows in the mid and end stations.

e. Corner Station Right Beam Manifold Section - Results are plotted in Figures 27a thru 27g. This section was analyzed in the low and high frequency regions only. Results at the beam splitter (Figs. 27a-c) are typical, but with slightly lower levels than for other splitters because of the larger distances from sources. Near the sources, levels are high (Figs. 27d-e). The end gate valve, GV8, the low frequency levels are high (Figs. 27f-g).

f. Corner Station Remote Locations - With our low frequency model of the corner station, the response of a receiver on the side of a chamber opposite a source was analyzed. Results are plotted in Figures 28a thru 28f. The responses of Ham8 and Ham9 to the turbo pump in the diagonal (Figs. 28b,d) are higher than expected. This

is due to the "liveliness" of the Hams and the proximity of the source.

g. **Mechanical Room Sources** - The predicted maximum floor response near a chamber due to the turbomolecular backing pump and the vent and purge systems is shown in Figure 29a and 29b, respectively. The backing pump has a peak at 20 Hz, its mount resonance, and at 60 Hz, its operating speed. The compressor on the vent and purge system operates at 29 Hz. With both sources, the inclusion of the gap between foundations in our model would reduce the predicted levels, somewhat.

B. Shock

The effect of the high shock levels caused by the opening and closing of the pneumatically actuated gate valve was evaluated using existing vibration models. Acceleration power spectral densities (PSD) were created from the time histories shown in Figure 14 and 15. The force into the model was calculated by considering the valve to be a velocity source attached to the bellows. This assumes that the valve moves as a rigid mass with the beam tube, and the valve support has a negligible effect.

The valve is located in the corner station where we have only developed a low frequency model. The resulting PSD at BSC7 is shown in Figure 30a. The low frequency RMS acceleration at BSC 7 is 0.009 g. Assuming the peak levels are roughly twice the rms values, a 0.02 g peak response is predicted at the beam splitter.

To estimate the mid and high frequency response, the input was applied to the motor driven gate valve in the end station, GV19, shown in Figure 18a. The results are shown in Figure 30b. Greater attenuation is expected in the corner station area.

The effects of the 10" and 14" manual valves are estimated at various locations shown in Figures 30c-30e. These valves are hard mounted to the tubes and the measured accelerations are assumed to be the drive point values. The attenuation varies with the distance from the valves to the chambers.

C. Noise

1. Overview

The purpose of the acoustical models is to predict the noise level at critical receptor locations in the various Laser Vacuum Equipment Areas [LVEA] of the LIGO Stations generated during LIGO operational conditions by vacuum pumps and auxiliary equipment provided by PSI. The project specified operational noise criterion spectrum of NC-20 applies. Receptor locations include specific locations on the vacuum system components. Use was made of the July 1996 architectural and engineering drawings from Parsons, as well as vacuum system layouts and details provided by PSI.

The procedure involves modelling the LVEA's acoustically to reflect the dimensions and the sound absorption properties of all surfaces and contents and determining the various transmission paths for airborne sound from equipment located in the Vacuum Support Equipment Areas [VSEA] as well as from the equipment located within the LVEA. Finally, combined noise levels are calculated at typical receptor locations based on the quantity and distances of the various sources.

The elements incorporated in the model include the following.

a. Noise Sources - Based primarily on measured sound pressure level in dB re 20 micropascal in octave bands from 31.5 to 8 kHz center frequency the levels are normalized to a 3 ft distance. Although the defined NC spectrum extends down only to 63 Hz, current practice in noise control includes at least the 31.5 Hz octave band. In order to provide a more complete description especially for larger sources such as compressors, all of the calculations include the 31.5 Hz band. The NC curve is extended to 31 Hz, at the same slope it has between 63 and 125 Hz, for information only.

b. Room Acoustics - All of the tall and sparsely furnished LVEA's can be expected to produce highly diffuse reverberant sound fields beyond the direct field of the sources. An exception could be the relatively narrow south and east branches of the Corner Station wherein the sound fields of distant sources will keep decreasing with

distance at a modest rate, however, to be conservative and avoid computational complexity, this factor is not applied in the acoustic model. The sound level in the reverberant field is determined by the acoustical ceiling, the sound absorption of all other room surfaces including all equipment, as well as occupants.

c. Noise Reduction of VSEA Envelopes - The partitions, doors, and other potential airborne sound transmission paths, e.g. ducts penetrating the partitions, and seals around penetrations are combined to achieve a frequency dependent noise transmission path to the associated LVEA.

d. Receptor Noise Level Predictions - The noise from combinations of sources under various conditions can be predicted, based on the distances from the sources in the LVEA and from the VSEA as a combined sound source. The sources, being non-synchronous, i.e., uncorrelated, are combined on an energy basis. The predicted noise levels are compared to the NC-20 spectrum. In certain cases exceedances of the noise criterion are found, in particular due to the turbomolecular pump carts.

2. Vacuum System Noise - Equipment List

The potential airborne noise sources used in the acoustical models include all vacuum pumps and auxiliary equipment provided to LIGO by PSI that are located within the building envelopes of each Station and to which the project specified **operational** noise criterion contour of NC-20 applies. In the Corner Stations, the possibility exists that LIGO may be in operation while vacuum sub systems, which can be isolated from the operational vacuum segments via the gate valves, are down, e.g. during repairs. During such events the Vent and Purge Equipment may be in operation and its noise output is included at receiver locations at the operational segments. Vacuum pumps used during initial pumpdown such as roughing pumps are exempt from the noise criterion since LIGO is then **not** operational. Cryopumps are not expected to produce any airborne noise.

The following list identifies the vacuum equipment which potentially contributes to noise during LIGO operations.

Table 1. List of noise producing vacuum equipment for different LIGO stations for operational conditions.

CORNER STATION [WA, LA]

Equipment	Location	Quantity	Operation	Primary Noise Paths
Large Ion Pump	LVEA	8	Constant	Airborne noise from top of Beam Tube location
Small Ion Pump Controller	LVEA	28	Constant	Airborne from floor location
TMP Cart	LVEA	2	Intermittent	Airborne from pump and controller
V&P Compressor Intake Air	LVEA	1	Intermittent	Airborne from 6 in. pipe into LVEA
Large Ion Pump Controller	VSEA	8	Constant	Via VSEA envelope
TMP Backing Pump	VSEA	2	Intermittent	Via VSEA envelope
Vent & Purge Compressor	VSEA	1	Intermittent	Via VSEA envelope

MID STATION [WA]

Equipment	Location	Quantity	Operation	Primary Noise Paths
Large Ion Pump	LVEA	1	Constant	Airborne noise from top of Beam Tube
Small Ion Pump Controller	LVEA	5	Constant	Airborne from floor location
TMP Cart	LVEA	1	Intermittent	Airborne from pump and controller

Equipment	Location	Quantity	Operation	Primary Noise Paths
TMP Backing Pump	VSEA	1	Intermittent	Via VSEA envelope
Large Ion Pump Controller	VSEA	1	Constant	Via VSEA envelope

END STATION [WA, LA]

Equipment	Location	Quantity	Operation	Primary Noise Paths
Large Ion Pump	LVEA	1	Constant	Airborne noise from top of Beam Tube
Large Ion Pump Controller	VSEA	1	Constant	Via VSEA envelope
Small Ion Pump Controller	LVEA	3	Constant	Airborne from floor location
TMP Cart	LVEA	1	Intermittent	Airborne from pump and controller
TMP Backing Pump	VSEA	1	Intermittent	Via VSEA envelope

3. Acoustic Field Calculations

The sound level produced at a given receptor location, e.g. a chamber, or a particular area of a beam manifold is the combination of all sources operating under the selected condition. Sources located within the LVEA, such as TMP's, produce sound levels at the receptor affected only by distance, if close by, or acoustical absorption if much further away. Sources located in the adjacent VSEA are typically noisier but their sound output is significantly attenuated by the envelope of the VSEA.

The calculated noise levels are based on the diffuse field equation for non-directional sources in rooms. The sound pressure level, in dB re 20 micro Pascal, is

$$L_p = L_w + 10 \log\left[\left(\frac{1}{4\pi r^2}\right) + \frac{4}{R}\right] + 10\,dB$$

where L_w is the acoustic power level in dB re 10^{-12} watts, r is the distance between source and receiver in ft, R is the room constant. The calculations are repeated at each octave band center frequency yielding reverberation times, average absorption coefficients, and room constants. The latter is the total effective sound absorbing area in the space having n different materials, equal to

$$R = \sum_n S_n \alpha_n$$

where S is the area of an specific absorbing material, in sq ft, and α is the sound absorption coefficient of that surface. The product $S\alpha$ has the units of Sabins and represents an equivalent area of perfect absorption. R includes the additional effect of air absorption applicable at higher frequencies and significant in large spaces. Persons are assigned a given number of Sabins. The critical distance at which the direct field component, the first term in the above equation, equals the reverberant field component, the second term in the brackets, is given by

$$r_{crit} = \frac{1}{4}\sqrt{\frac{R}{\pi}}$$

Sound sources in these spaces will generate highly diffuse reverberant sound fields beyond the direct fields of the sources. The calculated crossover, or critical, distance occurs at about 11 ft in the smaller Mid and End Stations and at about 22 ft in the Corner Stations.

The reverberation time of the spaces in seconds is given by the simple equation,

$$T = 0.05\ V/R$$

where V is the space volume in cu ft and R is the room constant.

The sound power levels for the sources in the LVEA's are obtained by calculating the equivalent sound power level for a point source having the measured sound pressure level at 3 ft. The sound power due to sources in the VSEA's is obtained from the intensity (assumed to be uniform over the partition in the vicinity of the equipment) by combining the measured source levels at 3 ft. The radiated power is then the product of the intensity and the surface area of the partition. The transmission loss of the partition, including all flanking paths, is subtracted to obtain the transmitted power into the LVEA. This simple approach is based on the fact that on the source side the partition is in the direct field while the receptor locations are all in the reverberant field of the partition. For the Corner Station the effective radiating area used is 1990 sq ft while it is 550 sq ft for the Mid and End Stations. As described above, the sound power radiated by the partition is found to be about ten times greater than the total reverberant sound power in the VSEA due to the same sources. This justifies the use of the simplified model in providing conservative receptor noise levels from these sources.

4. Room Acoustic Models

The Corner, Mid, and End Station LVEA's are large and tall and sparsely furnished. The Corner Station has a volume below the ceiling of about 1 million cubic feet. Due to the geometric similarity of the End Station and the Mid Station (WA), the End Station is used as the acoustic model for both.

Except for an acoustical ceiling with a modest absorption rating the remaining room surfaces are sound reflective. The planned acoustical ceiling product is USGypsum,"Clean Room Panel", Item #56090 whose absorption coefficient averages about 60%. Although, the sound absorption of all other room surfaces including all vacuum equipment, is quite small, averaging about 5%, the large surface areas involved

this contribution to absorption is included. The absorption due to a few occupants is also included.

The calculated average absorption coefficient and the reverberation times for the Stations are fairly independent of frequency in the range of 63 Hz to 4 kHz. In this frequency range the absorption coefficients of common materials are available from handbooks down to 125 Hz based on standardized test procedures, e.g. ASTM C423, and can be estimated quite reliably to 63 Hz based on published research reports. The uniformity of sound absorption down to low frequencies results from the ceiling panels being backed by deep air spaces and the 10 to 20% absorption values in the lower octave bands typically exhibited by the gypsum board wall panelling. In contrast, the concrete floor slab and the rigid metal vacuum components provide very small absorption values, about 3%, at all frequencies. The average reverberation time is about 2.2 seconds in the Corner Station and around 1.8 seconds in the End and Mid Stations, typical of industrial environments.

5. Sound Transmission Through VSEA Envelopes

The effective transmission loss [TL] includes flanking paths via ductwork, pipe penetrations, and access doors. These various factors are considered in the acoustic model, as applicable. Airborne sound transmission from VSEA's to the adjoining LVEA involve a variety of paths including:

- Common partitions
- Ductwork passing through space
- Personnel access doors
- Seal around piping and cables to vacuum equipment
- Flanking transmission via roof

With the exception of some minor recommended changes discussed in the Section 8

"Comments on Drawings", the partitions descriptions and dimensions are taken from R.M. Parsons drawings.

a. <u>Sound Transmission Individual Envelope Components</u> - The transmission loss for each octave band even if the construction does not precisely duplicate any laboratory or field tested partition can be estimated based on prior experience and a large quantity of published information on sound transmission through various building materials. The partition descriptions are on Drawing WA-A428.

Sound transmission loss values for gypsum wall board (GWB) partitions are based primarily on data contained in United States Gypsum Co. (Chicago, IL) Publication SA-921, 1990 edition, and Publication CS-139/USG/10-84. The transmission loss data in these publications extend down to 31 Hz, in some cases, well below the standard ASTM E90 test frequency lower limit of 100 Hz. Although these low frequency data do not claim conformance to the standard, they convey useful information for dealing with control of low frequency machinery noise.

The large round ducts can pickup sound in the VSEA through what is called "break in" and transmit it to the LVEA via air terminal devices, ie. diffusers and registers. Examples of such ducts running through the VSEA's are shown on the mechanical drawings, such as plan H212 and section H242. The leakage via these paths is not a major factor since the ducts are round and hence stiff. An exception is the transition area from round to rectangular duct in the return duct for the Corner Station which is reflected in the path TL.

Since the vacuum equipment is attached to the building structure in various ways and is directly or indirectly in contact with vacuum vessels and manifolds via air and cooling water pipes, flexible bellows, electrical conduits, and instrumentation cables <u>structureborne noise</u> paths of undesirable dynamic energy are inevitable. The transmission via these paths is controlled through the "first order" abatement techniques for the vacuum equipment, including vibration isolation elements, flexible pipe

connectors, and damping materials. The joint between foundation slabs surrounding each LVEA is useful in controlling flanking path transmission of both airborne and structureborne noise.

The following transmission loss values have been used in the acoustic path model between the VSEA's and the LVEA's. The combined transmission loss depends on the effective surface area of each component.

Table 2. Transmission Loss Estimates for VSEA Envelope Components. Values in dB.

	Octave Band Center Frequency, Hz								
Envelope Component	31	63	125	250	500	1k	2k	4k	8k
PARTITION: **Mid & End** - [cavity wall, Type 11]	14	23	33	42	50	51	52	52	52
PARTITION: **Corner** - [cavity wall, Type 15]	22	30	36	50	55	55	55	55	55
INTERIOR DOOR: **Mid & End:**- direct [gasketed]	12	18	20	28	27	29	32	34	35
INTERIOR DOOR: **Corner:** via Access Space	20	30	35	42	50	50	50	50	50
RETURN AIR DUCT: **Mid & End** - 16" dia. duct and floor register	36	36	33	31	30	31	31	28	32
RETURN AIR DUCT: **Mid & End** - 32" dia. via intake above acoustical ceiling	34	34	34	35	41	45	50	55	55
RETURN AIR DUCT: **Corner** - 42" dia. via partition to floor register	31	30	28	43	50	50	50	50	50
SUPPLY AIR DUCT: **Corner:** via diffusers	46	39	31	25	28	27	28	34	40
FLANKING VIA EXPOSED ROOF DECK: **All**	25	30	35	40	45	50	55	55	55
PENETRATION at Pipe Bridge: **Corner Station**	10	15	16	17	18	18	19	20	22

b. Estimated Transmission Loss Through VSEA Envelopes - Combining the transmission loss values tabulated above for the Mid or End Station and Corner Station on the basis of the areas involved in each component the following results were obtained. In the case of the Corner Station, the assumed transmitting envelope below the acoustical ceiling includes 40 ft of the southerly wall and the 40 ft of the westerly wall portion not overlapped by the Access Area, other than the path via the door. In the Mid and End Stations the whole partition below the acoustical ceiling is used.

Table 3. Transmission Loss For VSEA Envelopes. Values in dB.

	Octave Band Center Frequency, Hz								
STATION	31	63	125	250	500	1k	2k	4k	8k
End or Mid [550 sq ft]	14	23	31	40	41	43	45	46	48
Corner [1990 sq ft]	22	30	32	40	44	45	45	44	45

6. Receptor Noise Levels

The vacuum equipment noise levels are calculated at the following representative receptor locations taken from the LIGO list [12]. The octave band spectrum of these levels compared to the NC-20 criterion is shown in the corresponding figures. The receptors and the sources are identified in Figs. 16a-c. Unless otherwise noted the receptor elevation is 2 m. The End Station results apply to comparable locations in the Mid Station as well.

a. Corner Station Receptor ID 1a: 5 m south of HAM-1 - Fig. 31a shows that without the two TMP Carts or the Vent and Purge Compressor in operation the predicted noise level from the remaining vacuum equipment is below the design criterion. However, with either of these systems

in operation, especially the TMP Carts which are typically close to beam tubes and vacuum chambers the design goal for airborne noise is not met.

Individual contributions by the Compressor and its Air Intake shown in Fig. 31b and are both lower than the TMP Cart noise at and above 250 Hz. Below 250 Hz, the Compressor and the Air Intake noise contributions are predicted to be higher than the TMP system. There is some uncertainty about this equipment's source levels because the actual equipment was not available for measurements, however, the values used are believed to be conservative..

b. **Corner Station Receptor ID 1b: 5 m north of HAM-7** - The calculated noise level results (Figs. 31c and d) are similar to those for Receptor 1b, with only the TMP Cart and Vent and Purge Compressor operations leading to exceedances of the noise criterion. The noise level from the TMP Backing Pump alone is shown in Fig. 31d and it is found not to contribute to the exceedance.

c. **Corner Station Receptor ID 1e: BSC-7** - The calculated noise levels at this location (Fig. 31e) also reflect the dominance by operations of the TMP and Vent and Purge systems as is found at the other locations in the Corner Station.

d. **Corner Station Receptor ID 3d: TMP Nozzle of Cryopump-2** - As shown in Fig. 31f, the close proximity of the TMP Cart to this location increases the noise levels at and above 250 Hz by about 10 dB in all octave bands compared to the other Corner Station receptors discussed above. At those locations the TMP Carts are at least 3 m or further from the receptors.

e. **End Station and Mid Station Receptor ID 1a and 1b : BSC-9 Nozzles** - Results are shown in Fig. 32a. Since the smaller Vent and Purge system is not used during LIGO operation in the End Stations, the exceedance of the noise criterion occurs only at and above 250 Hz and is due solely to noise from

intermittent TMP Cart operations. The same noise levels are anticipated for both Receptors 1a and 1b.

f. End Station Receptor ID 2a and Mid Station Receptor ID 2: Manifold Section A-7 - Results are presented in Fig. 32b. For this location the calculated noise levels during intermittent TMP Cart operation are about 7 dB higher than for the other End Station Receptor due to the closer proximity of the TMP Cart.

7. Conclusions

The calculated noise levels from the vacuum pumps and auxiliary equipment are expected to meet the project noise criterion of NC-20 during operational conditions except during intermittent operations of the turbo pump carts and, in the case of the Corner Stations, when the vent and purge compressor is in operation. Minor modifications and clarification of the construction details of the VSEA envelopes are recommended to help achieve the favorable results.

8. Comments on Drawings

The drawing package dated 12 July 1996 has been reviewed and several minor changes and additions affecting the isolation of Vacuum Support Equipment Area from the Laser Vacuum Equipment Areas are recommended. If the recommendations are not incorporated they may affect the predicted noise levels.

a. Corner Station VSEA Partition

(DWGS: WA-A-505, -161, -28) - Change Type 11/H1 partition on the Mechanical Equipment Room [MER] side to Type 15/H1 [2 layers of 5/8 in. gypsum wall board].

b. Mid and End Station Partitions

(DWGS: WA-A-201, -202, -428) - Type T3 insulation is not required in the VSEA partition; Type T2, with a thickness equal to that of the studs, is preferable.

c. Acess Doors to VSEA's

(DWGS: WA-A-201, -202, -426, -505) - The relevant doors are numbered on the drawings as 210C [Mid], 310C [End], and 106B [Corner]. Detail 11 on A-426 shows a basic drop seal for the bottom edge, however, no seals for the head and jambs are indicated.

The gaskets for head, jambs, and threshold should incorporate permanently soft elastomers such as neoprene, silicone rubber, or EPDM; PVC material is not acceptable. Products suitable for these doors include self adhesive *Stanley* [Series 5050, "Double-Guard"], *Pemko* [Series S-88], Zero [Series 188], or equivalent head and jamb gaskets. Alternatively, tubular gaskets with carrier channels are acceptable but require a sealant between the channels and the door frame. Drop seals are maintenance prone, however, if used they should be "heavy duty" type such as *Zero* 365 or 367 or *Pemko* 4301/RL or 4301/PKL Series, or approved equal by *Reese, National Guard Products*, or *Stanley.* Preferred alternative bottom gasket include [a] a saddle and a door mounted sweep gasket such as *Pemko* 313 or 317 or equivalent or [b] a low profile threshold with a tubular compression gasket such as *Zero* Model 564, or equivalent. All gaskets should be installed to result in a compression of between 25 and 50 percent of the unloaded thickness. All gaskets should continuous. Drop seals should minimize clearances at the ends of the drop bar.

d. Seals Around Penetrations - There is no complete drawn description or general note regarding the seals required around all structural, duct, pipe, and conduit penetrations of the VSEA/MER partitions. These seals must be continuous

and include caulking on both sides of the partition. Various commercially available backer materials and permanently non-hardening sealants can be used for this purpose.

Seals of this sort are also required around the pipes, cables, and other connections between the Vacuum Support equipment components and the Vacuum equipment in the LVEA's for which openings are being provided; see e.g. DWG A-251, Section D and A-553, Section C. Due to possible changes in these connections the sealing system should permit easy opening and resealing. Use of mastics, for example, FSP 1000 "Firestop Putty" by International Protective Coatings Corp., Ocean Township, NJ, or equivalent, is suggested.

e. <u>Joints between Partitions and Roof Structure</u>

(DWG: WA-A-422) - Details 9 and 10 show a satisfactory closure where partitions run parallel to the ribs of the metal roof deck. There is no corresponding detail for the perpendicular intersection with the ribs. The latter typically includes a preformed elastomeric insert or fibrous fill stuffed in all openings. It is important that all rib openings be sealed completely and involve a filler material which is sufficiently dense to prevent excessive sound penetration.

REFERENCES

1- Vacuum Equipment Specification, LIGO Facility, LIGO-E94-0002-01-V, Rev. 1, 28 March 1995, p.11.

2 - C.M. Harris, Handbook of Acoustical Measurements and Noise Control, (3rd Ed., McGraw-Hill Book Co., NY, 1991) pp. 43.4-43.5.

3 - J.S. Bendat and A.G. Piersol, Engineering Applications of Correlation and Spectral Analysis, (John Wiley & Sons, NY, 1980) pp. 264-270.

4 - Summary of Concepts and Reference Design for LIGO, Cal. Instit. of Tech, February 1992.

5 - C.M. Harris and C.E. Crede (Ed), Shock and Vibration Handbook, Vol. 1, (McGraw-Hill Book Co., NY, 1961) pp. 10.24-10.25.

6 - M.C. Junger, "Bubble-Generated Forces and Resulting Structure-Borne Noise", CAA Tech Memo: TM/U-2392-2041 to Richard Bagley of PSI (26 August 1996).

7 - W.L. Haberman and R.K. Morton, "An Experimental Investigation of the Drag and Shape of Air Bubbles Rising in Various Liquids", David W. Taylor Model Basin Report No. 802, Sept. 1953.

8 - J.B. Turpin, Shock Test of LIGO G44E Valve, from, GNB Report (9 Sept. 1996).

9 - Kyle Martini, "GNB Pneumatic Valve Shock Analysis", CAA Memo to Richard Bagley of PSI (30 Dec. 1996).

10 - Kyle Martini, "10" and 14" Manual Valve Shock Measurements," CAA Memo to Richard Bagley of PSI (9 Dec. 1996).

11 - LIGO Technical Foundation Analyses Executive Summary and Discussions.

12 - John Worden, "Focal Receiver Points as Requested by CAA for their Vibration and Acoustics Analysis," LIGO Tech Memo TM 37, to Richard Bagley (5 Aug. 1996).

13 - LIGO Technical Foundation Analyses Executive Summary and Discussions, The Ralph M. Parsons Company Contract Number: PP150969 (4 December 1995).

14 - Richard H. Lyon, Statistical Energy Analysis of Dynamical Systems, (The MIT Press, Cambridge, MA, 1975).

15 - S. H. Crandall and R. Lotz, "On the Coupling Loss Factor in Statistical Energy Analysis", J. Acoust. Soc. Am., 49, 352-356 (1971). Also, J. Garrelick, "Dynamic Response of Coupled Systems: A Comparison Between Statistical Energy and Deterministic Systems", CAA Technical Report U-392-213 prepared for The

Office of Naval Research under Contract N-00014-69-C-0056 , Structural Mechanics Program, (Sept. 1972).

16 - L. Cremer, M. Heckl and E.E. Ungar, Structure-borne Sound, (Springer-Verlag, Berlin, 1973), Ch. V.

17 - W. Maurice Ewing, Wenceslas S. Jardetsky, and Frank Press, Elastic Waves in Elastic Media, (McGraw-Hill Book Company, New York, 1957), 315.

18 - Miguel C. Junger and David Feit, Sound, Structures and their Interaction, (The MIT Press, Cambridge, MA, 1986), Ch 7.

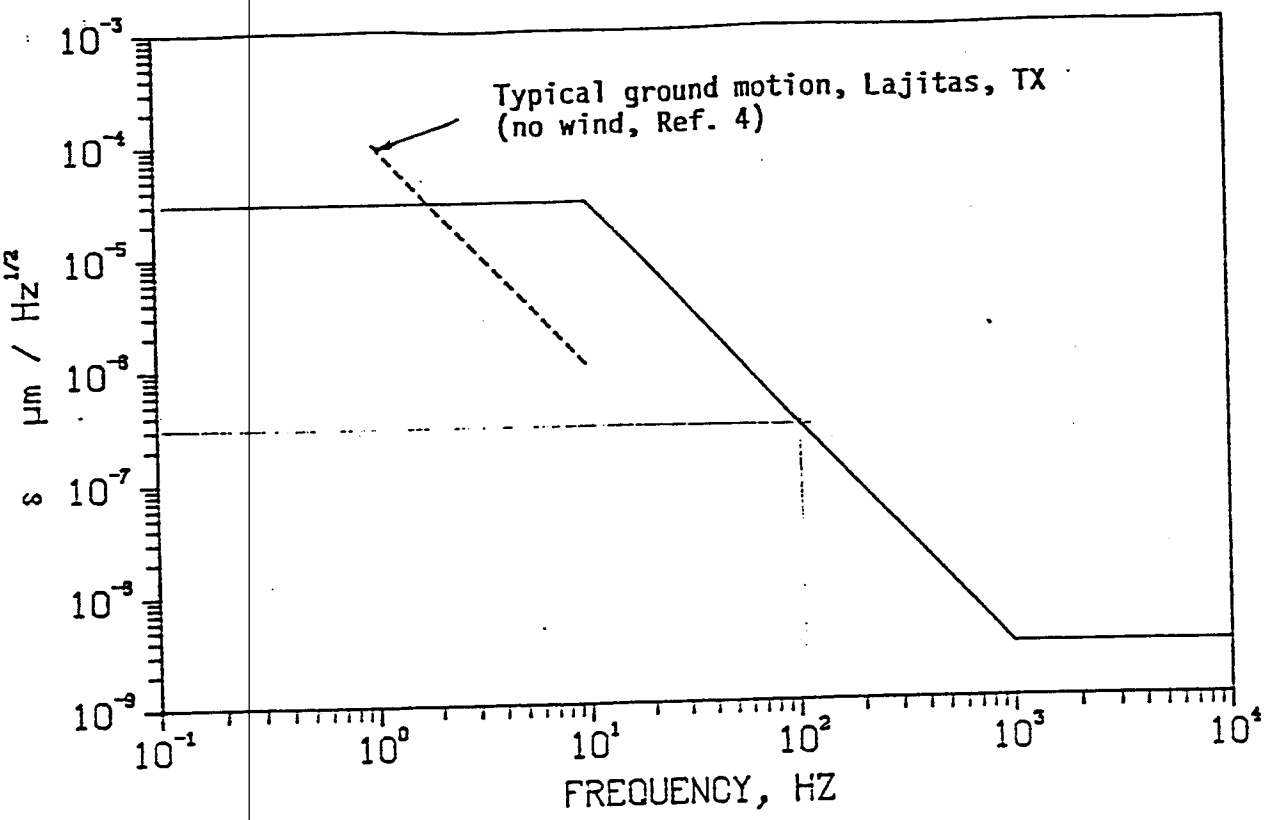

(a) Displacement

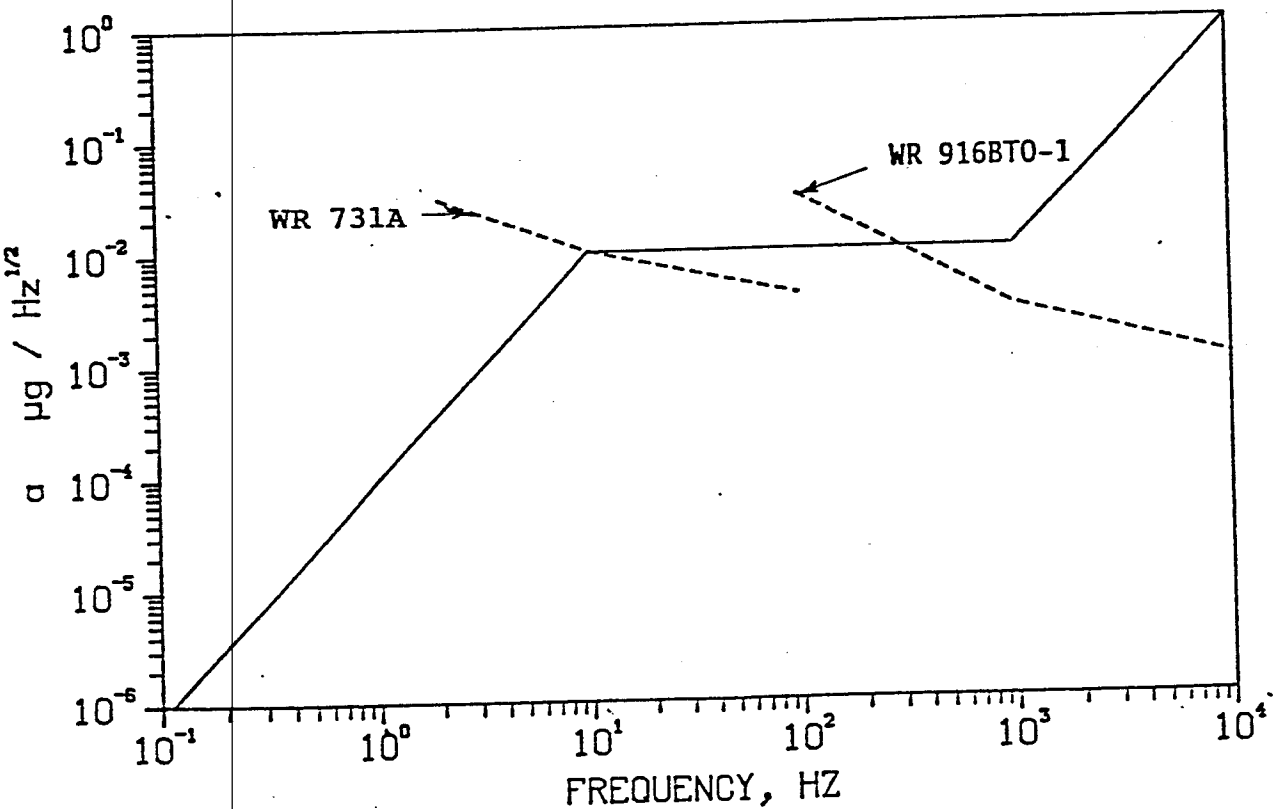

(b) Acceleration

Fig. 1 - LIGO Displacement and (equivalent) acceleration specifications

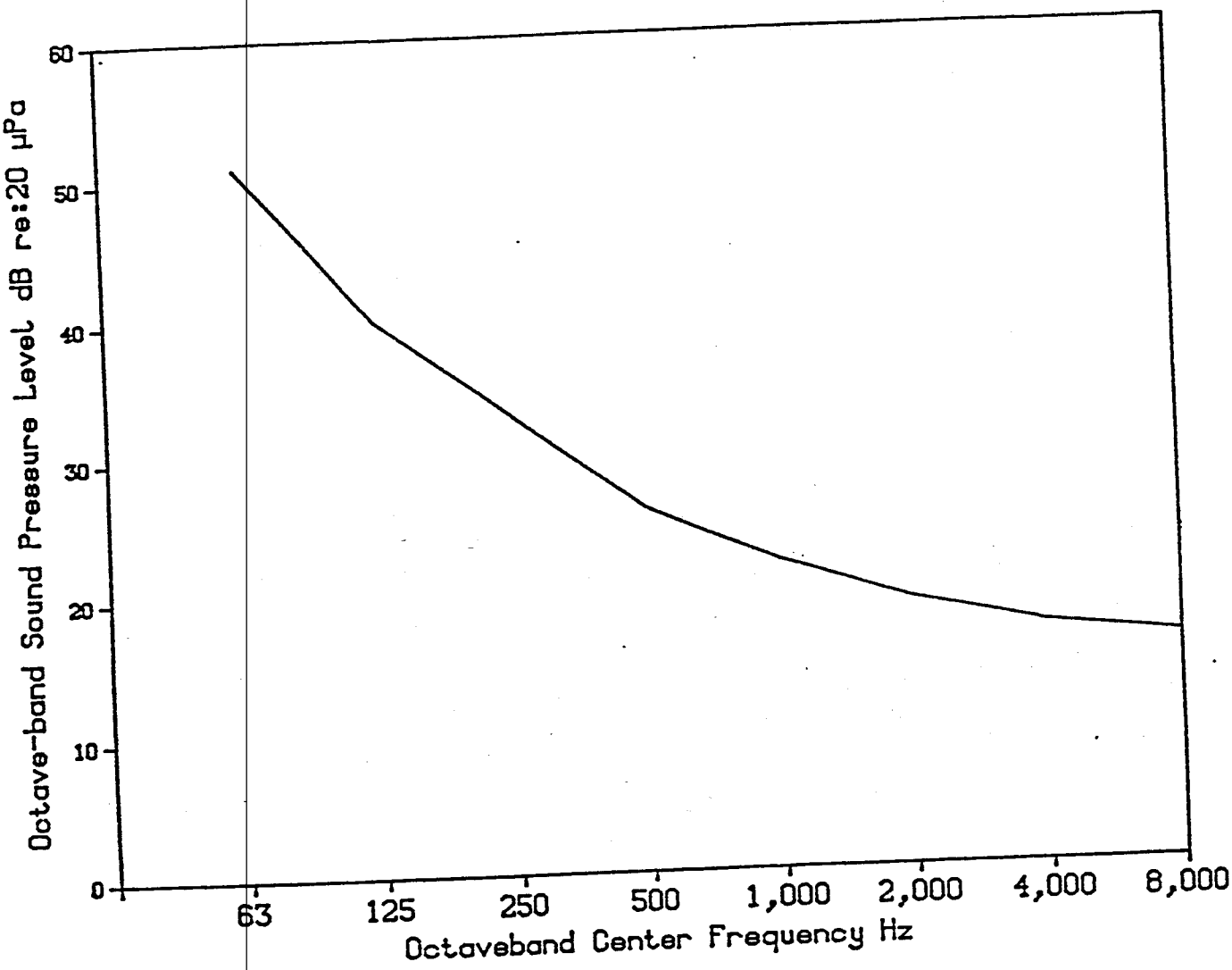

Fig. 2 Noise criterion-20 (NC-20) octave band sound pressure levels.

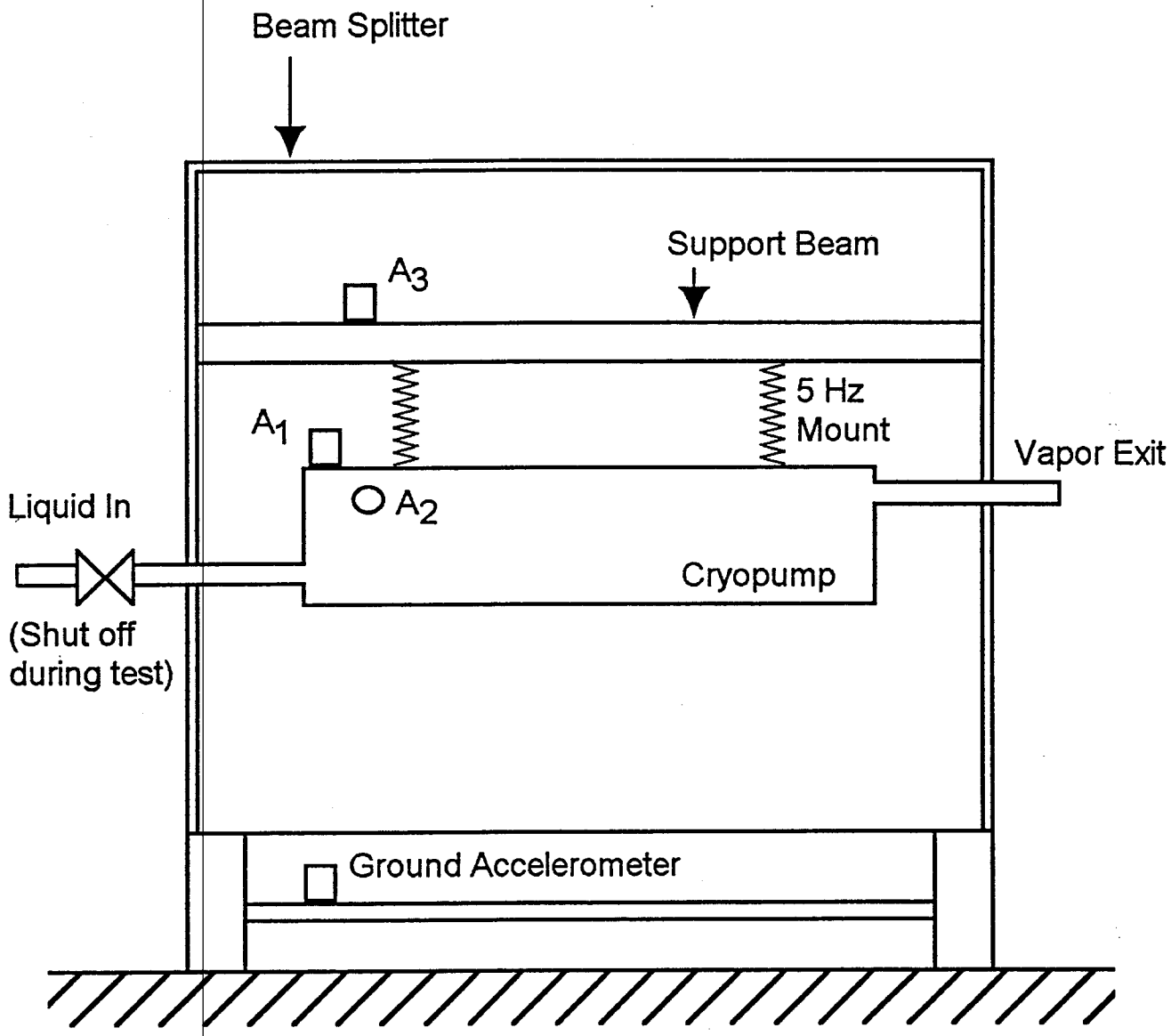

Fib. 3a - Cryopump Vibration Test

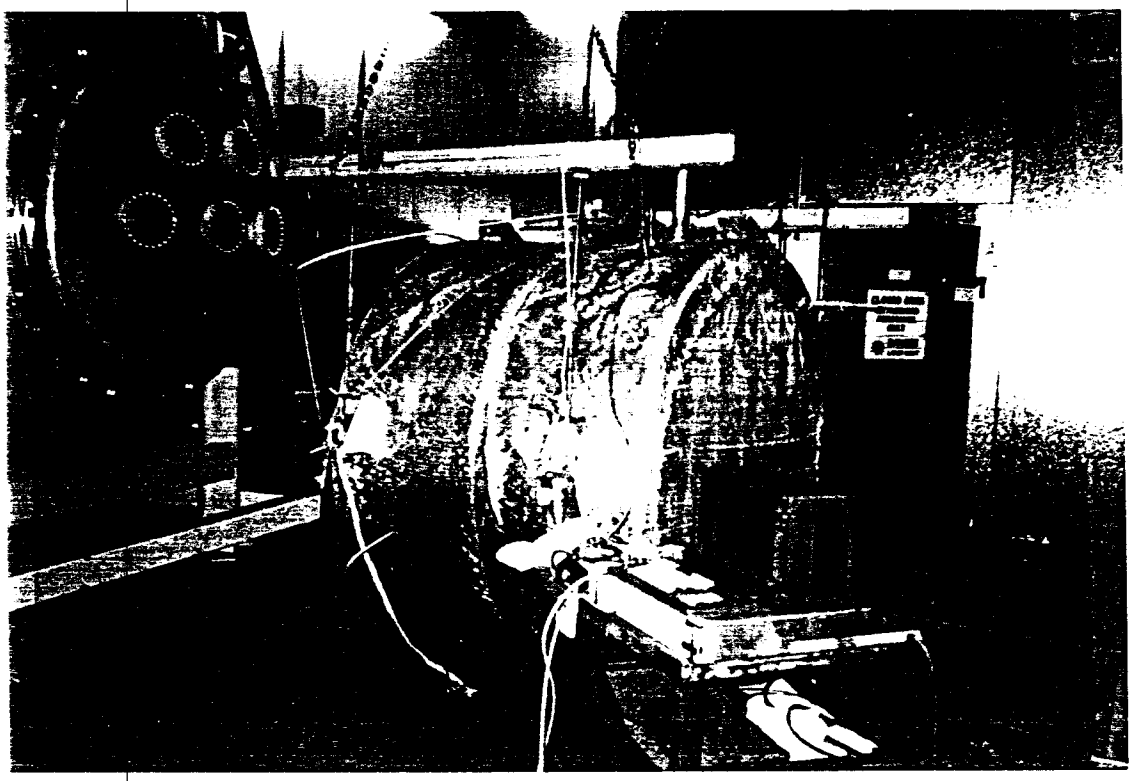

Fig. 3b - Photograph at Cryopump

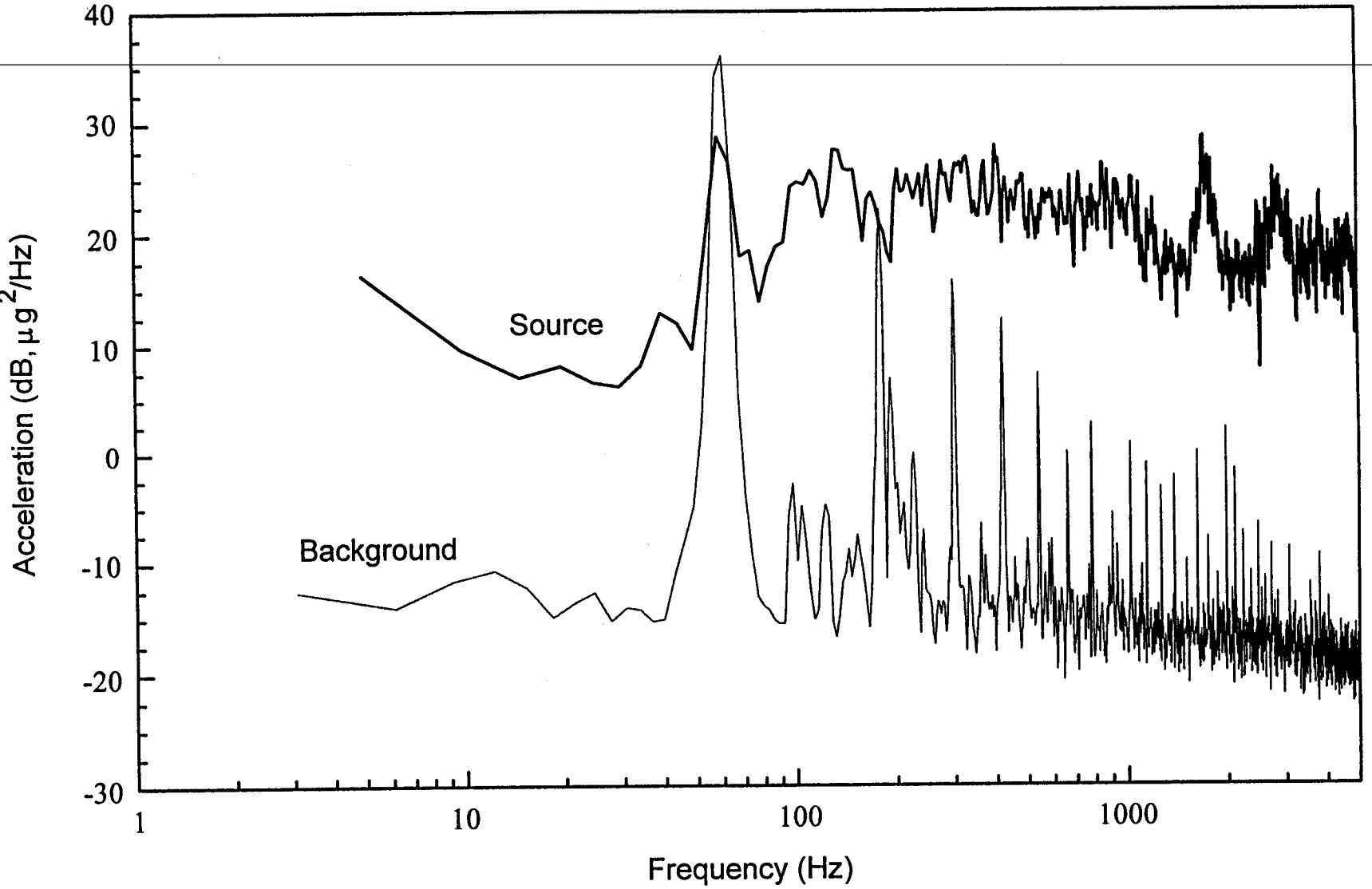

Fig. 3c - Cryopump Source Levels Compared with Background Levels
Horizontal Direction

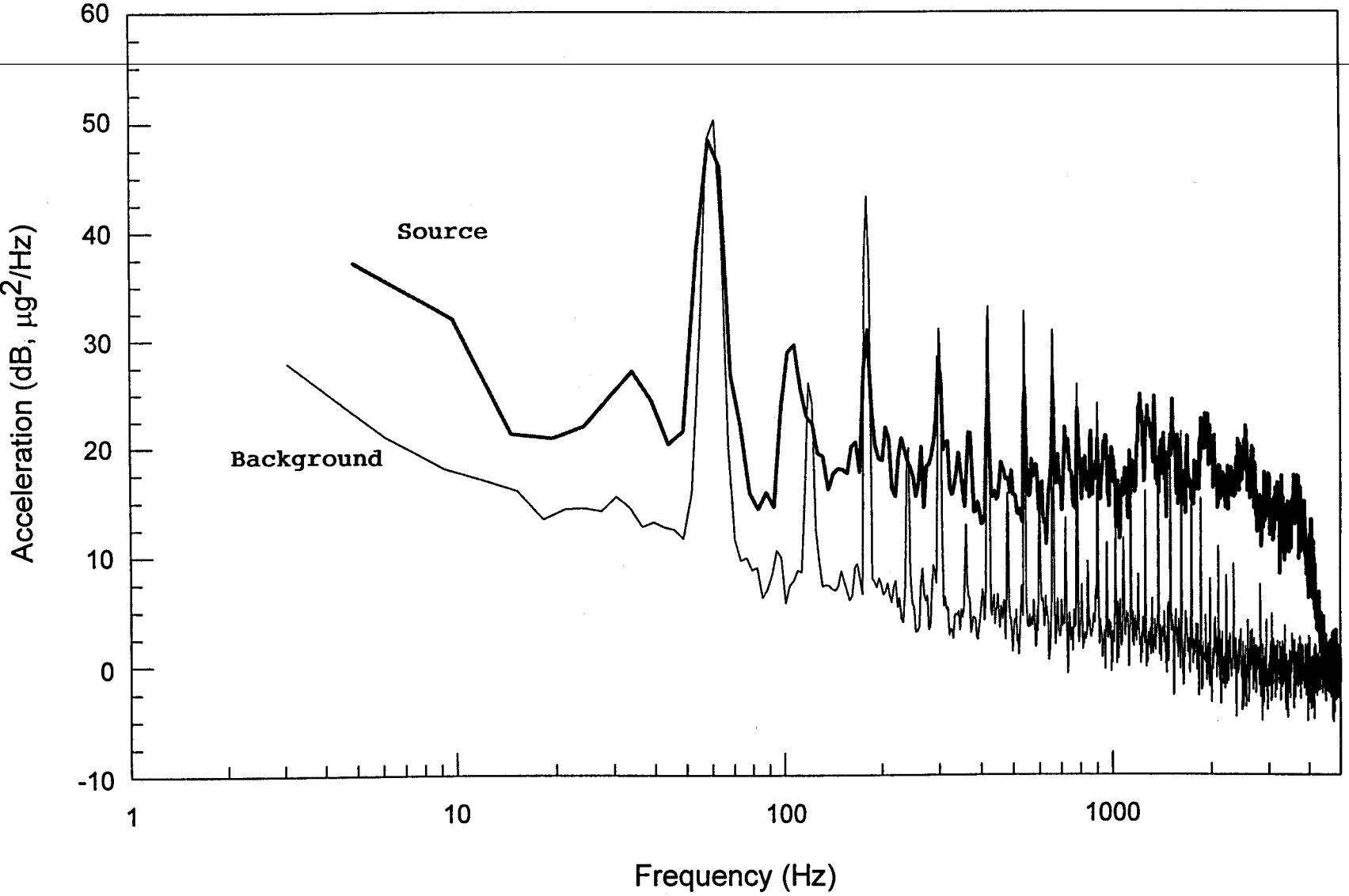

Fig. 3d - Cryopump Source Levels Compared with Background Levels
Vertical Direction

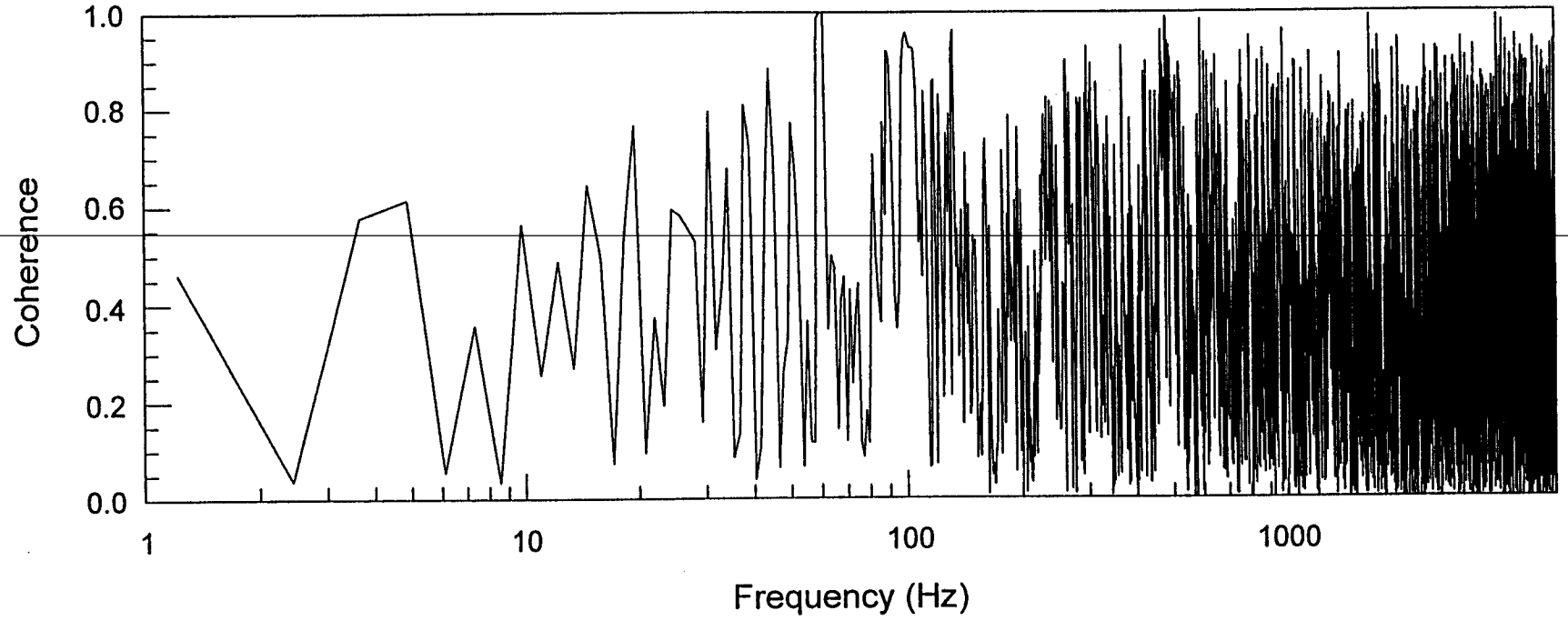

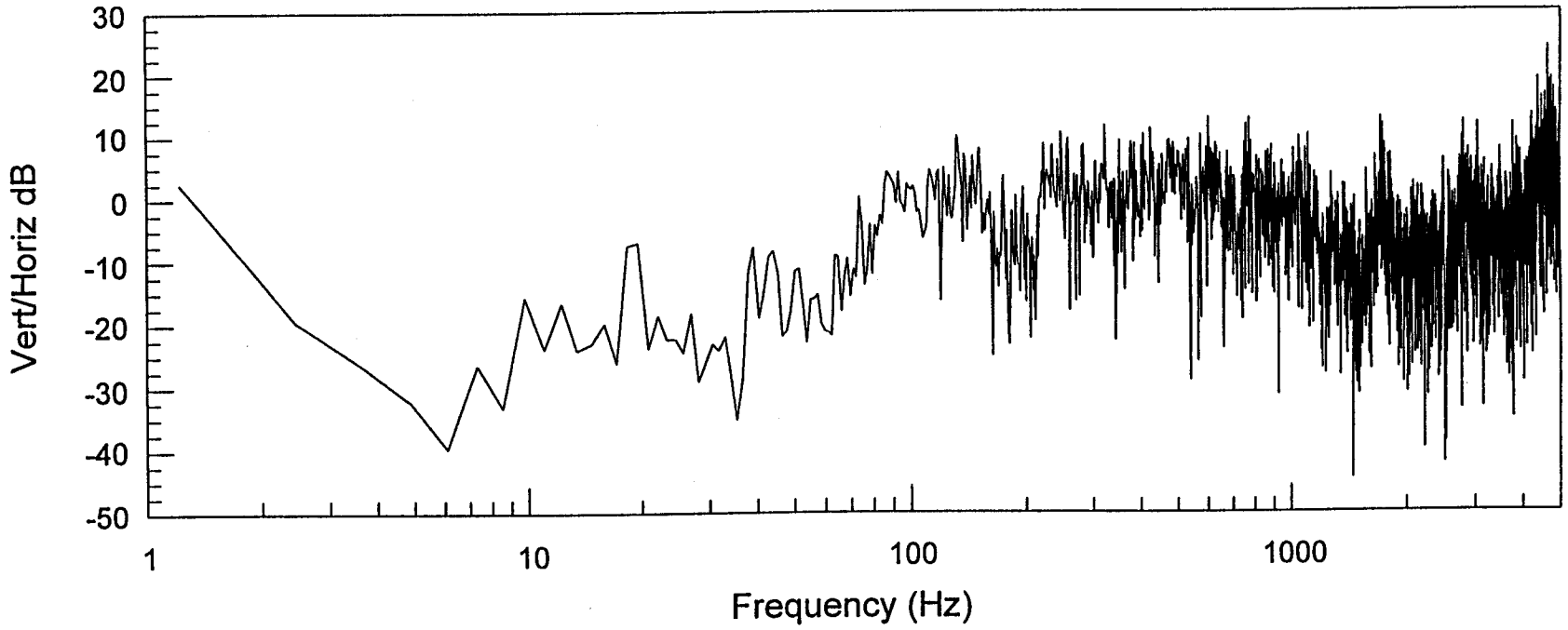

Fig. 3e - Cryopump - Comparison between Vertical and Horizontal Vibrations

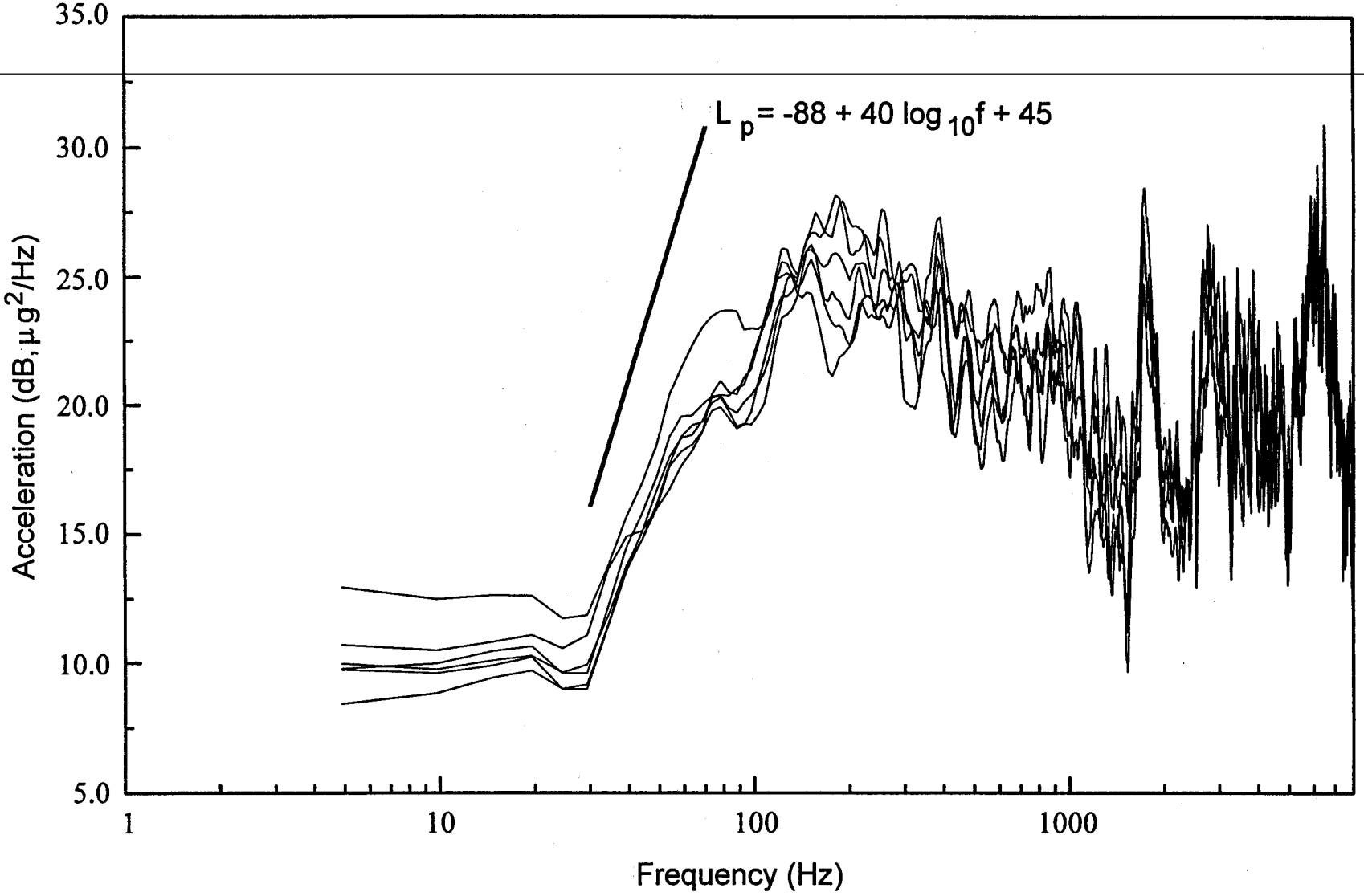

Fig. 3f - Cryopump Source Level for Various Flow Rates - Data Smoothed

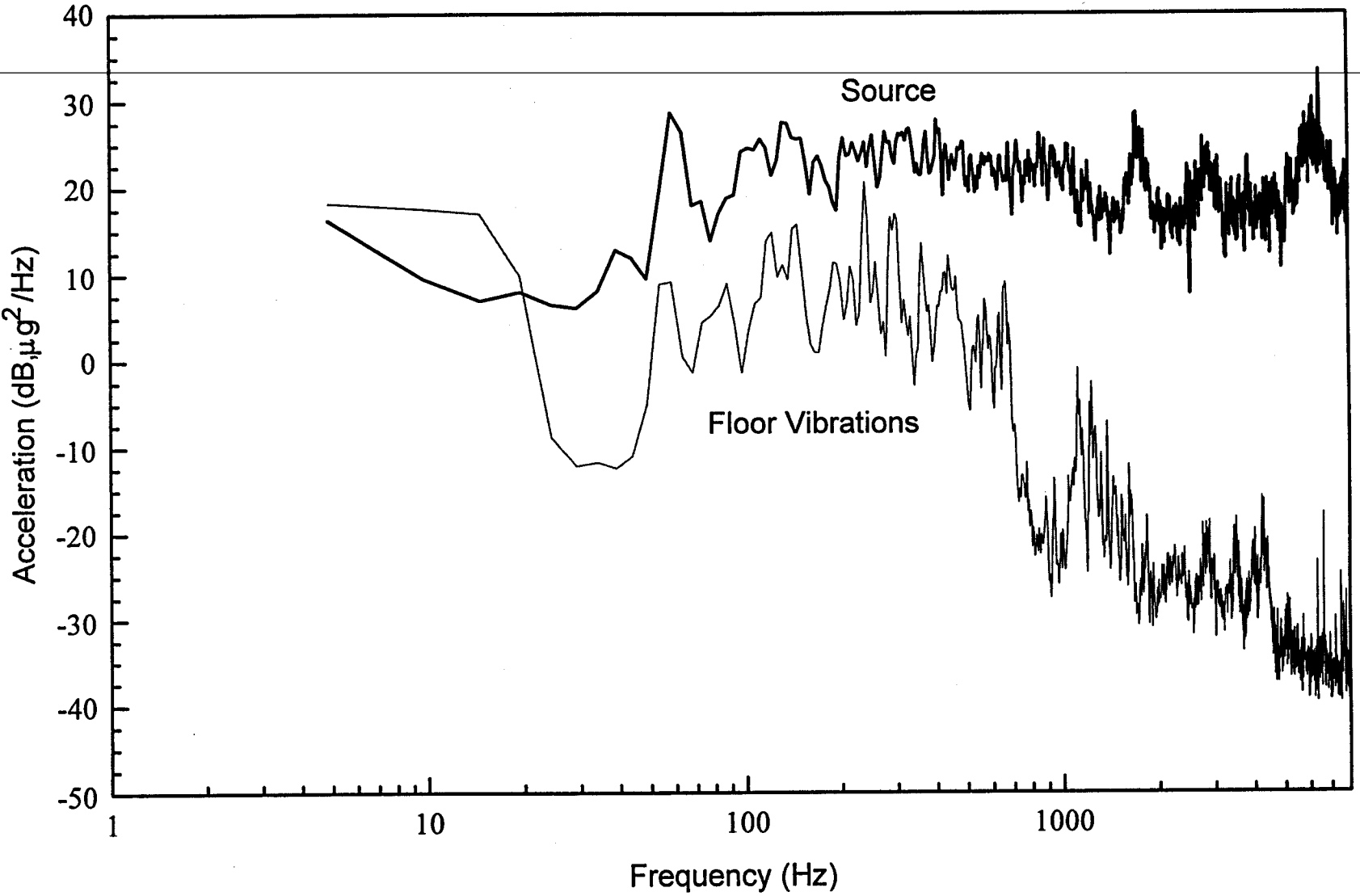

Fig. 3g - Cryopump Source Levels Compared with Floor Vibrations

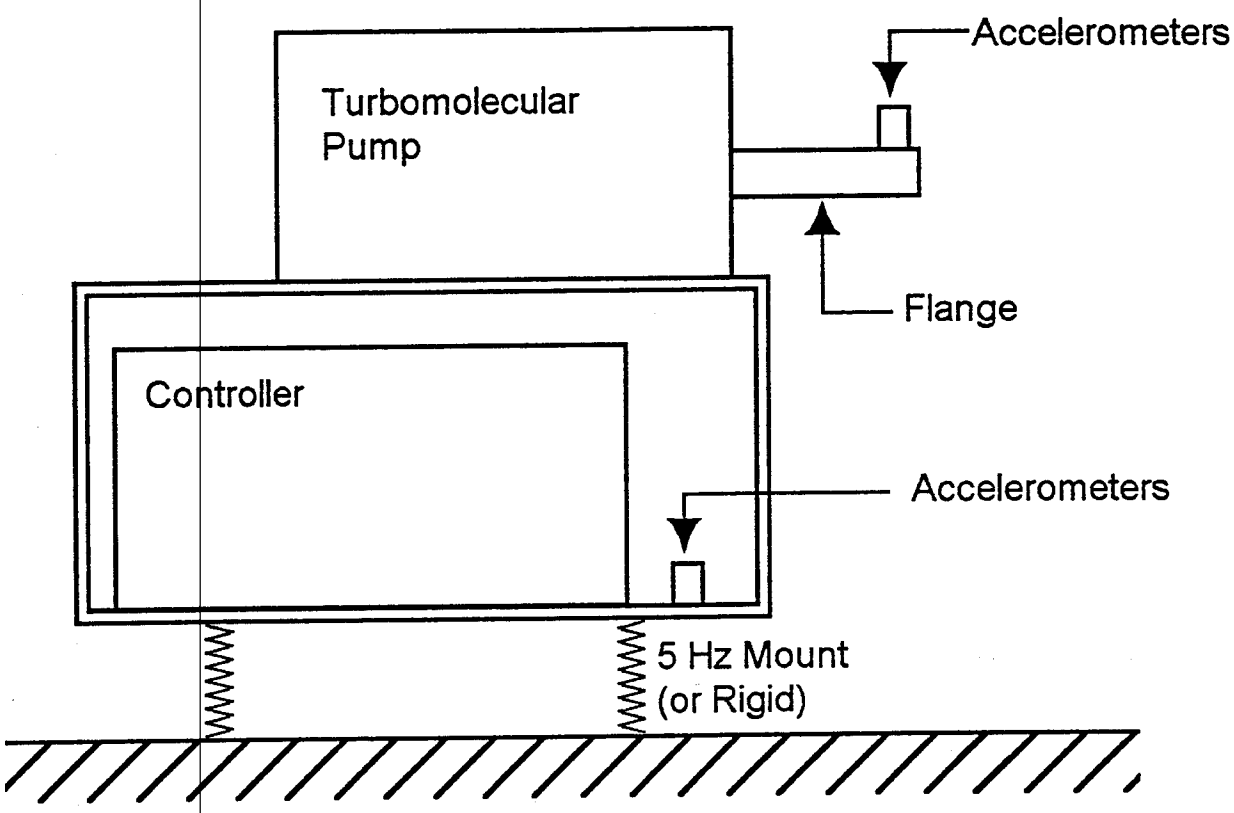

Fig. 4a - Turbomolecular Pump Vibration Test

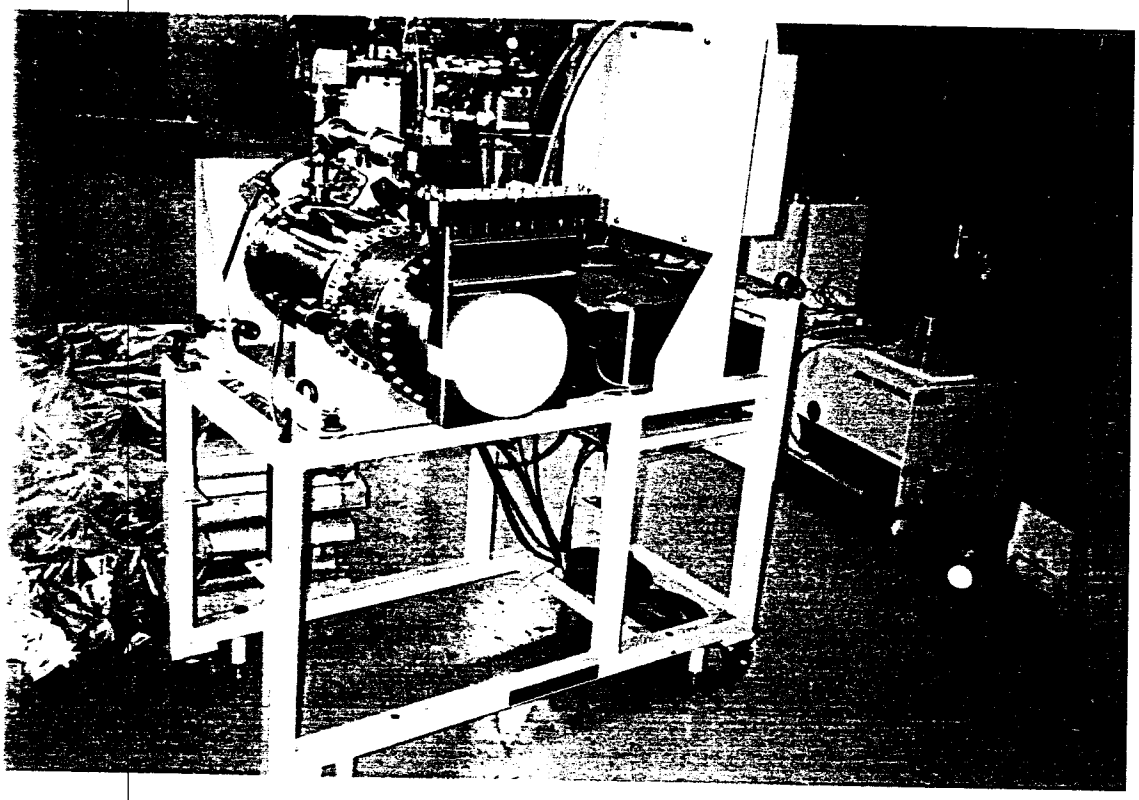

Fig. 4b - Photograph of Turbomolecular Pump

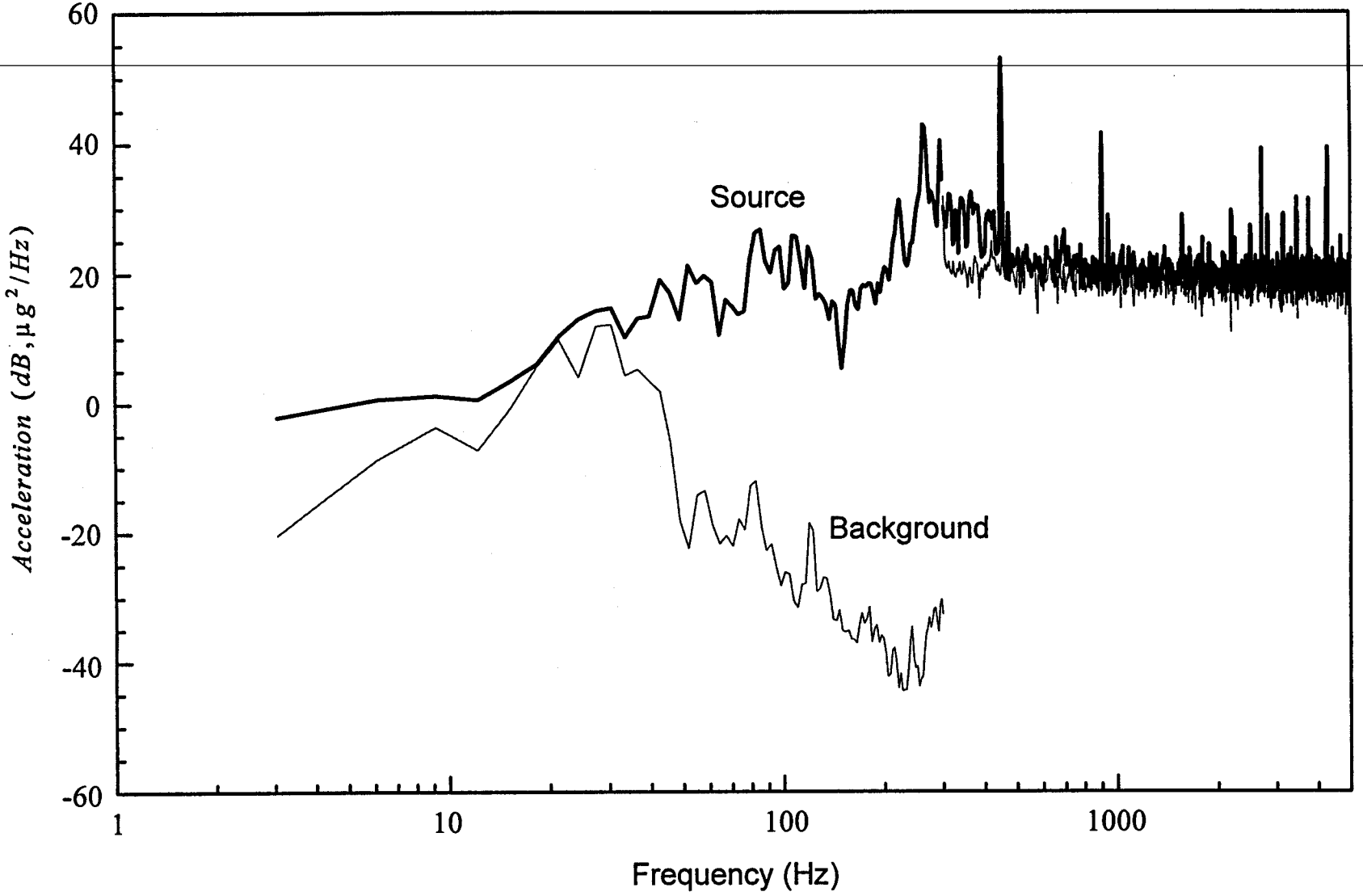

Fig. 4c - Turbomolecular Pump Vibration at Flange

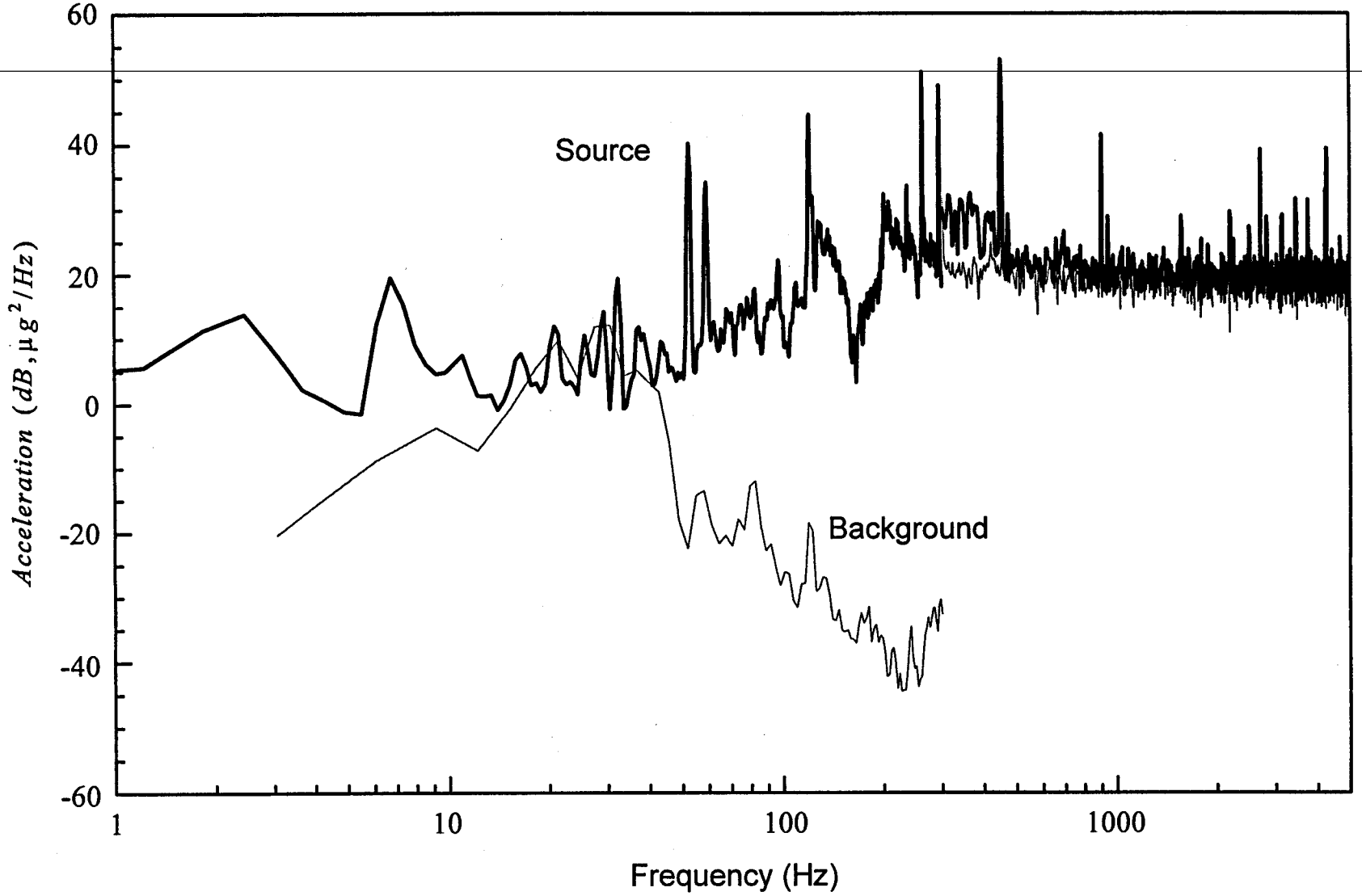

Fig. 4d - Turbomolecular Pump Vibration at Base

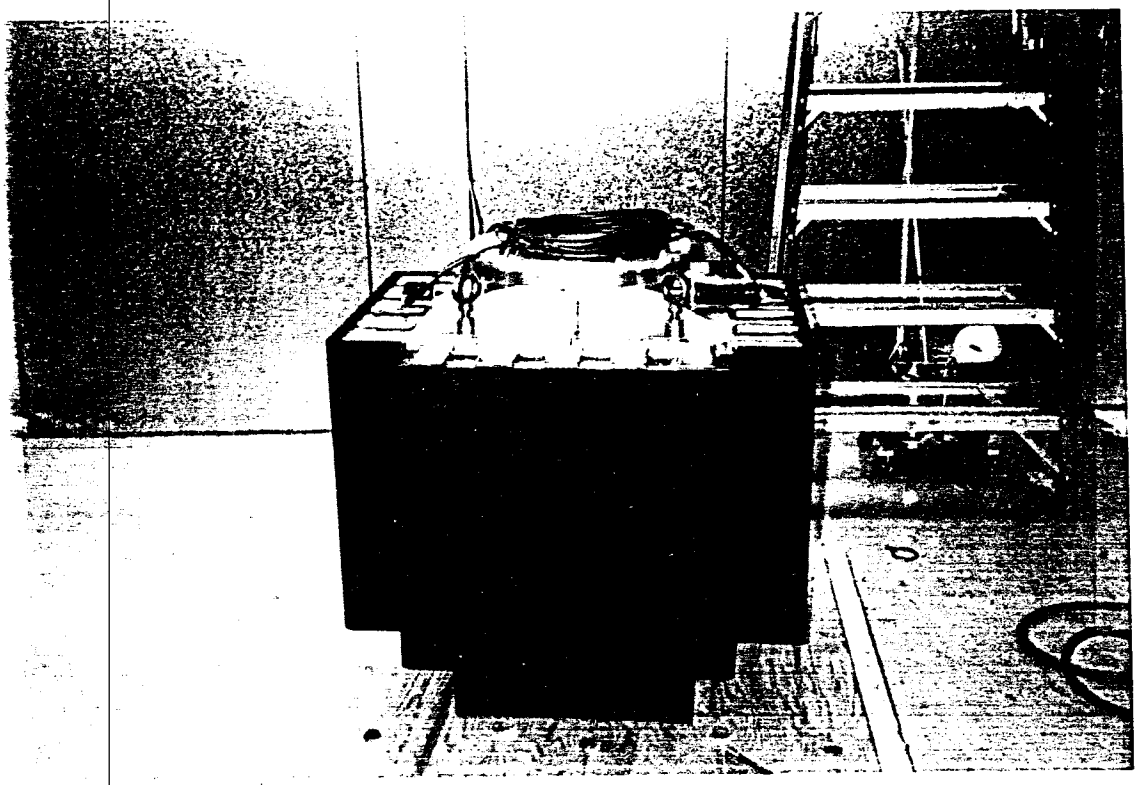

Fig. 5a - Photograph of Large Ion Pump

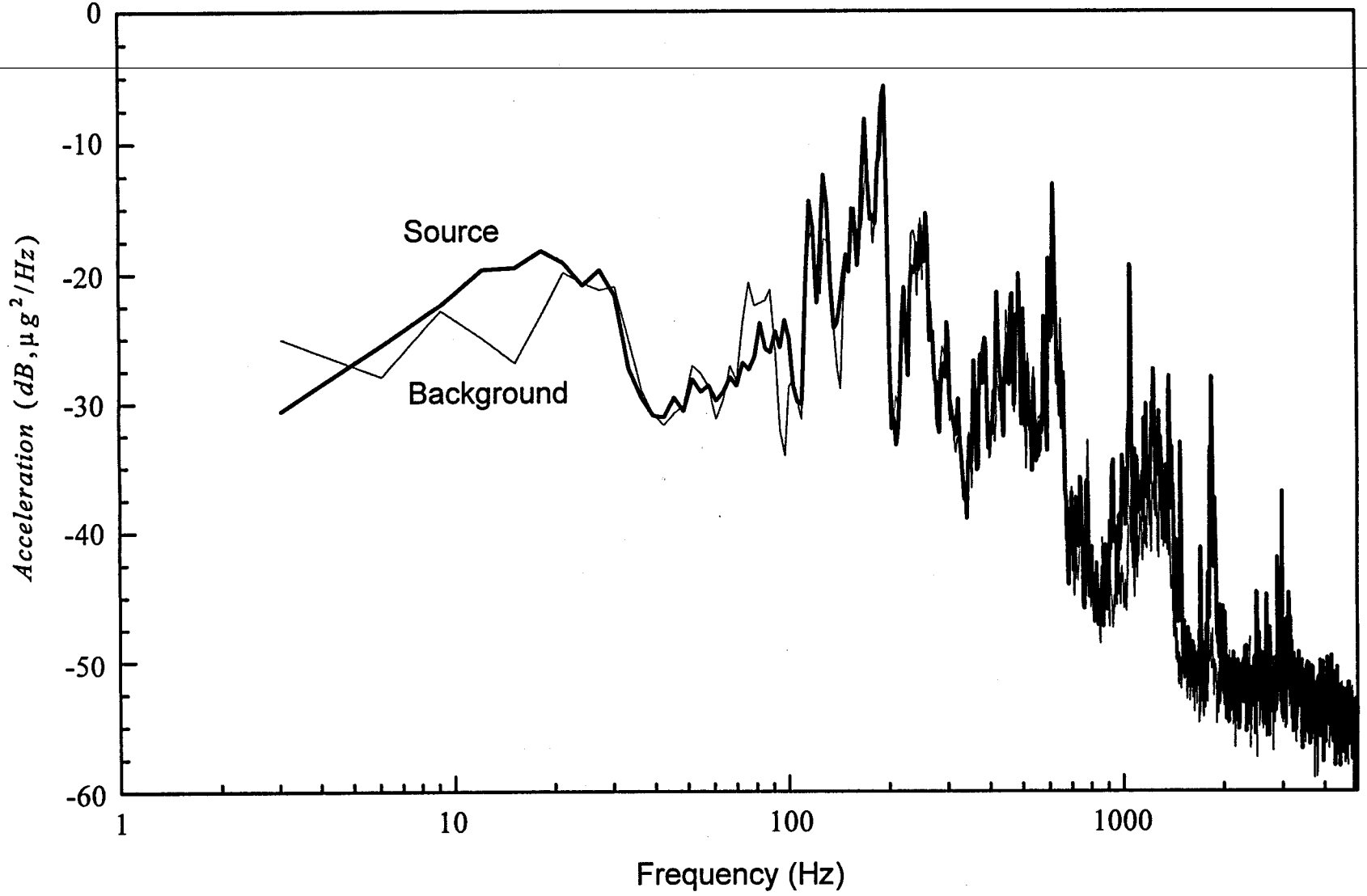

Fig. 5b - Large Ion Pump Vibrations

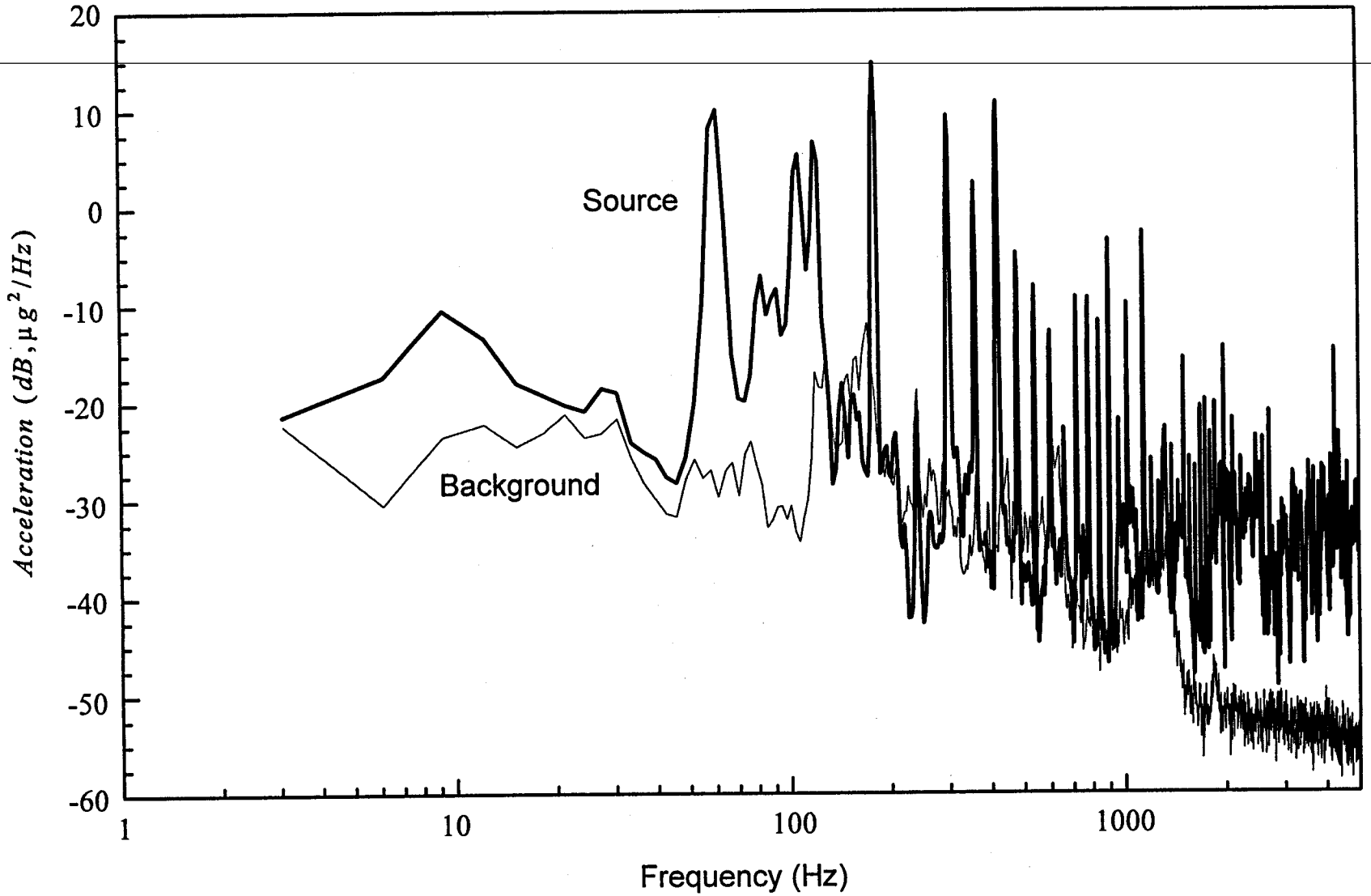

Fig. 6 - Small Ion Pump Controller Vibrations

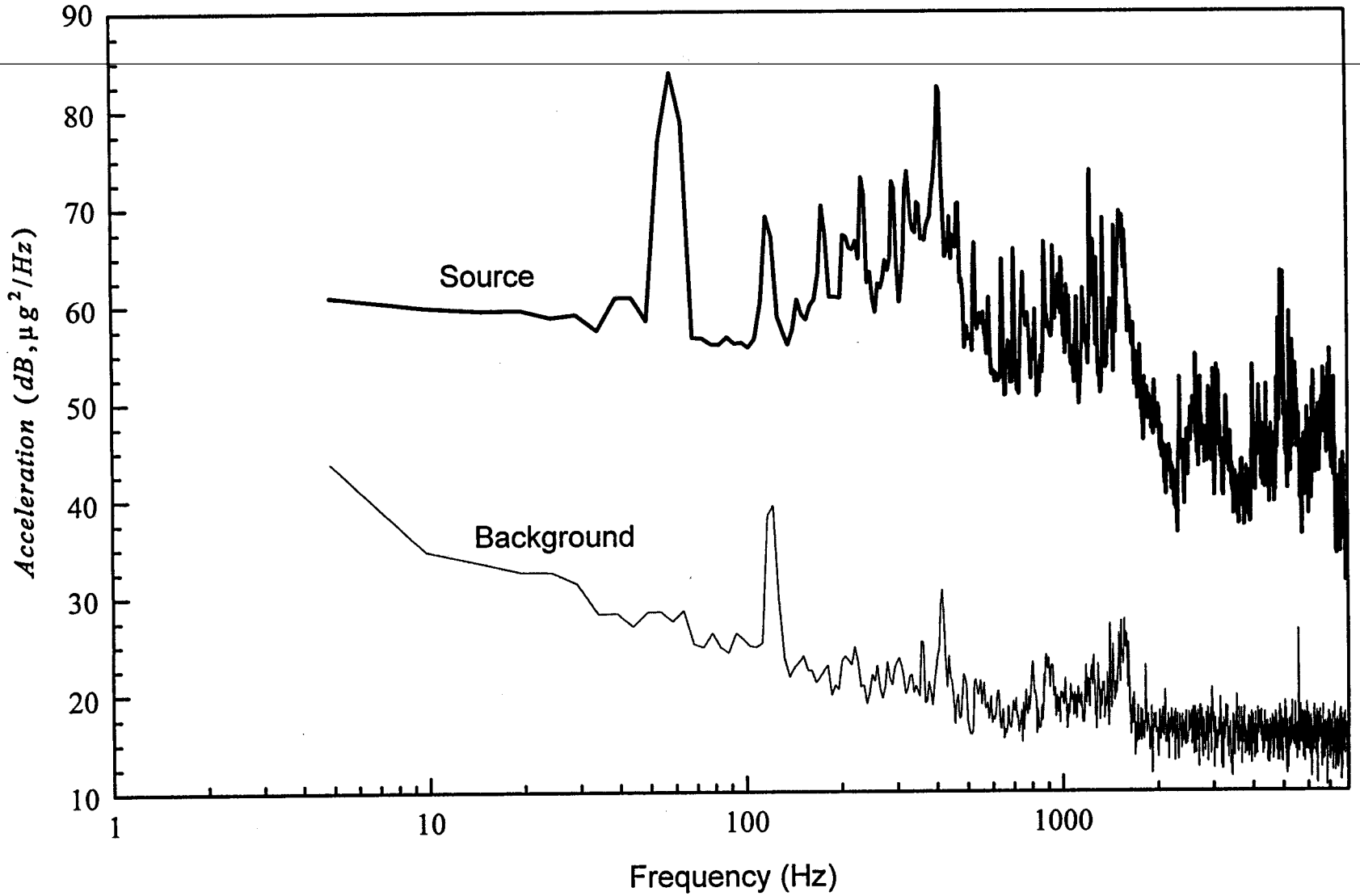

Fig. 7 - Turbo Backing Pump Vibrations

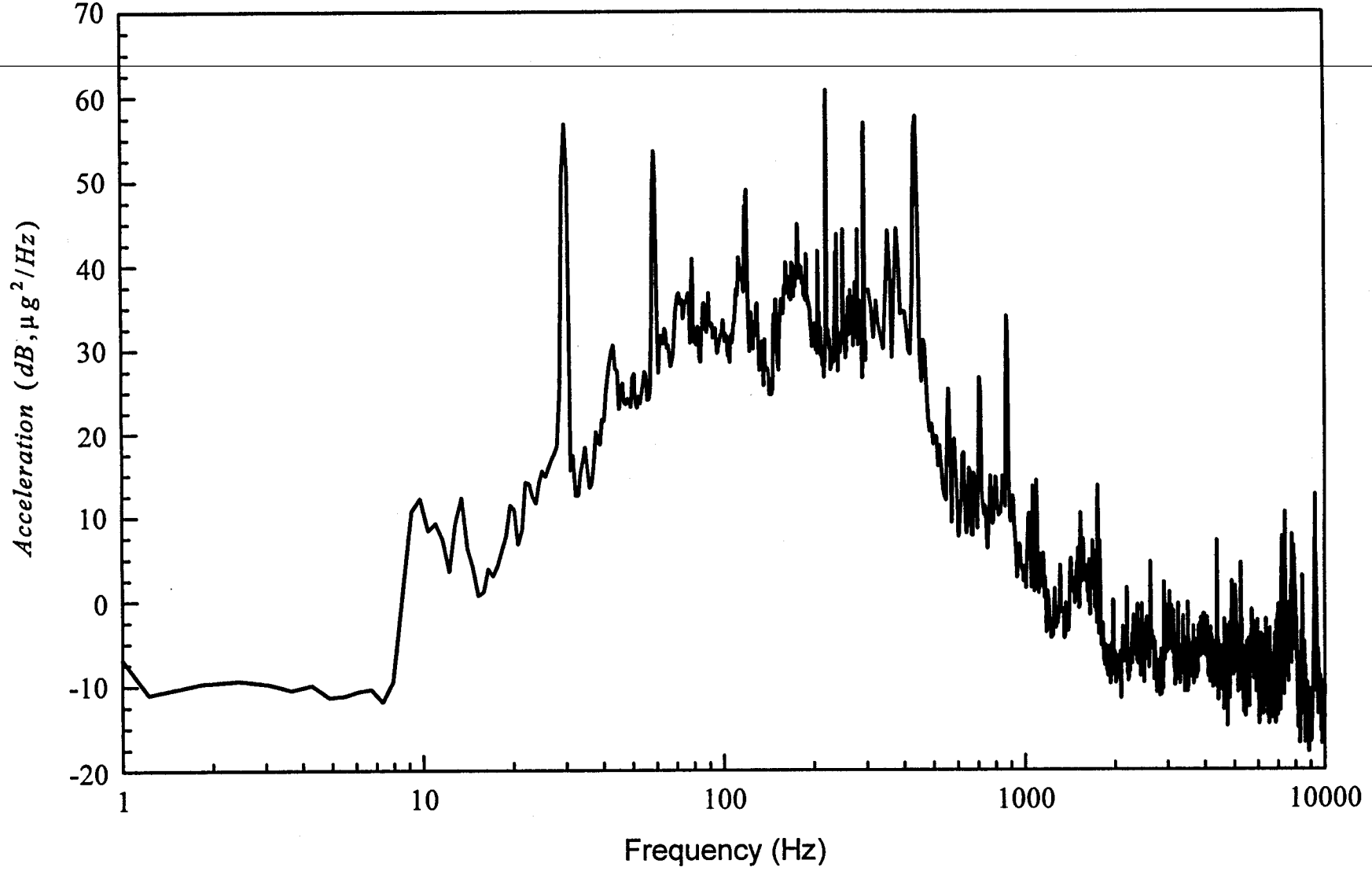

Fig. 8 - Vent and Purge System Vibrations

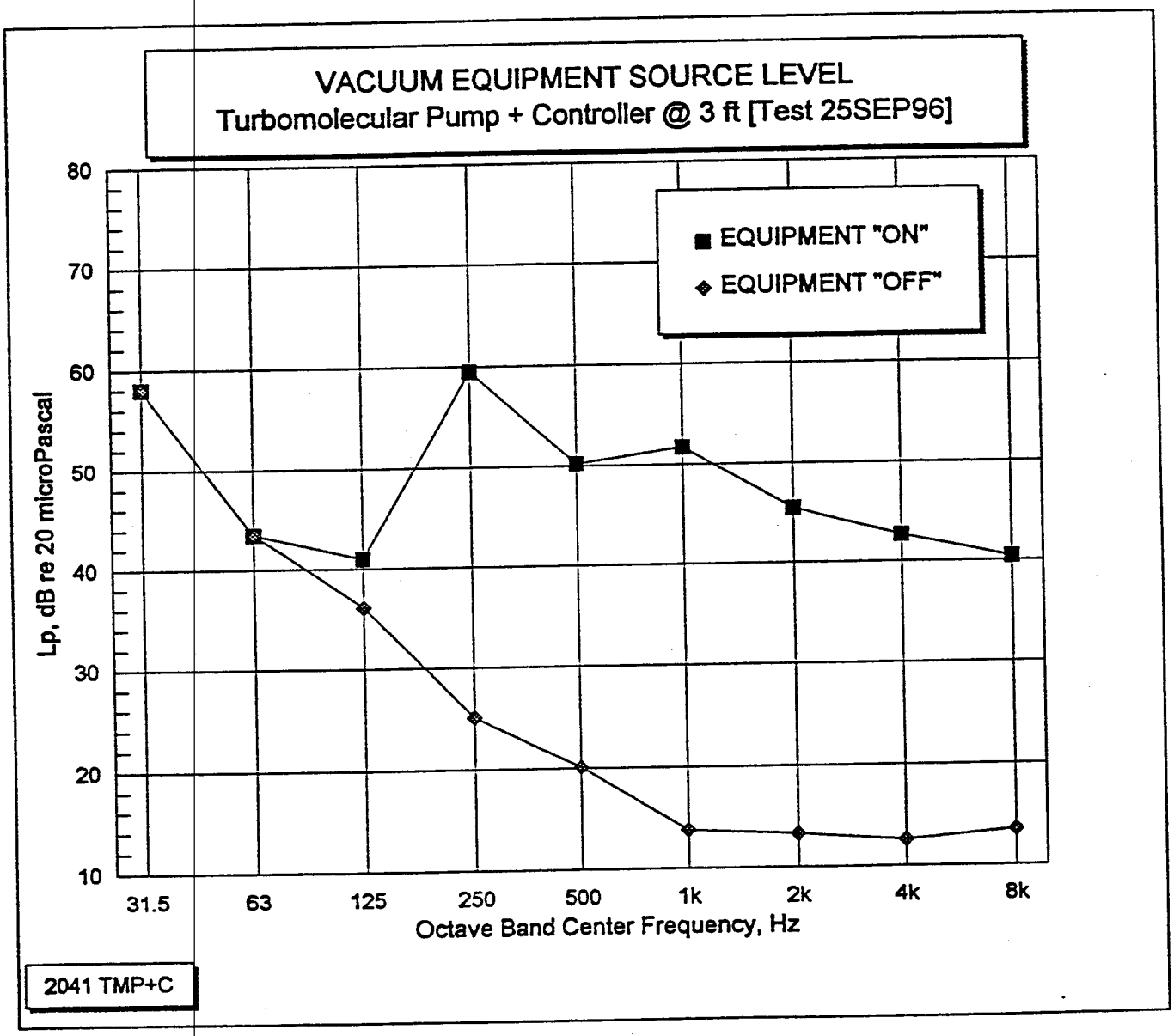
VACUUM EQUIPMENT SOURCE LEVEL
Turbomolecular Pump + Controller @ 3 ft [Test 25SEP96]
EQUIPMENT "ON"
EQUIPMENT "OFF"
Lp, dB re 20 microPascal
80
70
60
50
40
30
20
10
31.5
63
125
250
500
1k
2k
4k
8k
Octave Band Center Frequency, Hz
2041 TMP+C

Fig. 9

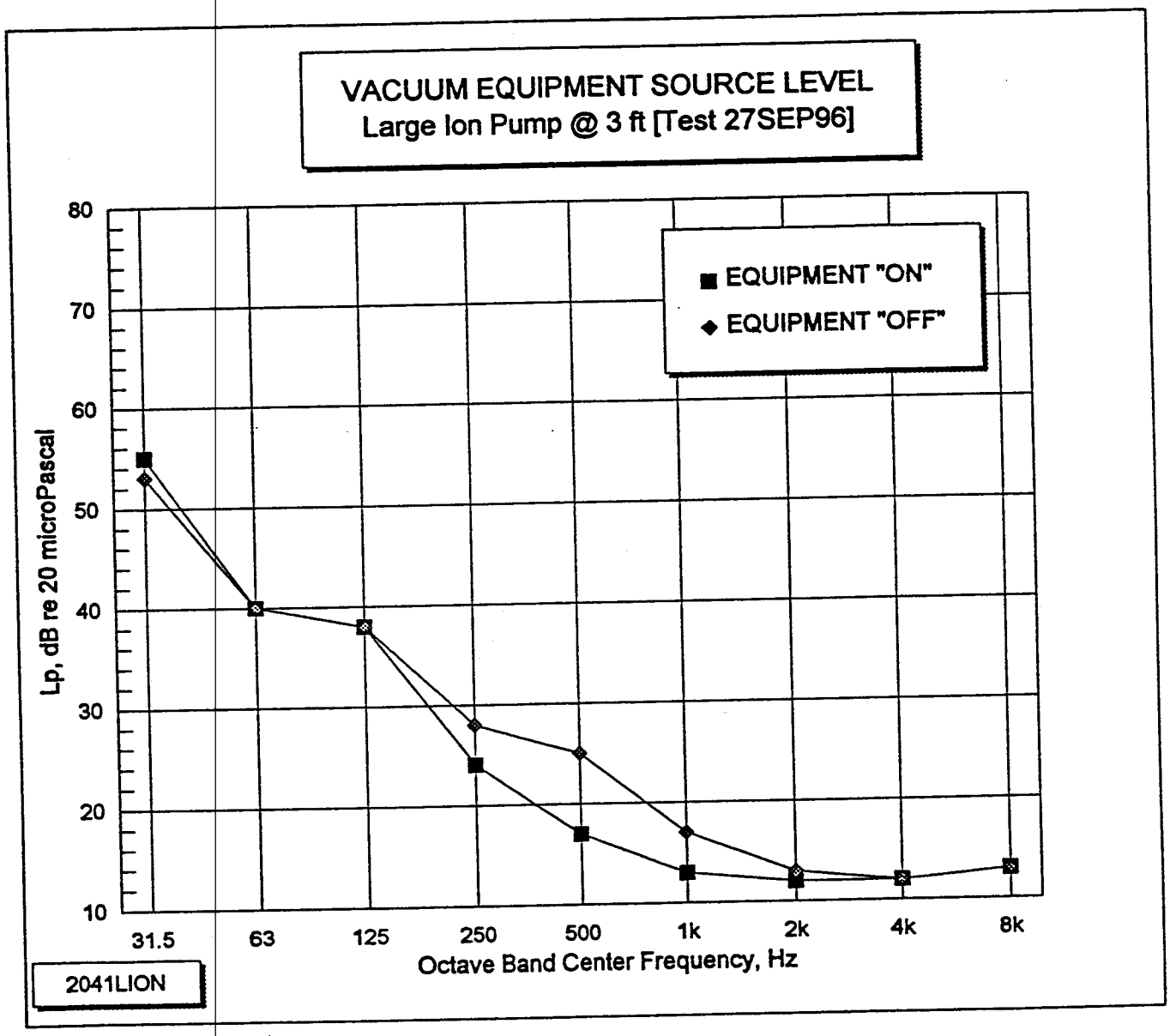
VACUUM EQUIPMENT SOURCE LEVEL
Large Ion Pump @ 3 ft [Test 27SEP96]
EQUIPMENT "ON"
EQUIPMENT "OFF"
Lp, dB re 20 microPascal
80
70
60
50
40
30
20
10
31.5
63
125
250
500
1k
2k
4k
8k
Octave Band Center Frequency, Hz
2041LION

Fig. 10a

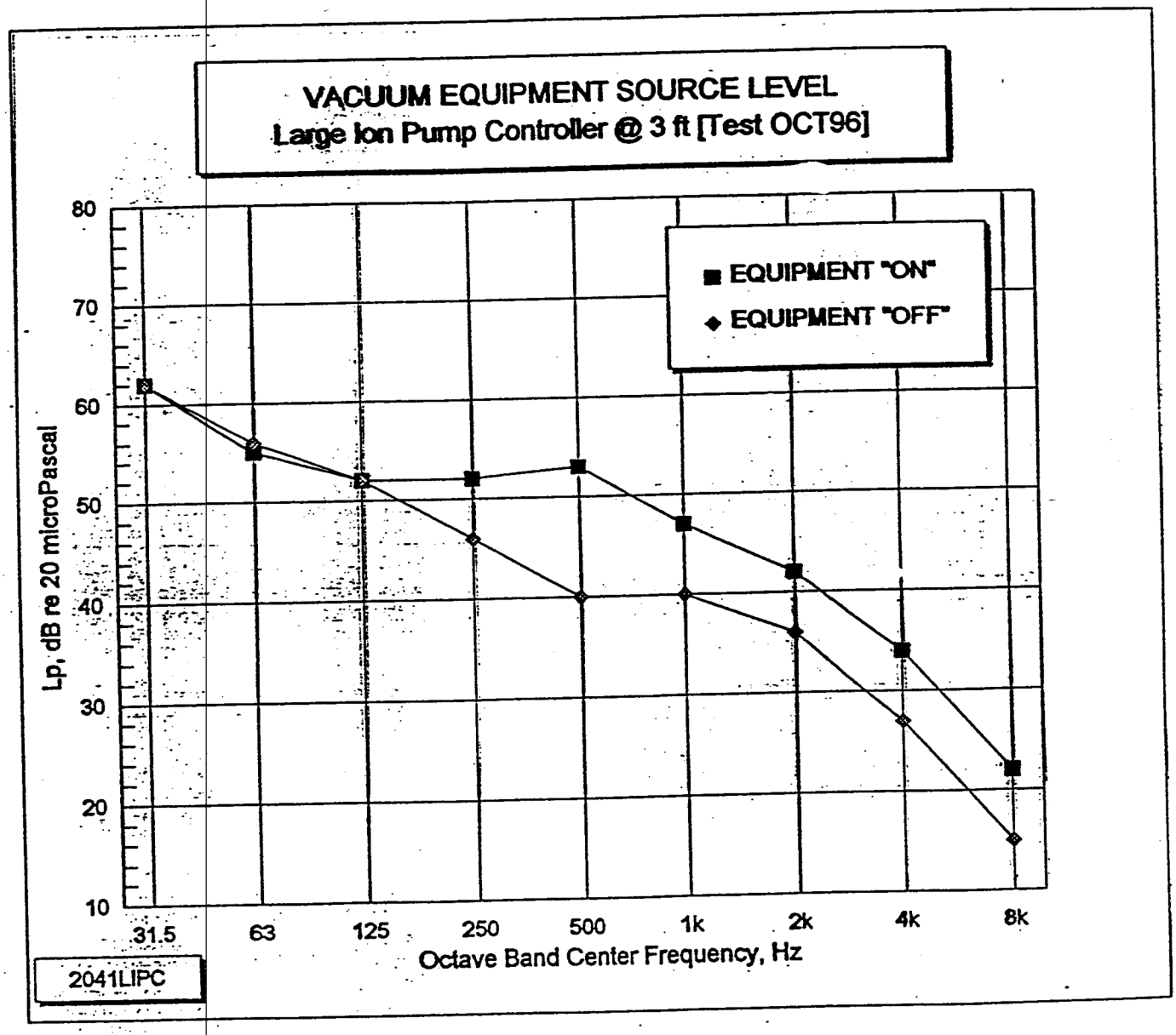
VACUUM EQUIPMENT SOURCE LEVEL
Large Ion Pump Controller @ 3 ft [Test OCT96]
EQUIPMENT "ON"
EQUIPMENT "OFF"
Lp, dB re 20 microPascal
80
70
60
50
40
30
20
10
31.5
63
125
250
500
1k
2k
4k
8k
Octave Band Center Frequency, Hz
2041LIPC

Fig. 10b

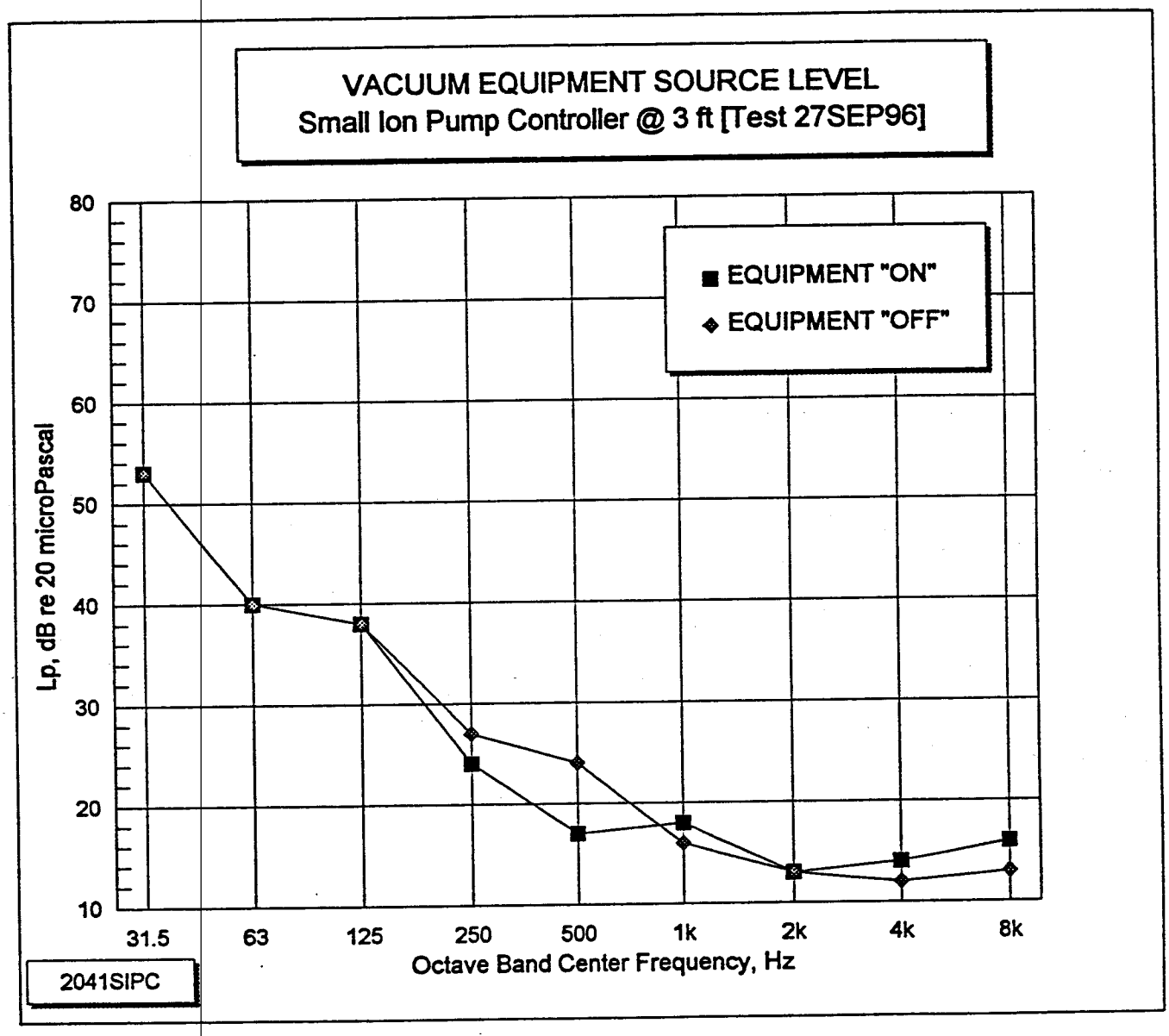
VACUUM EQUIPMENT SOURCE LEVEL
Small Ion Pump Controller @ 3 ft [Test 27SEP96]
EQUIPMENT "ON"
EQUIPMENT "OFF"
Lp, dB re 20 microPascal
80
70
60
50
40
30
20
10
31.5
63
125
250
500
1k
2k
4k
8k
Octave Band Center Frequency, Hz
2041SIPC

Fig. 11

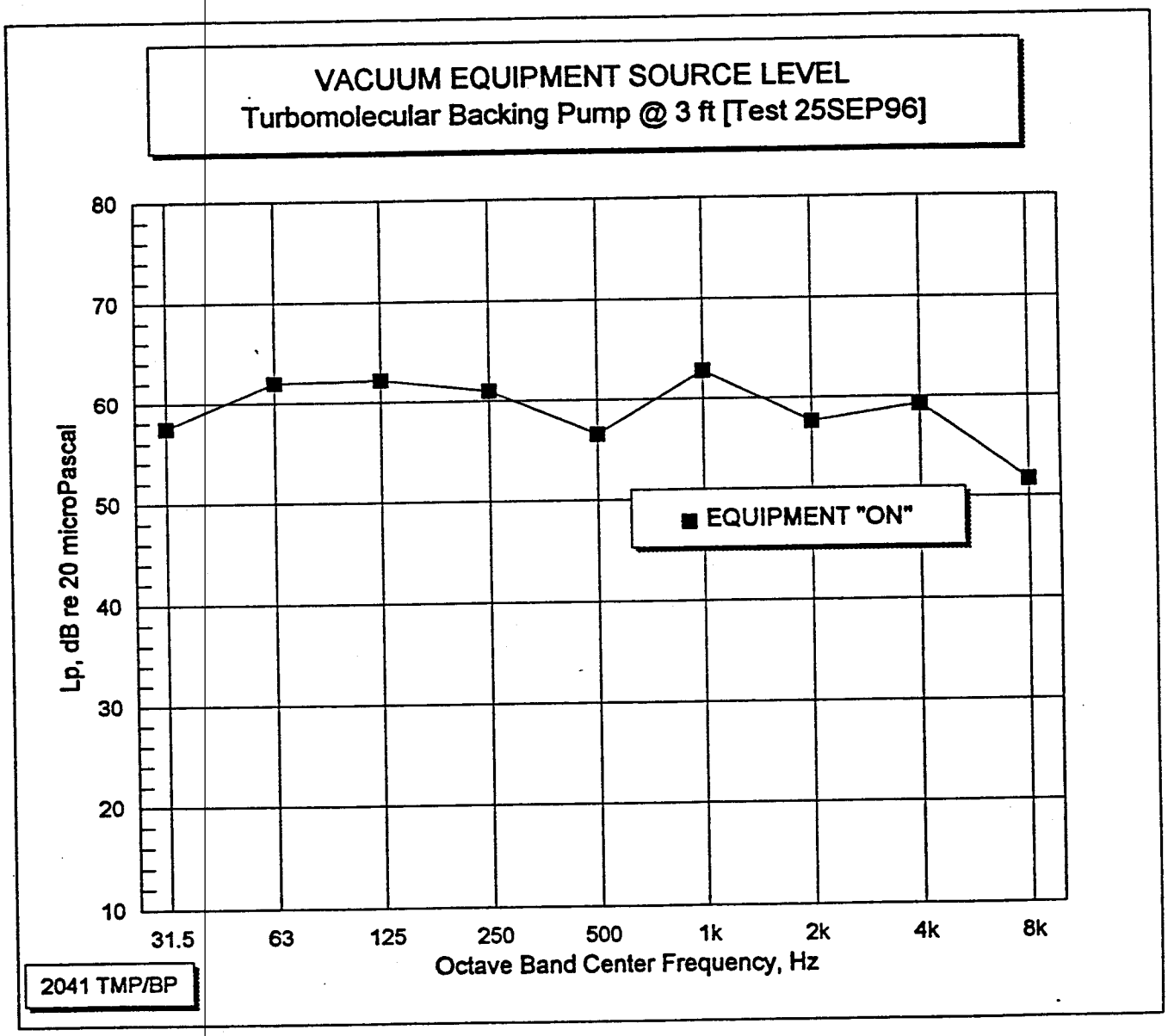
VACUUM EQUIPMENT SOURCE LEVEL
Turbomolecular Backing Pump @ 3 ft [Test 25SEP96]
80
70
60
50
40
30
20
10
Lp, dB re 20 microPascal
EQUIPMENT "ON"
31.5
63
125
250
500
1k
2k
4k
8k
Octave Band Center Frequency, Hz
2041 TMP/BP

Fig. 12

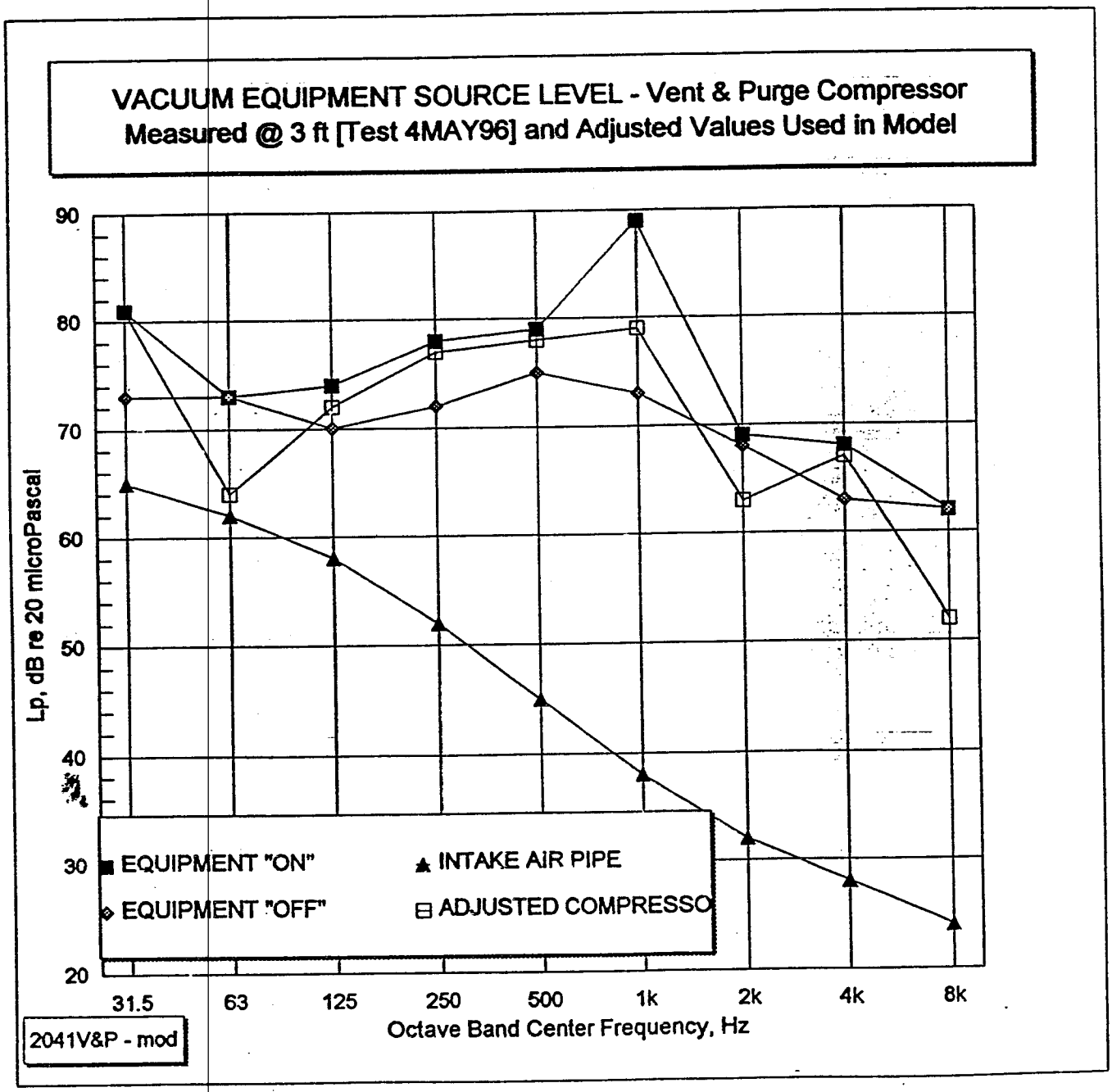
VACUUM EQUIPMENT SOURCE LEVEL - Vent & Purge Compressor
Measured @ 3 ft [Test 4MAY96] and Adjusted Values Used in Model
Lp, dB re 20 microPascal
90
80
70
60
50
40
30
20
31.5
63
125
250
500
1k
2k
4k
8k
Octave Band Center Frequency, Hz
EQUIPMENT "ON"
INTAKE AIR PIPE
EQUIPMENT "OFF"
ADJUSTED COMPRESSO
2041V&P - mod

Fig. 13

GNB P-G44P VALVE SHOCK TEST; 25 November 1996
CLOSING ("lockover"); AXIAL ACCELERATION

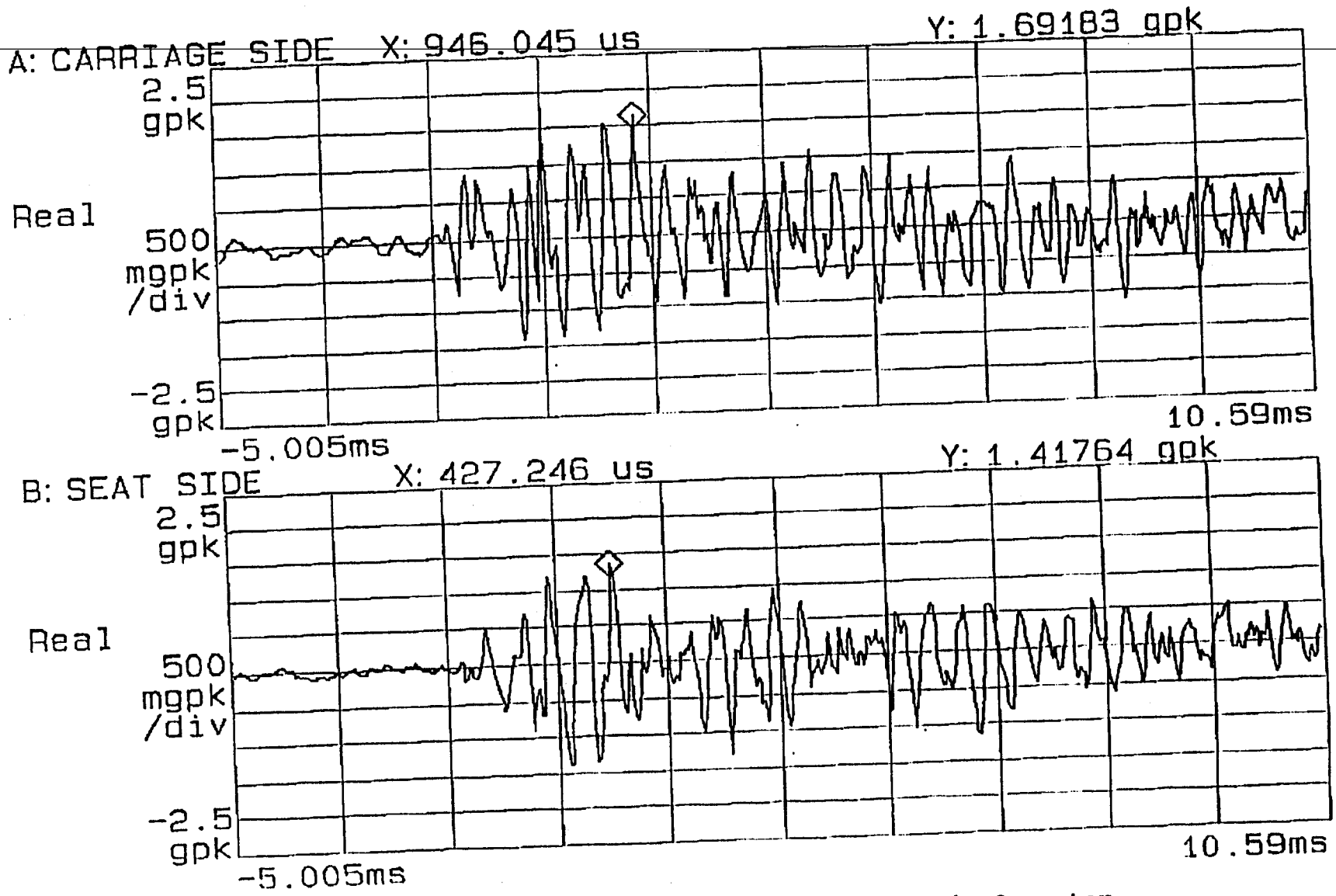

Fig. 14 - -44 Inch Gate Valve with Pneumatic Operator

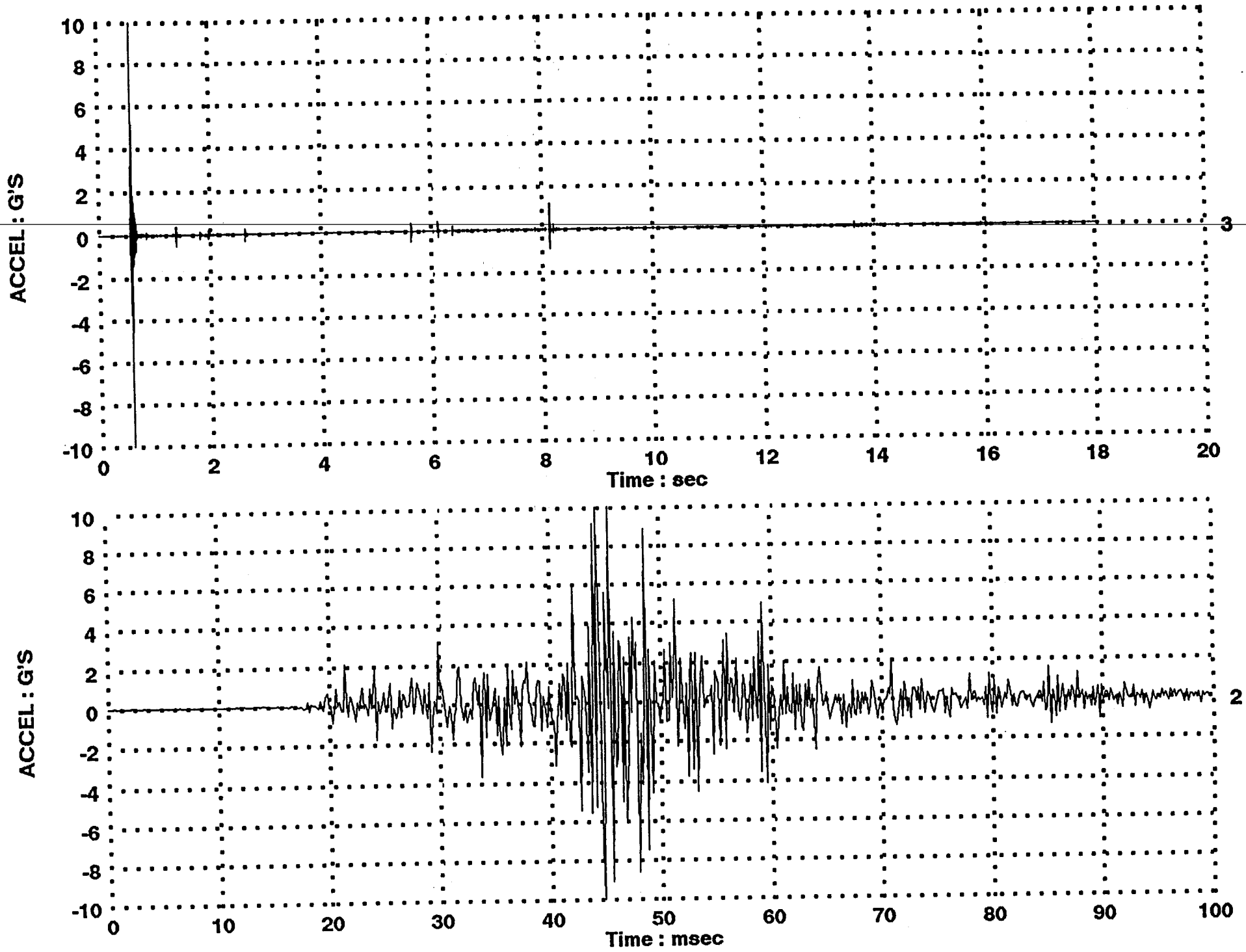

Fig. 15a – 10" HAND VALVE OPENING (BOTTOM GRAPH SHOWS PEAK EXPANDED)

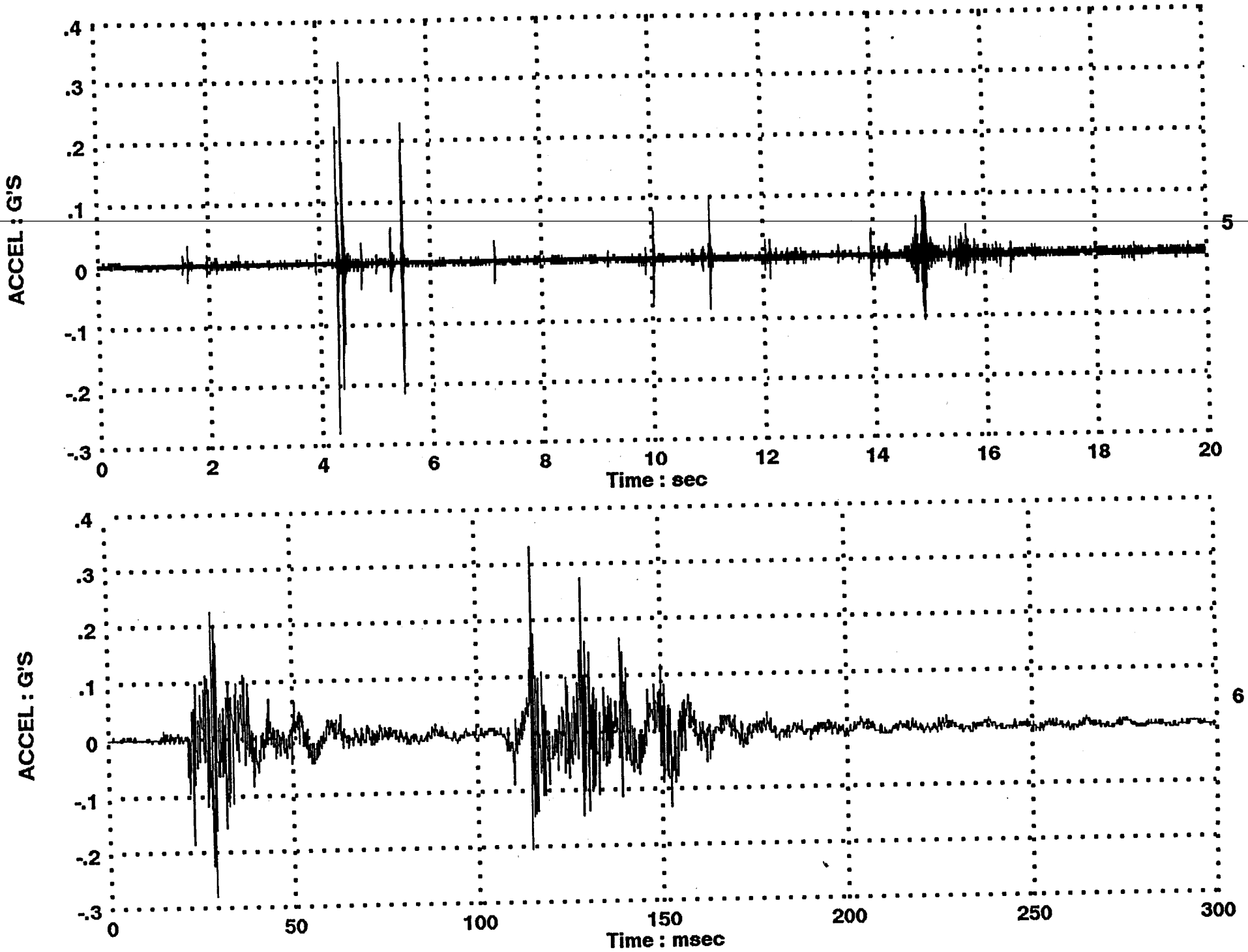

Fib. 15b - 14" HAND VALVE OPENING (BOTTOM ZOOM AT 4 SEC.)

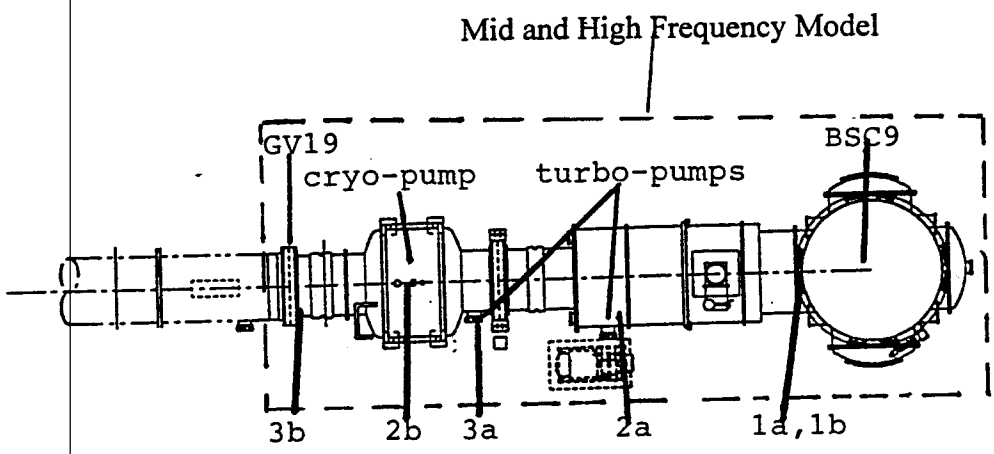

Fig. 16a

Sketch of Right End Station indicating the sources considered, receiver points and portions of station modeled in middle and high frequency analyses.

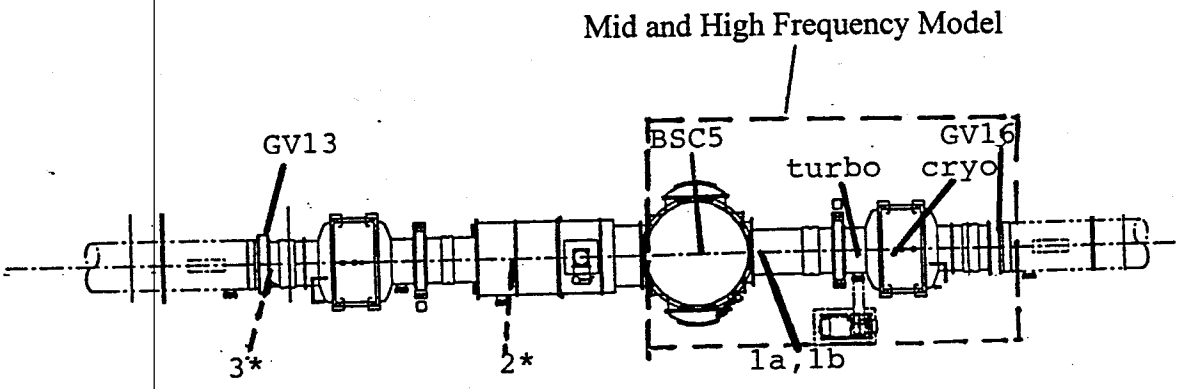

Fig. 16b

Sketch of Right Mid Station indicating the sources considered, receiver points and portions of station modeled in middle and high frequency analyses. Note receiver points 2 and 3 are similar to End Station points 2a and 3b for sources on left side of BSC5.

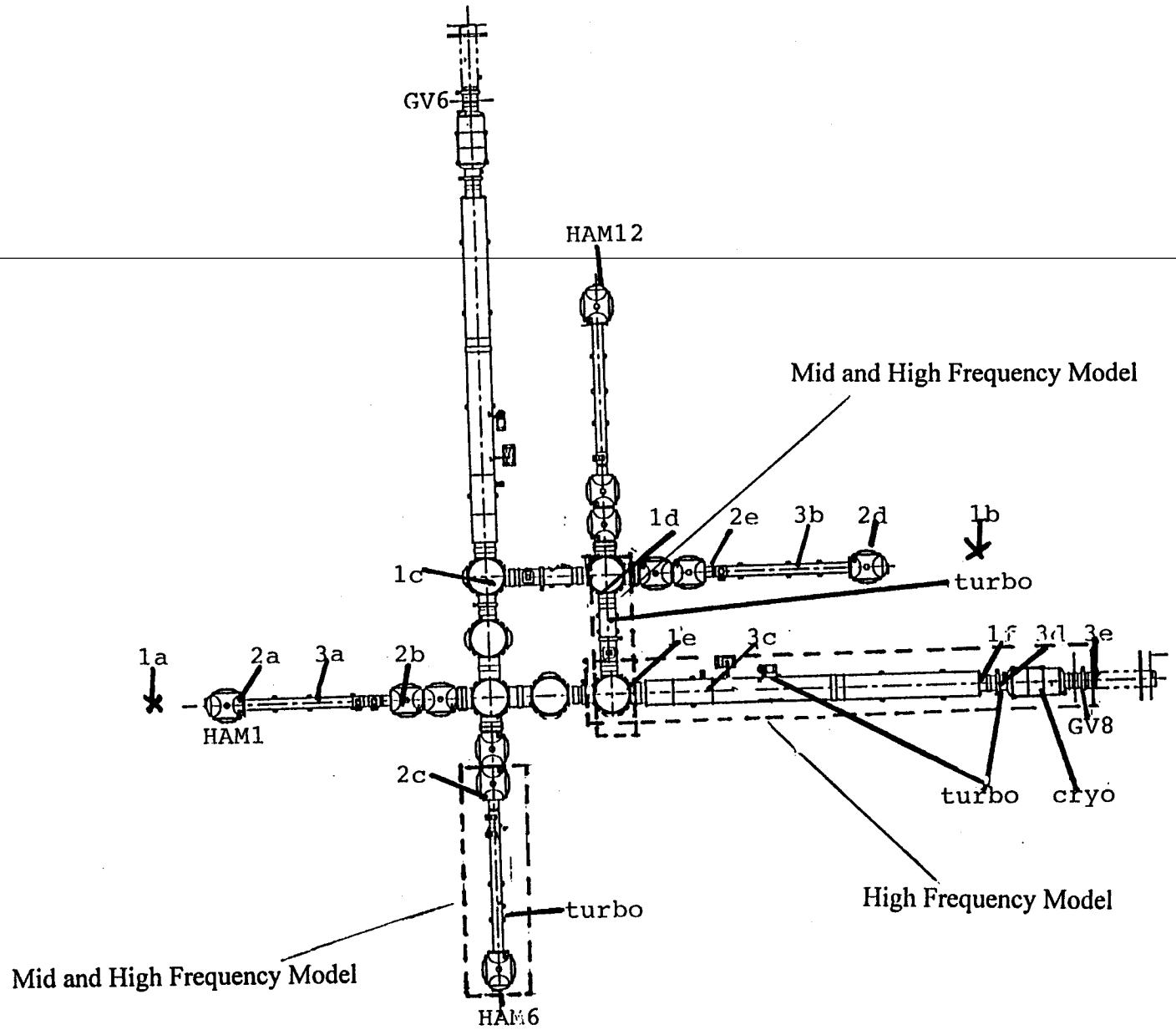

Fig. 16c – Sketch of Corner Station indicating the sources considered, receiver points and the portions of the station modeled in middle and high frequency analyses.

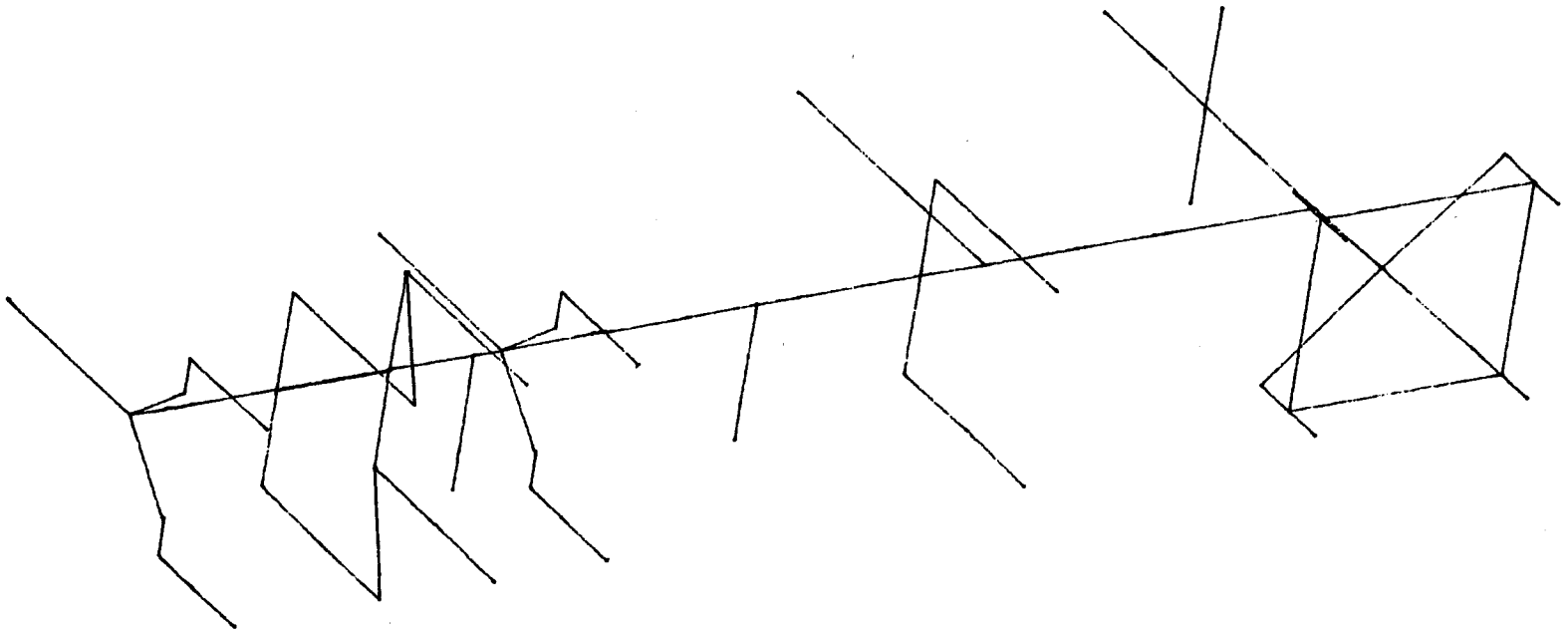

Fig. 17a - Plot of Low Frequency End Station Model

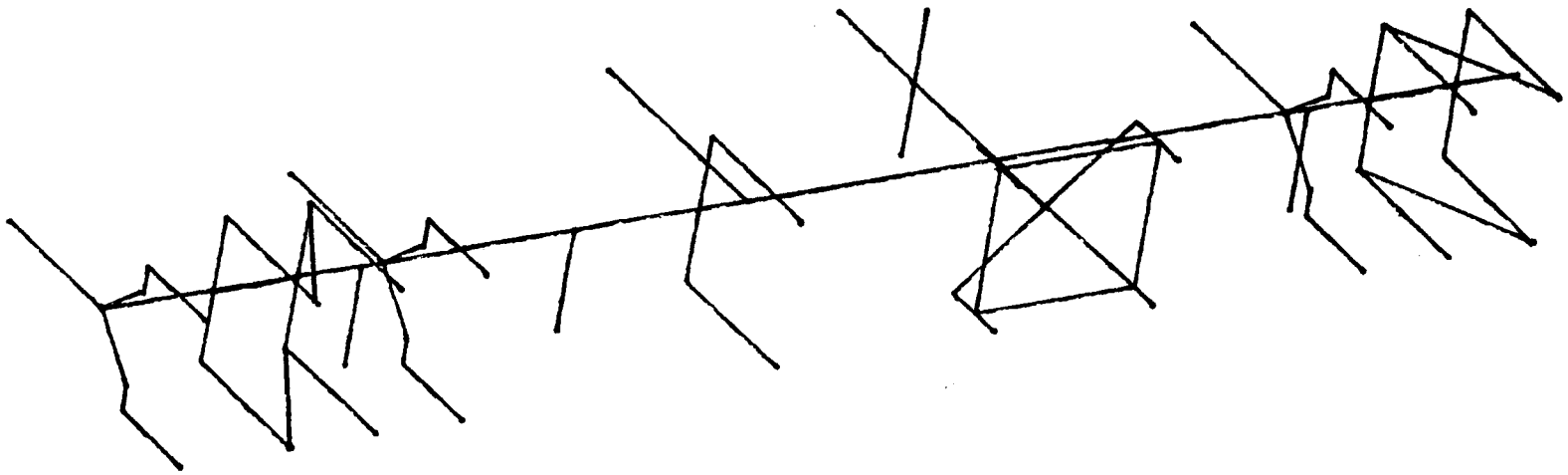

Fig. 17b - Plot of Low Frequency Mid Station Model

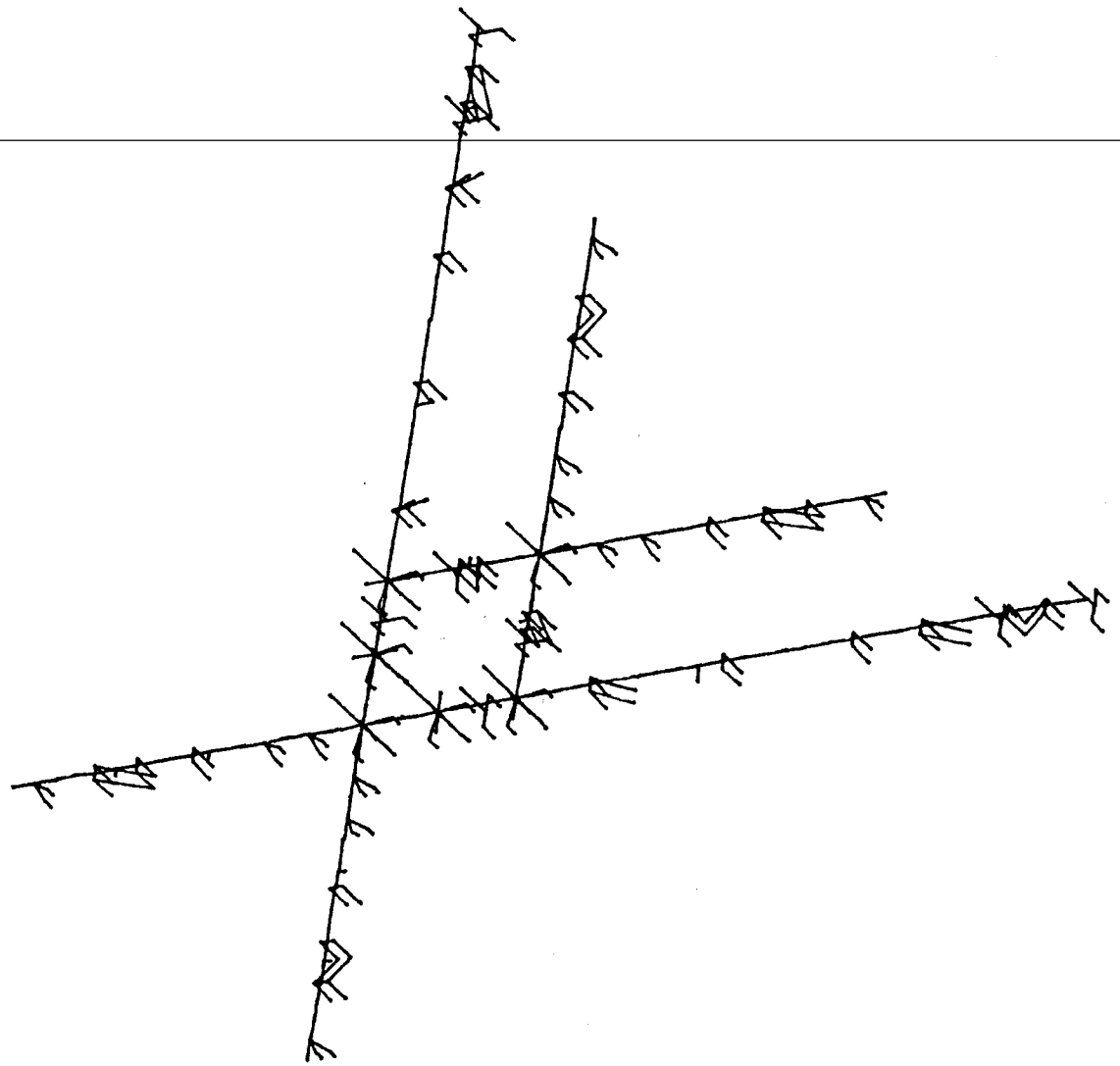

Fig. 17c - Plot of Low Frequency Corner Station Model

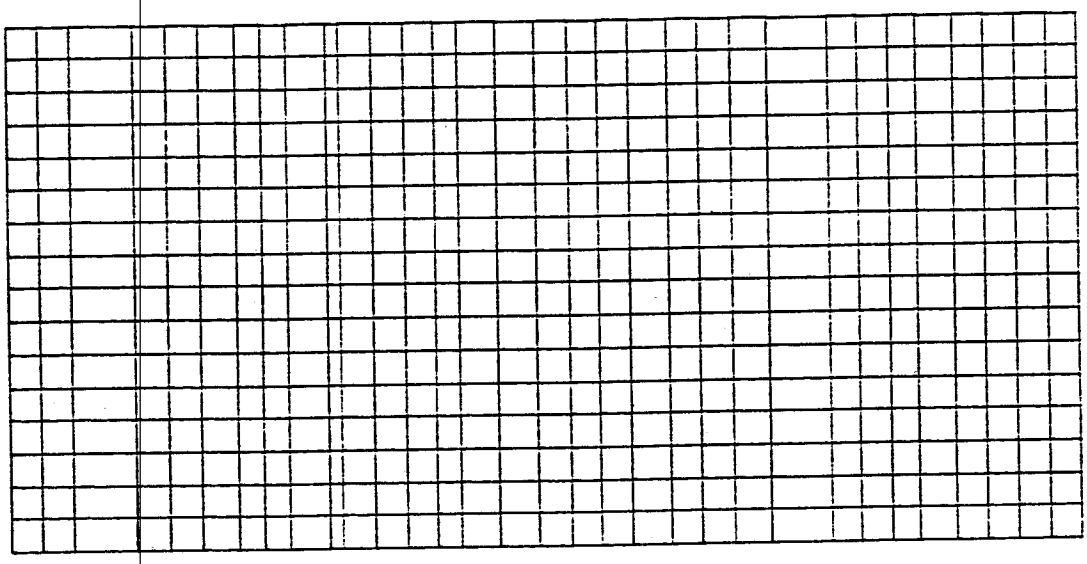

Fig. 17d - Plot of Foundation Model in End and Mid Station

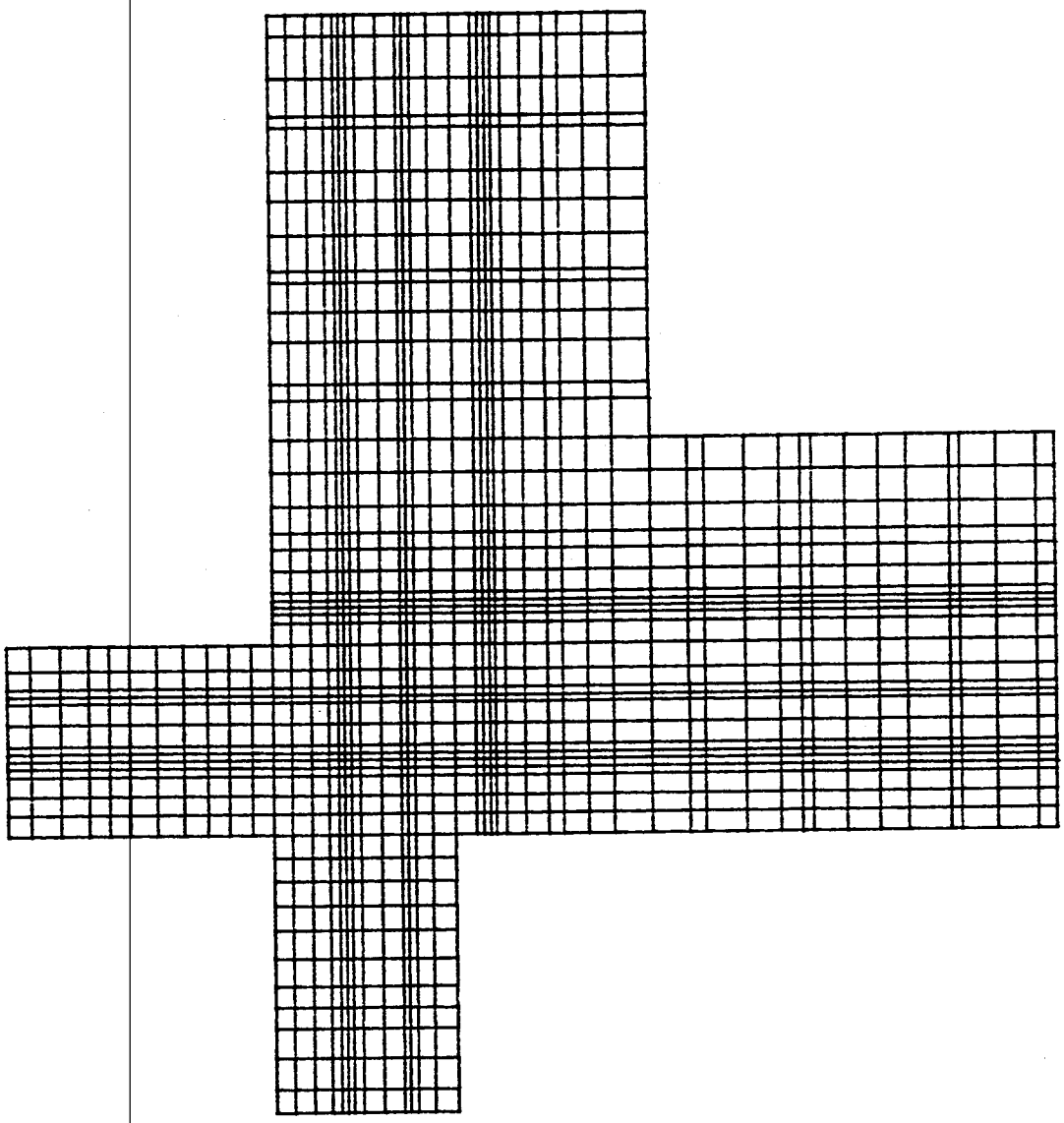

Fig. 17e - Plot of Foundation Model in Corner Station

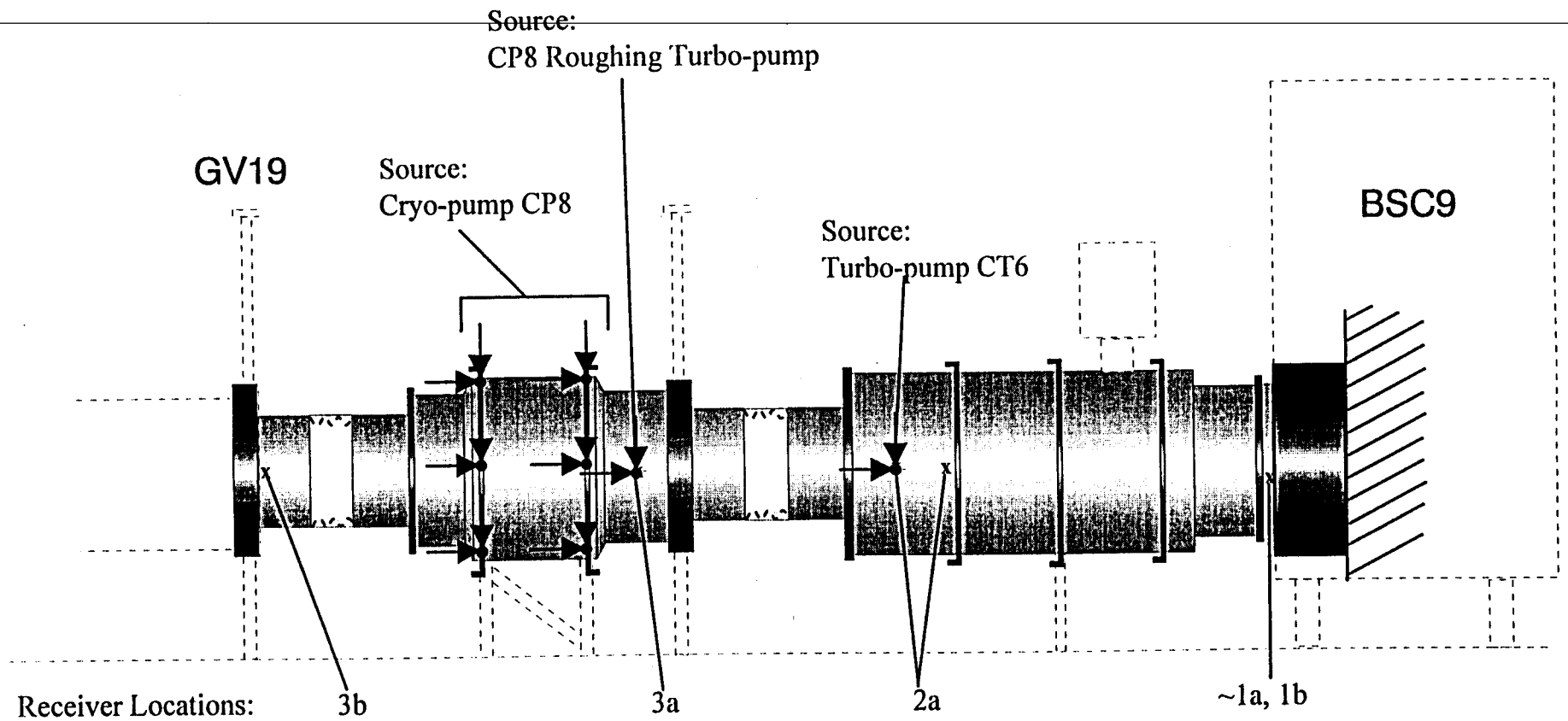

Fig. 18a - Schematic of Mid Frequency End Station Model

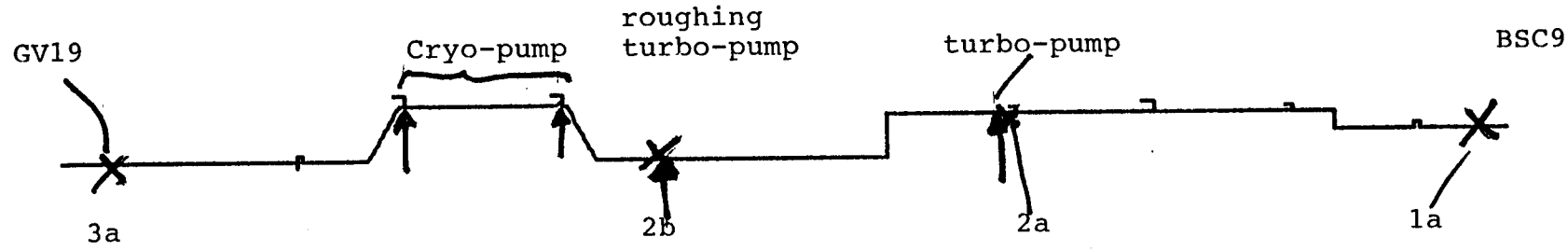

Fig. 18b - Plot of Mid Frequency End Station Model

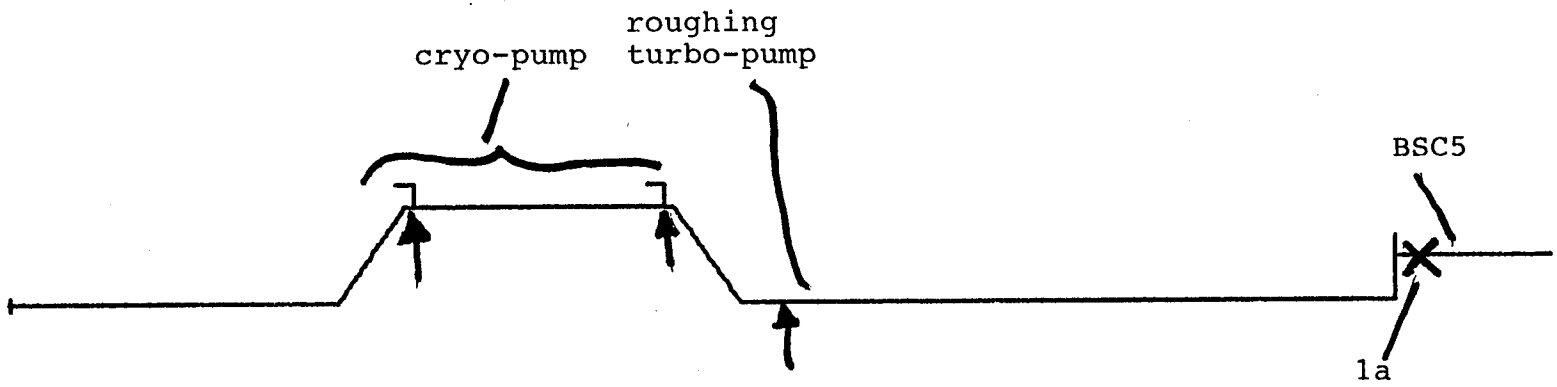

Fig. 18c - Plot of Mid Frequency Mid Station Model

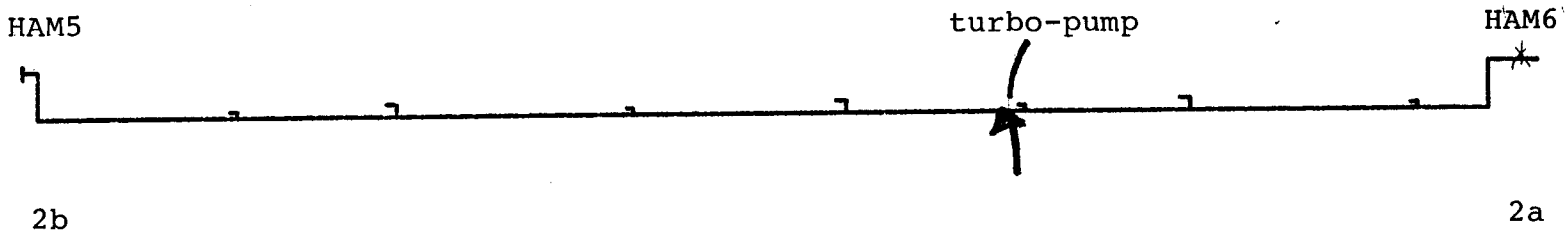

Fig. 18d - Plot of Mid Frequency Corner Station Model - Mode Cleaner Area

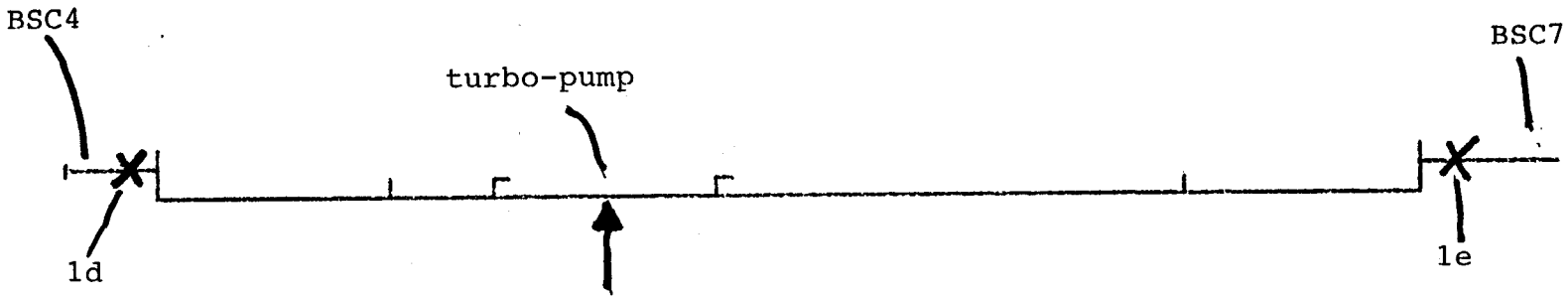

Fig. 18e - Plot at Mid Frequency Corner Station Model - Diagonal Area

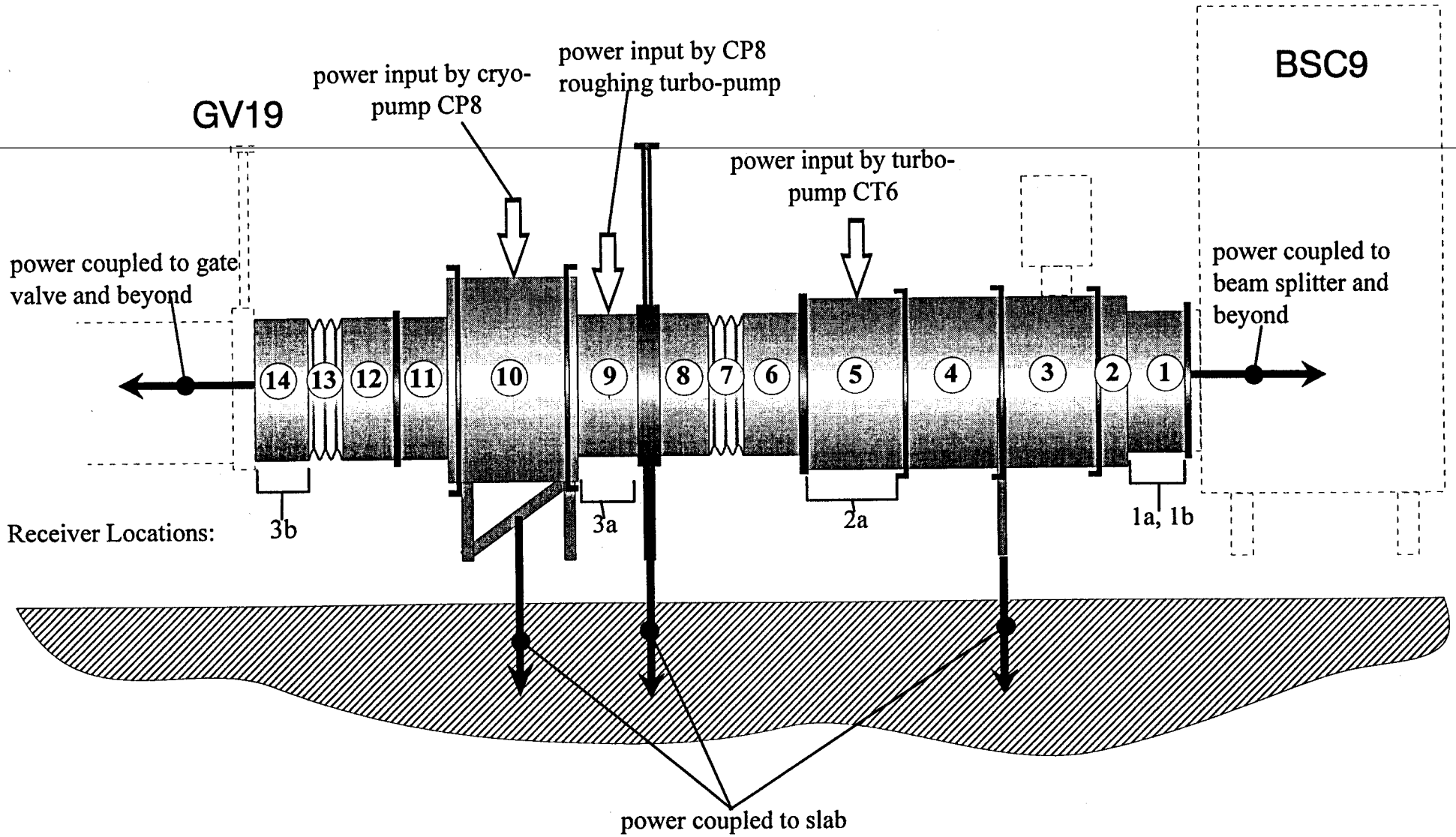

Fig. 19 - Schematic of High Frequency End Station Model

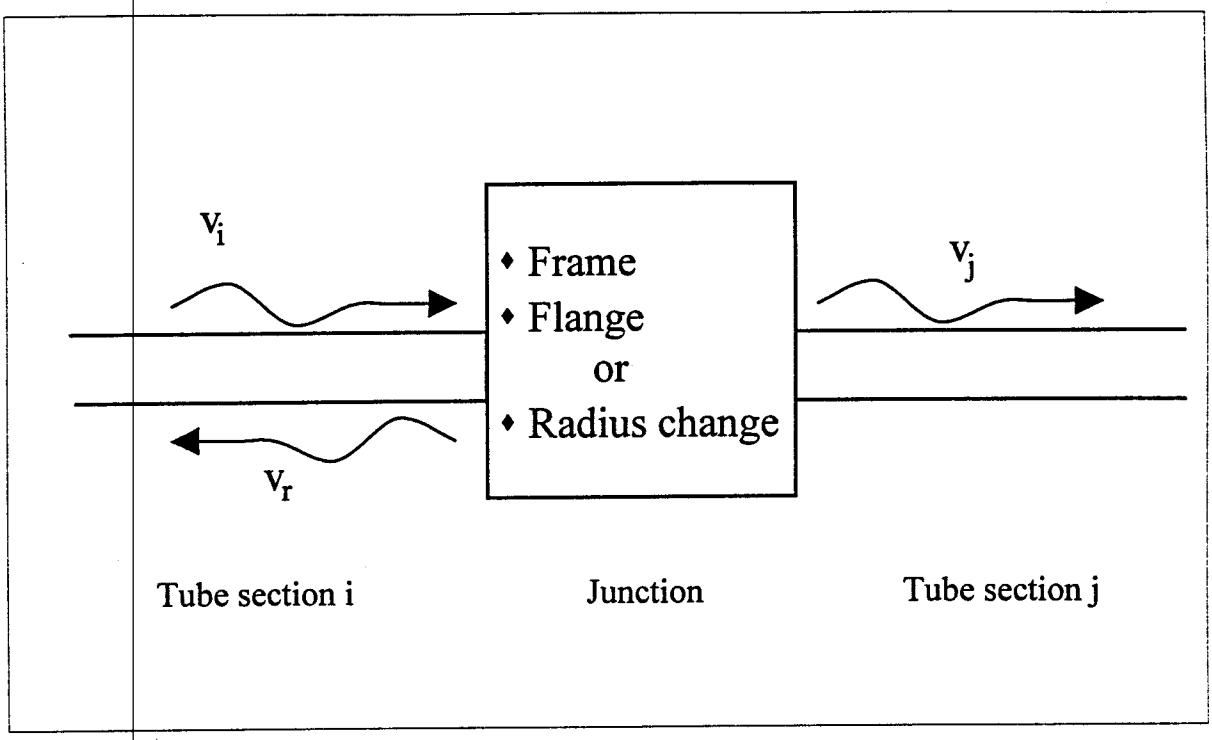

Fig. 20a – High Frequency Coupling of Flexural Waves Across Tube Junctions.

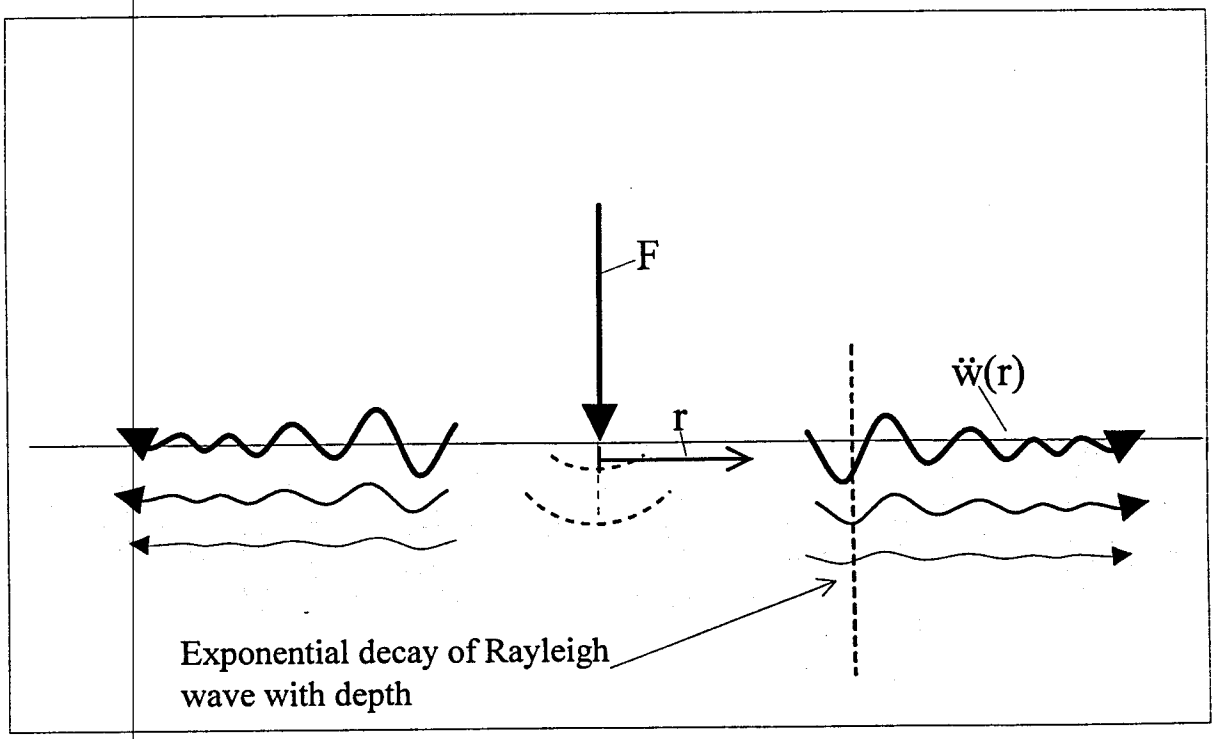

Fig. 20b – High Frequency Representation of Concrete Slab as Elastic Half Space.

Fig. 21 - Source-Path Interaction

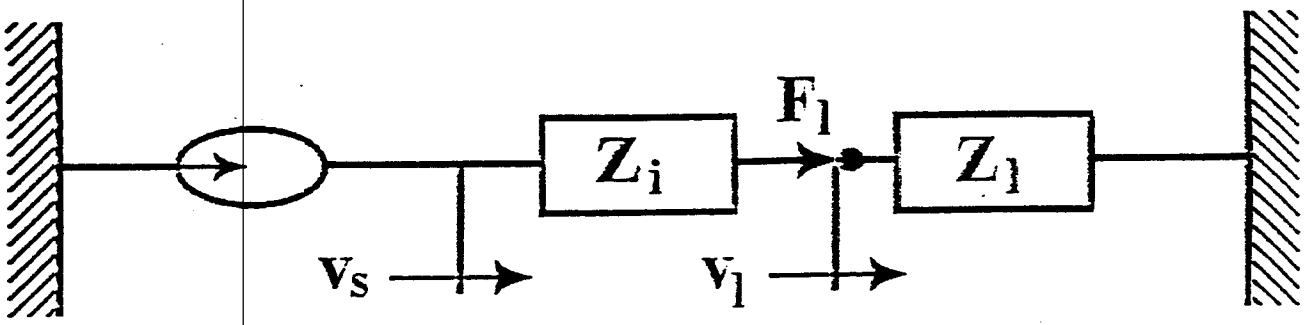

NORTON EQUIVALENT SOURCE

$$v_l = \frac{F_l}{Z_l} = \frac{v_s Z_i}{Z_i + Z_l}$$

v_s = FREE VELOCITY MEASURED AT SOURCE CONNECTION

Z_i = MEASURED INTERNAL IMPEDANCE OF SOURCE

Z_l = CALCULATED IMPEDANCE OF LOAD OR PATH INCLUDING 1ST ORDER REMEDIATION

v_l, F_l = VELOCITY AND FORCE AT INTERFACE

Fig. 22a - Force/Acceleration through Cryopump Support

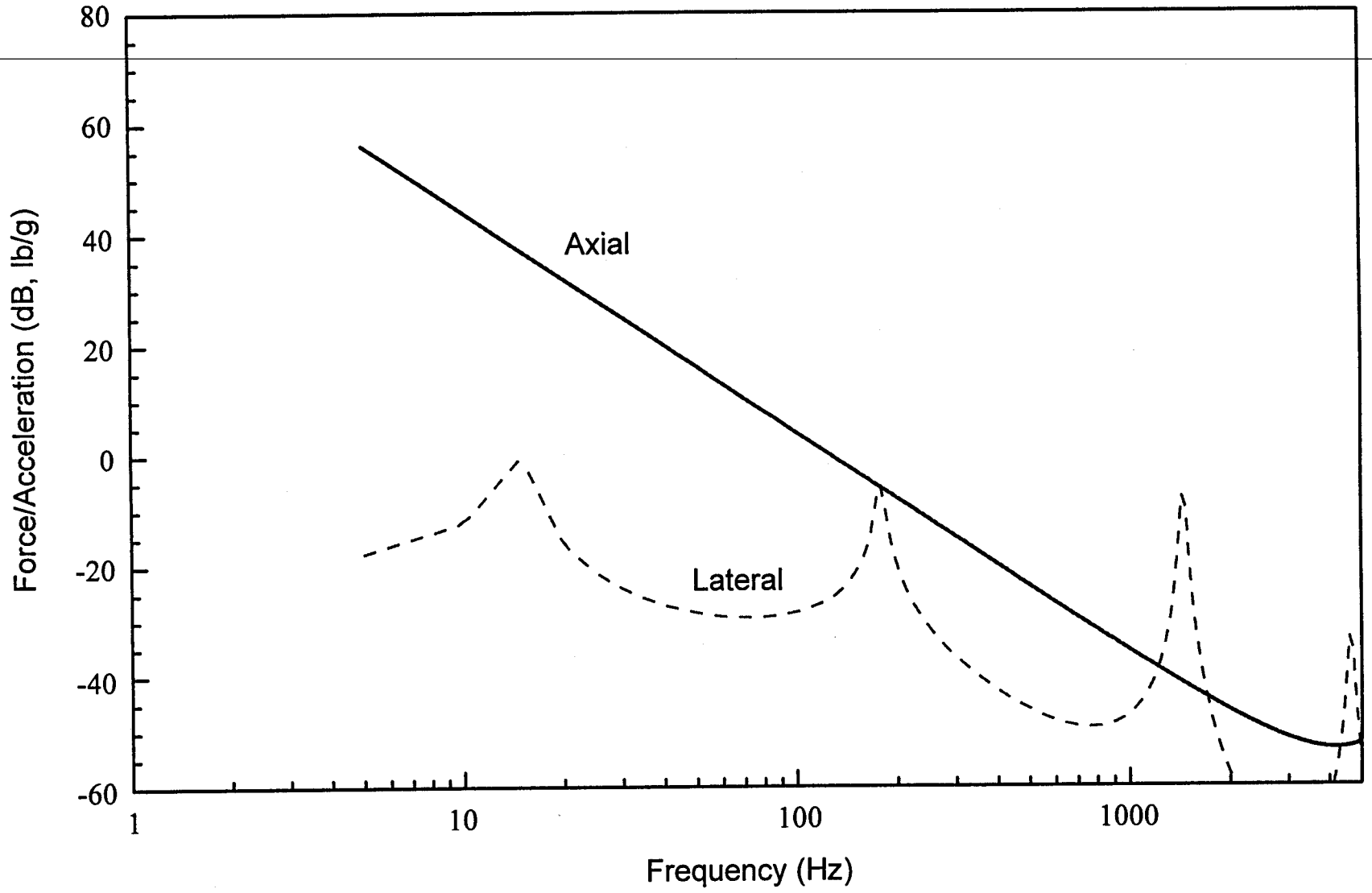

Fig. 22b - Force/Acceleration through Turbomolecular Pump Bellows.

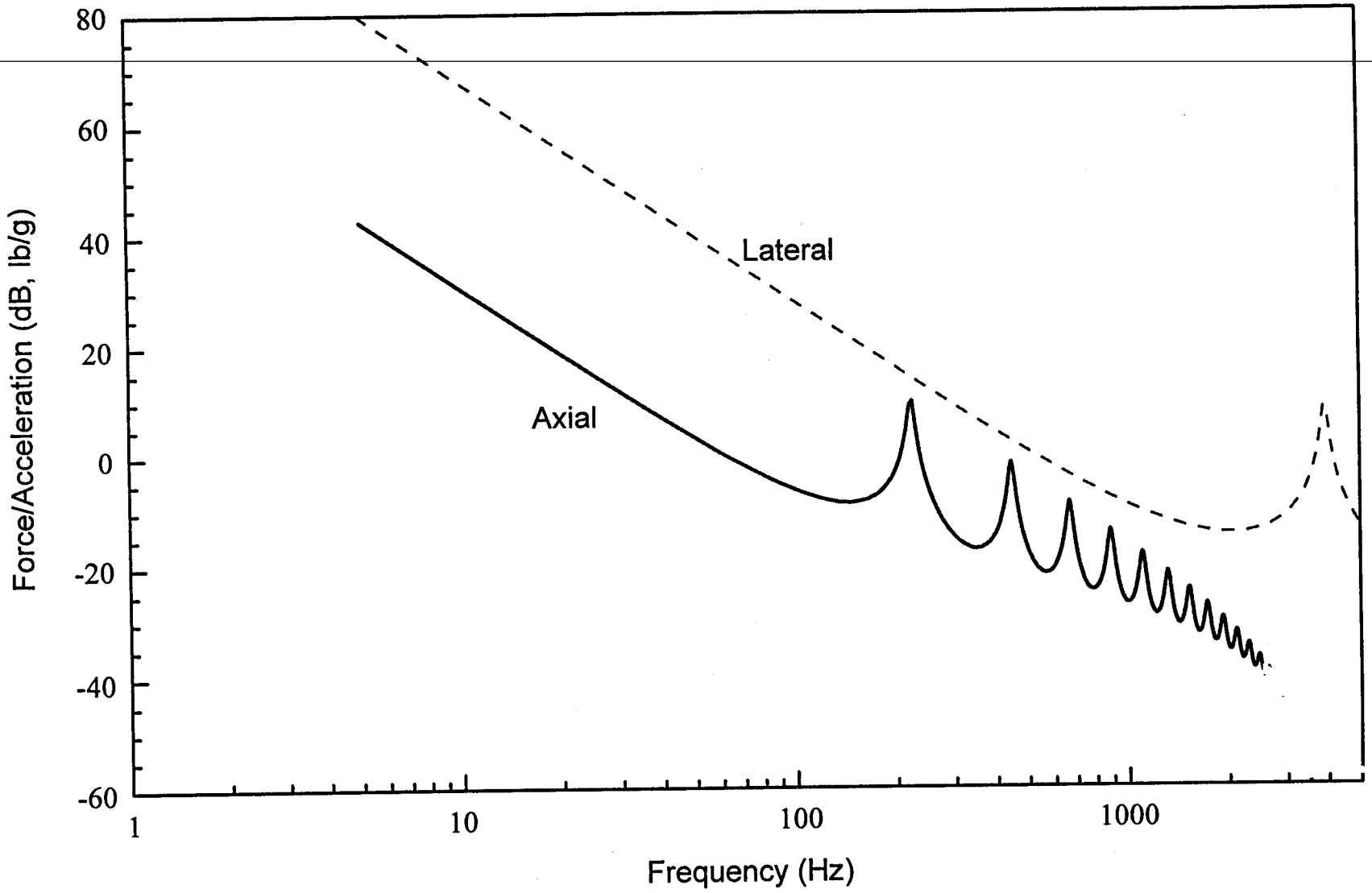

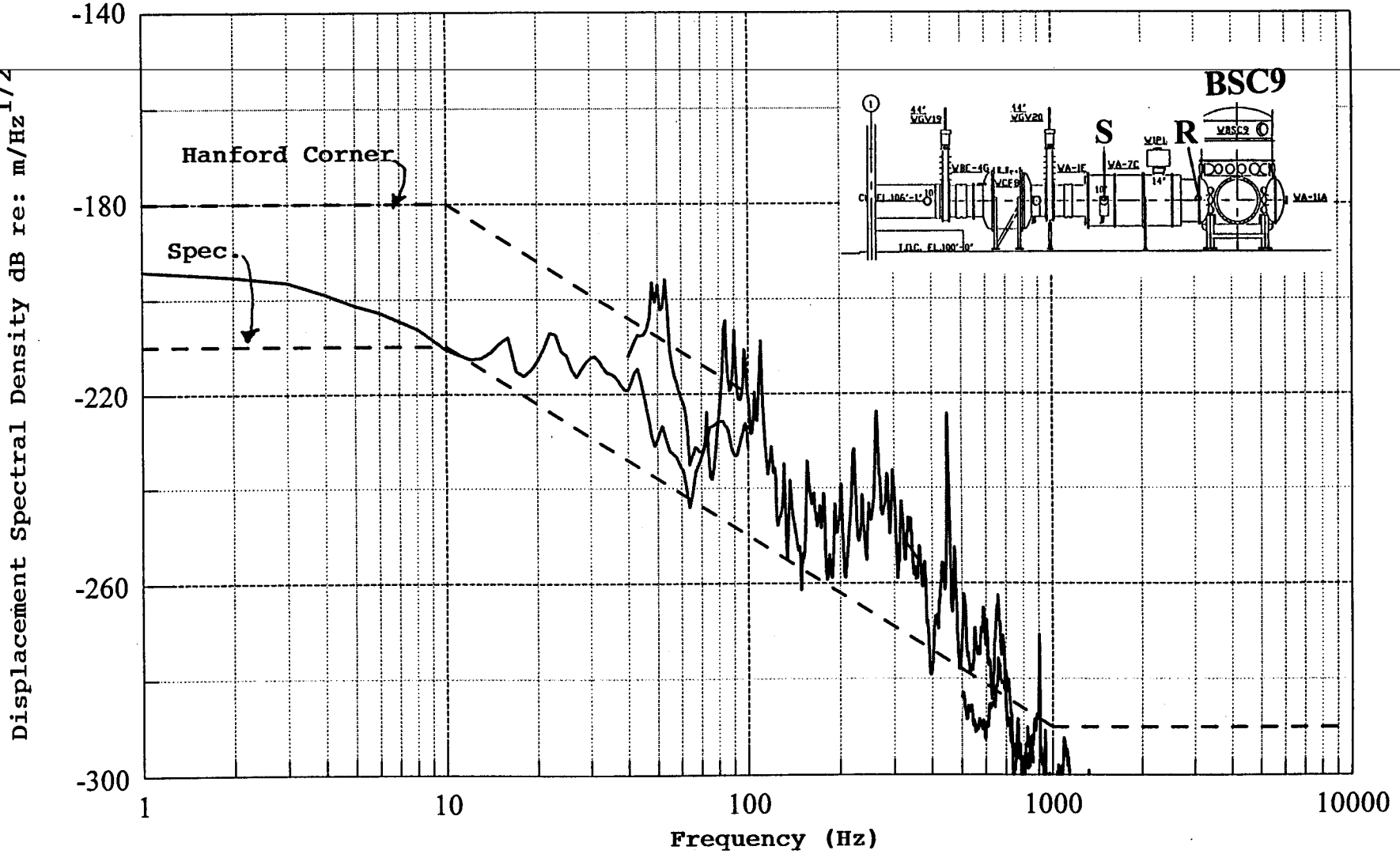

Fig. 23a – Predicted displacement spectra near Right End Station receiver location 1a, on tube near beam splitter BSC9 caused by operation of turbo-pump TC6.

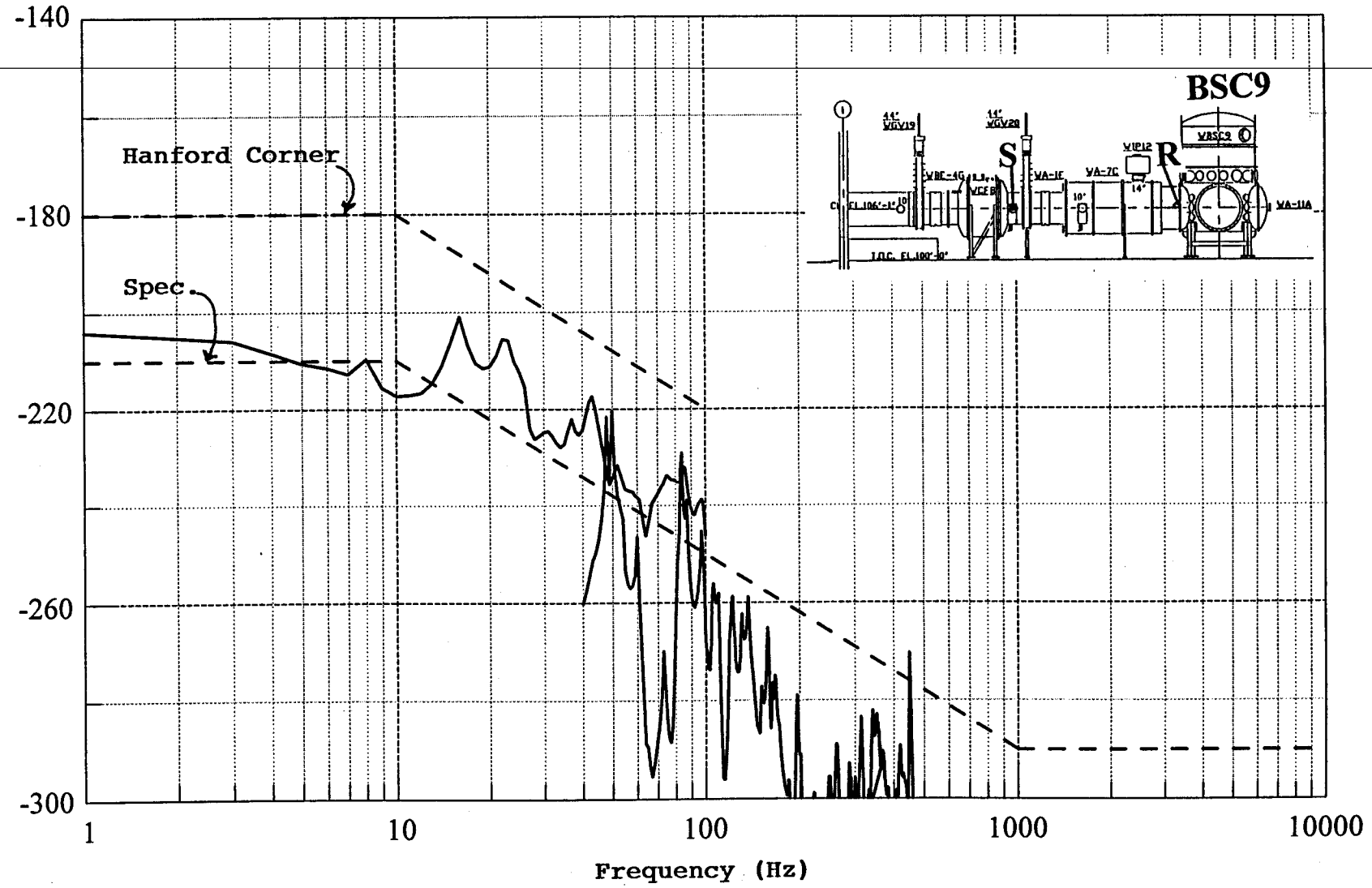

Fig. 23b – Predicted displacement spectra near Right End Station receiver location 1a, on tube near beam splitter BSC9 caused by operation of the roughing turbo-pump for CP8.

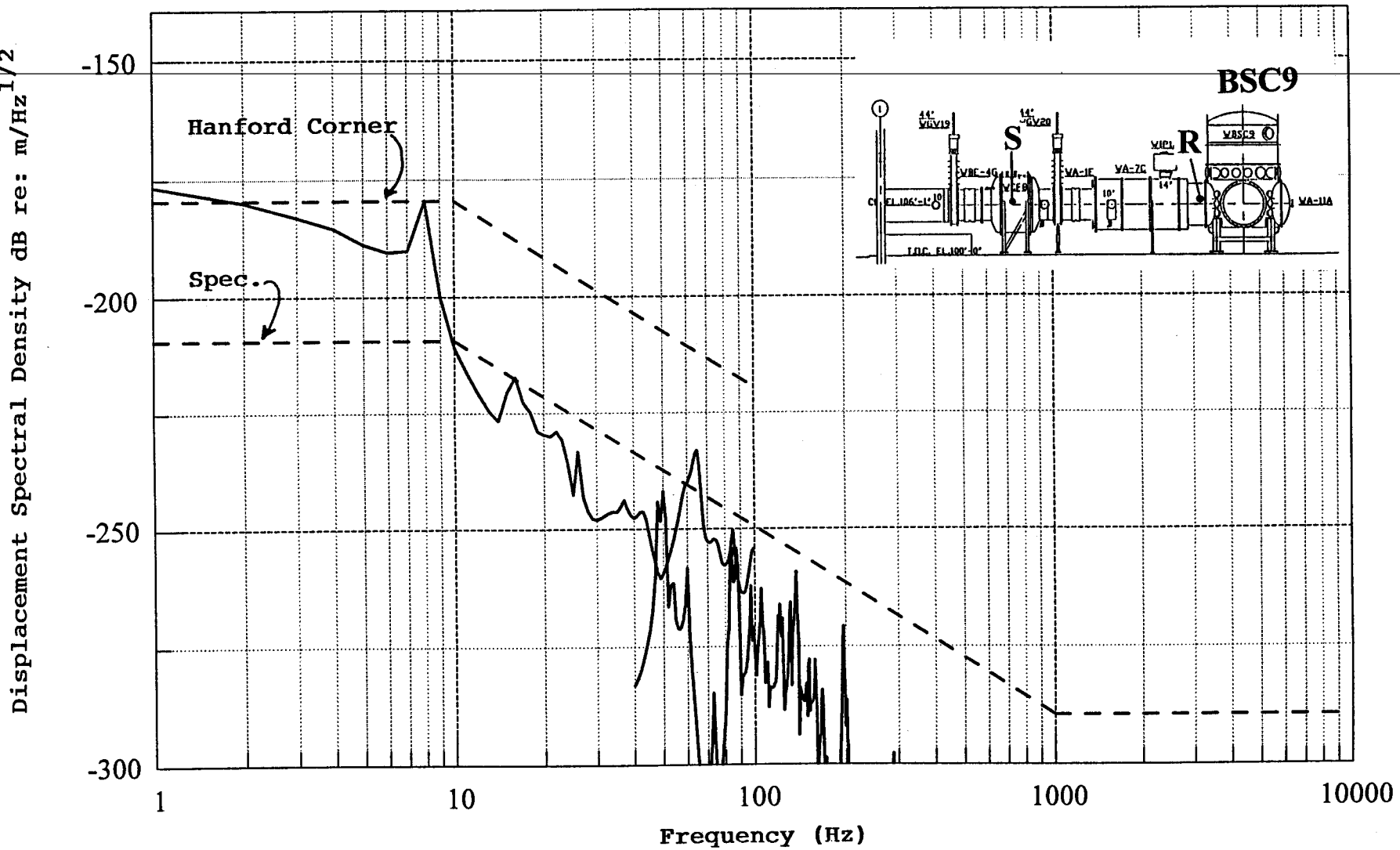

Fig. 23c – Predicted displacement spectra near Right End Station receiver location 1a, on tube near beam splitter BSC9 caused by operation of cryo-pump CP8.

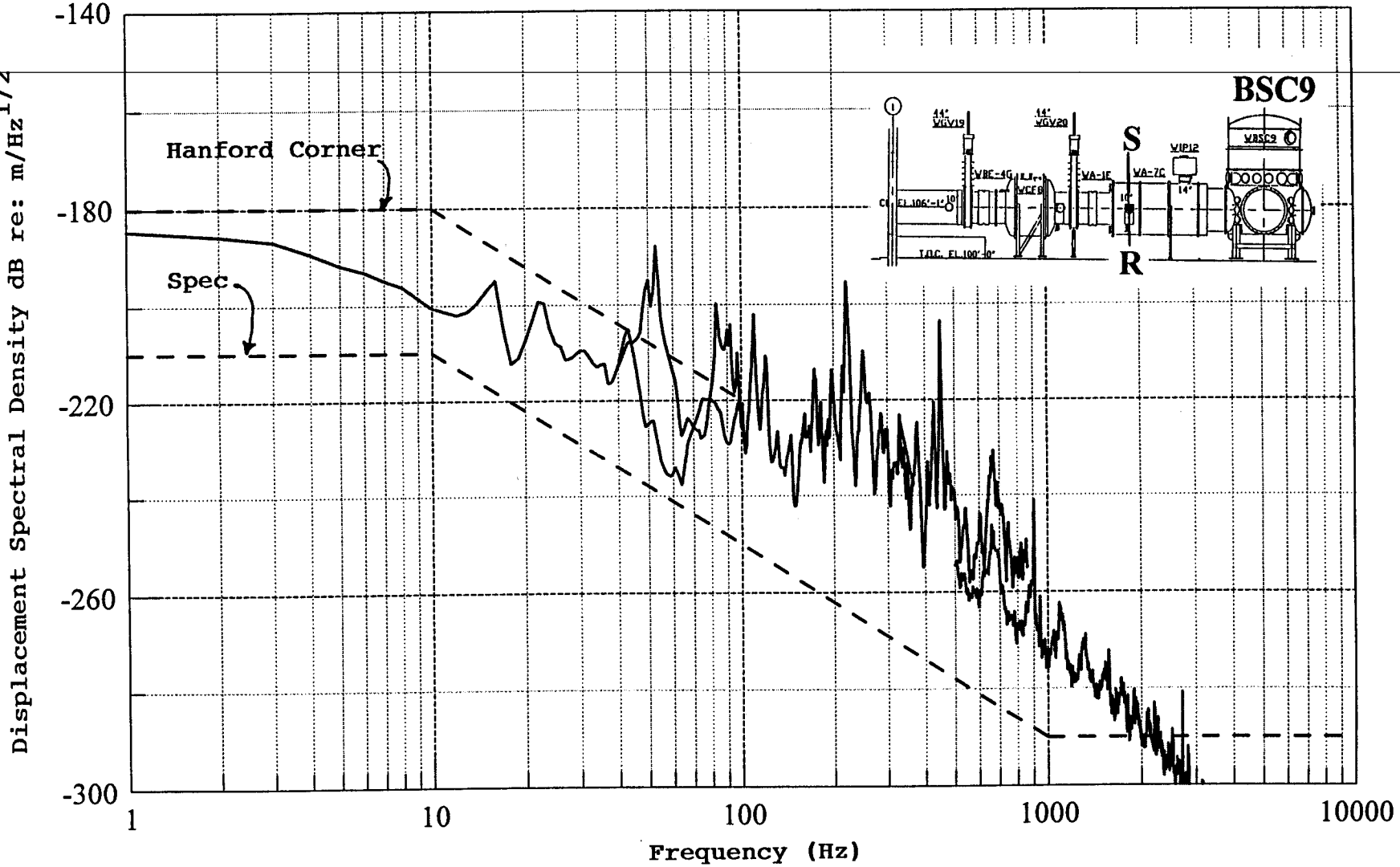

Fig. 23d – Predicted displacement spectra near Right End Station receiver location 2a, at TC6 on A-7C caused by operation of turbo- pump TC6.

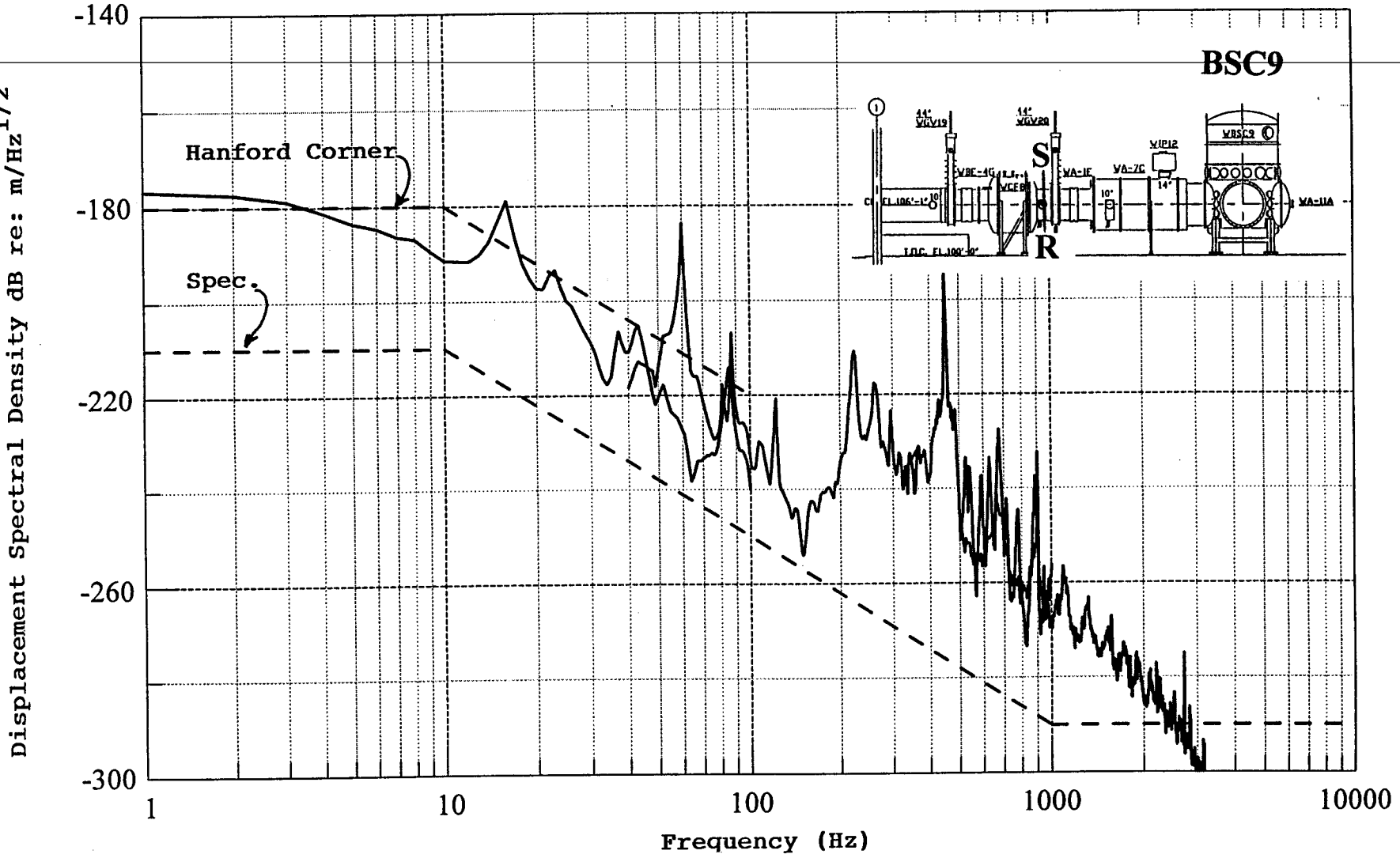

Fig. 23e – Predicted displacement spectra near Right End Station receiver location 3a, at the roughing turbo-pump on CP8 caused by operation of the roughing turbo-pump on CP8.

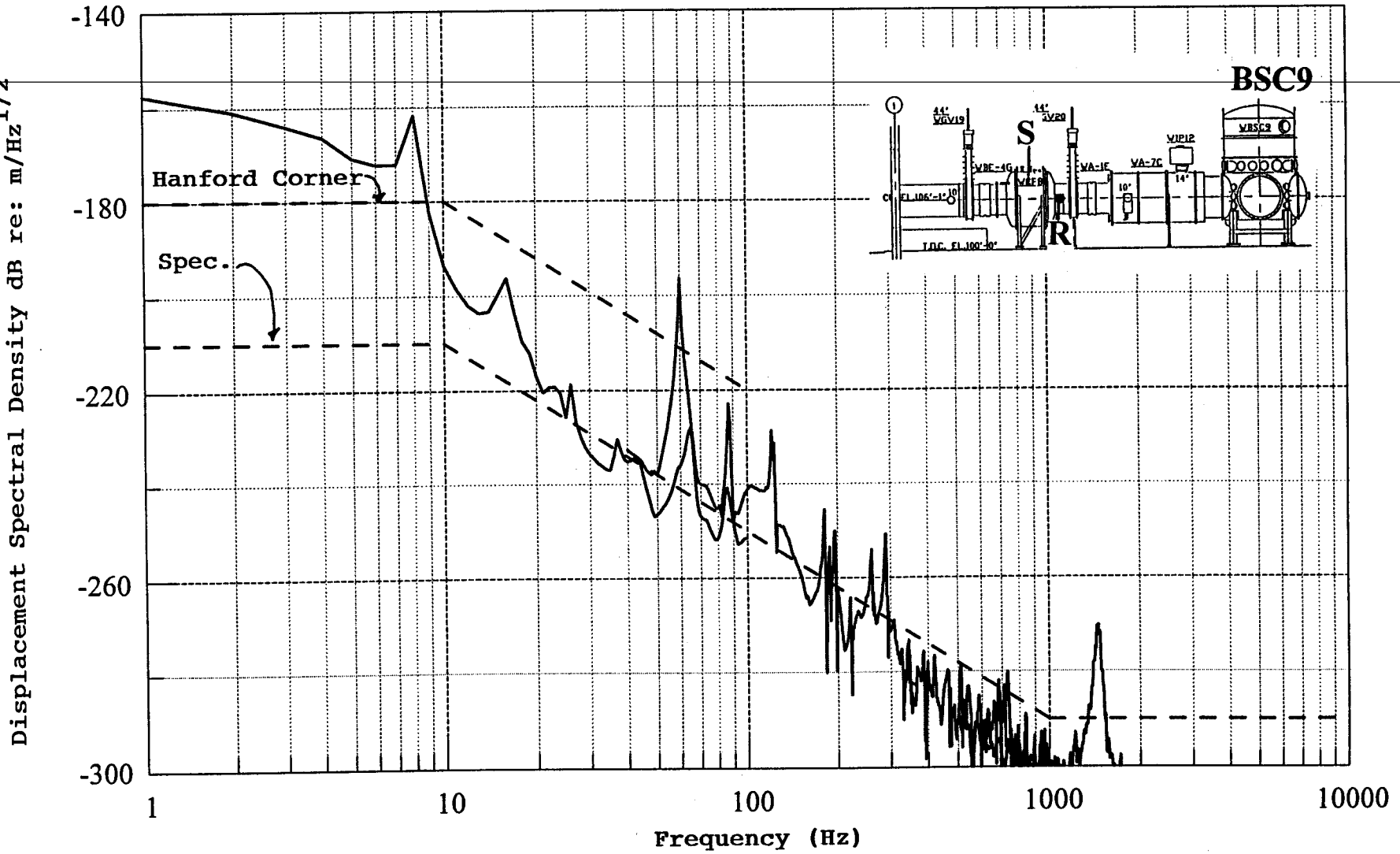

Fig. 23f – Predicted displacement spectra near Right End Station receiver location 3a, at the roughing turbo-pump on CP8 caused by operation of the cryo-pump CP8.

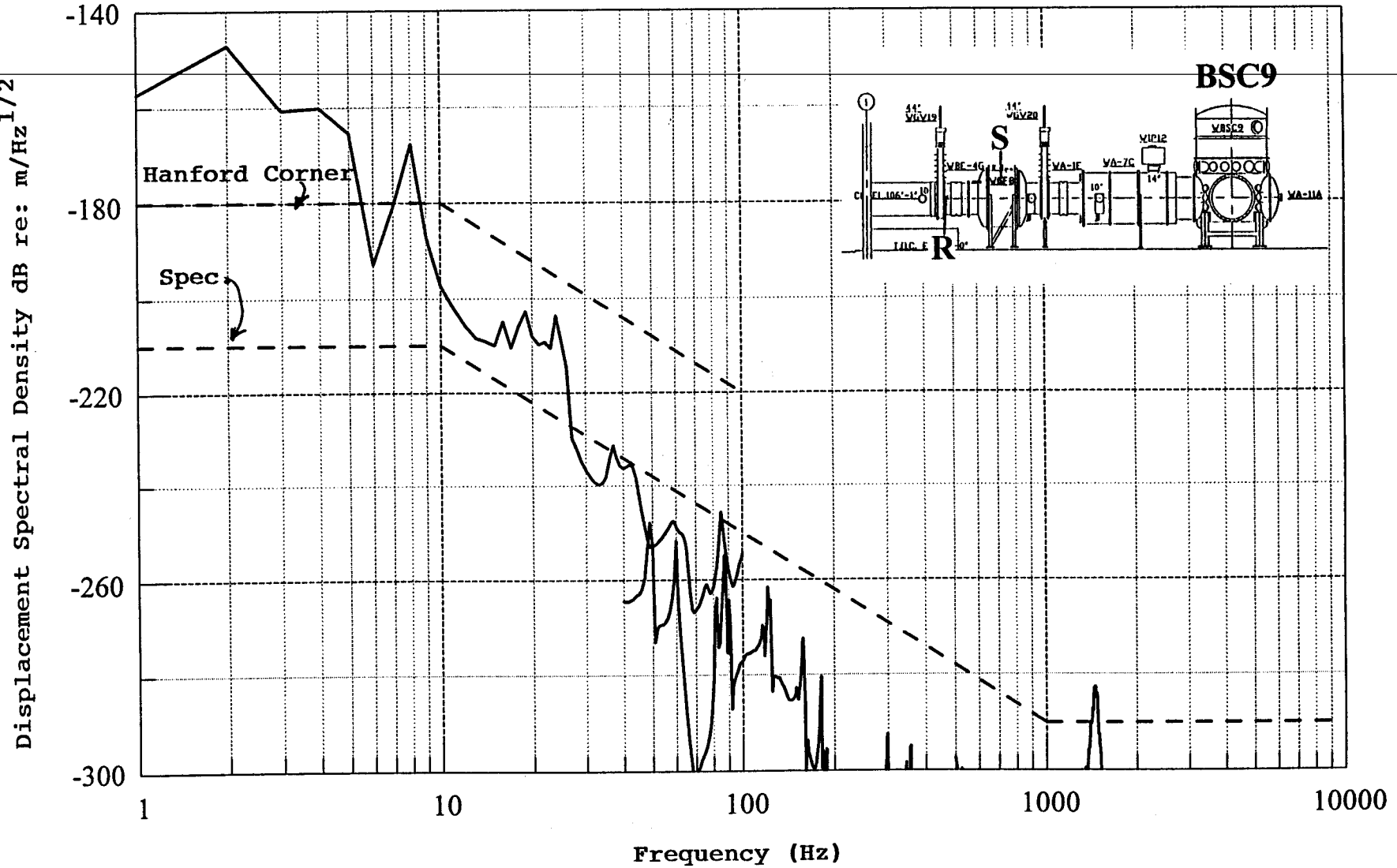

Fig. 23h -- Predicted displacement spectra near Right End Station receiver location 3b, near gate valve GV19 caused by operation of cryo-pump CP8.

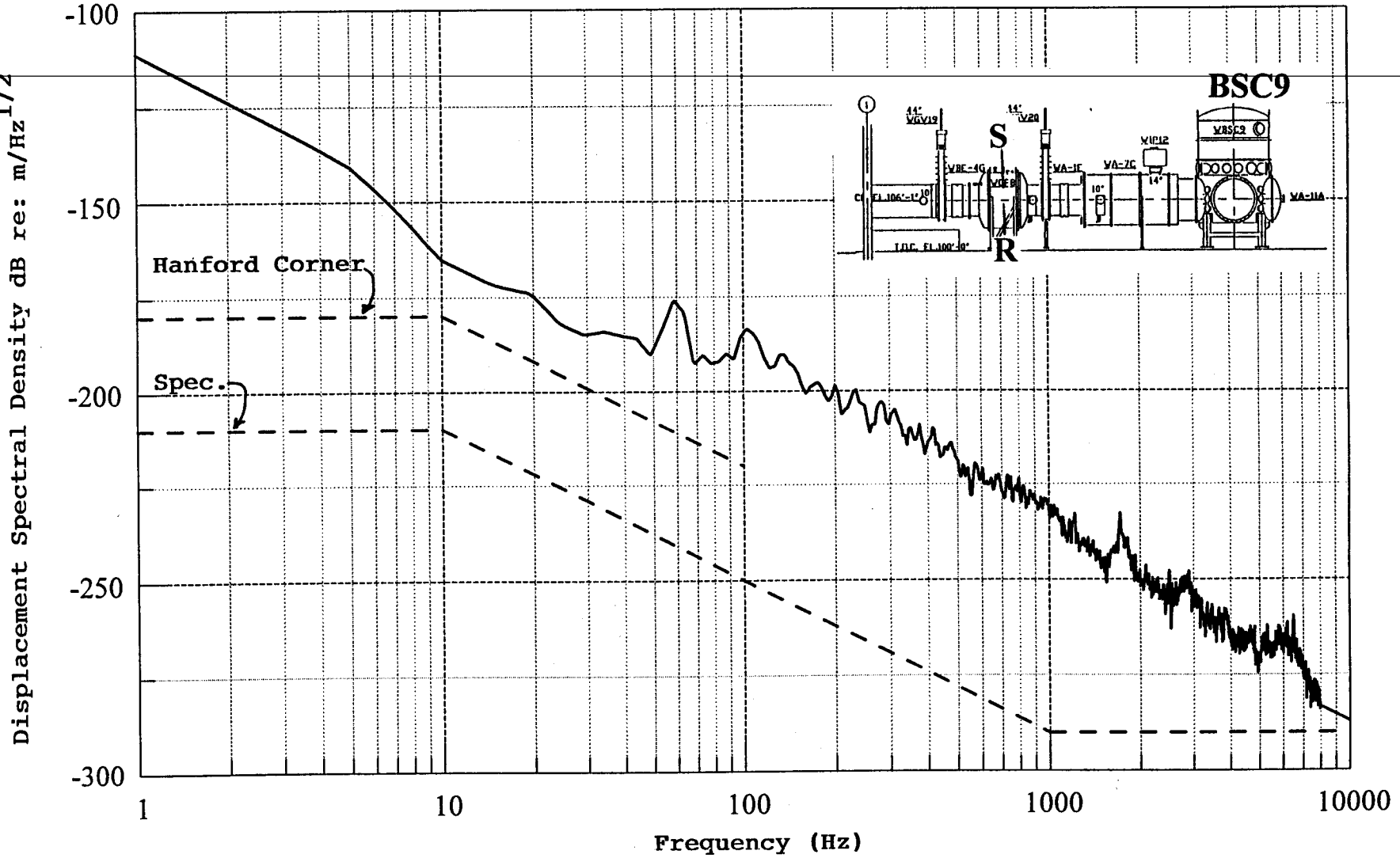

Fig. 23g – *Measured* displacement spectra near Right End Station receiver location 2b, at the cold surface of cryo-pump CP8 caused by the operation of cryo-pump CP8.

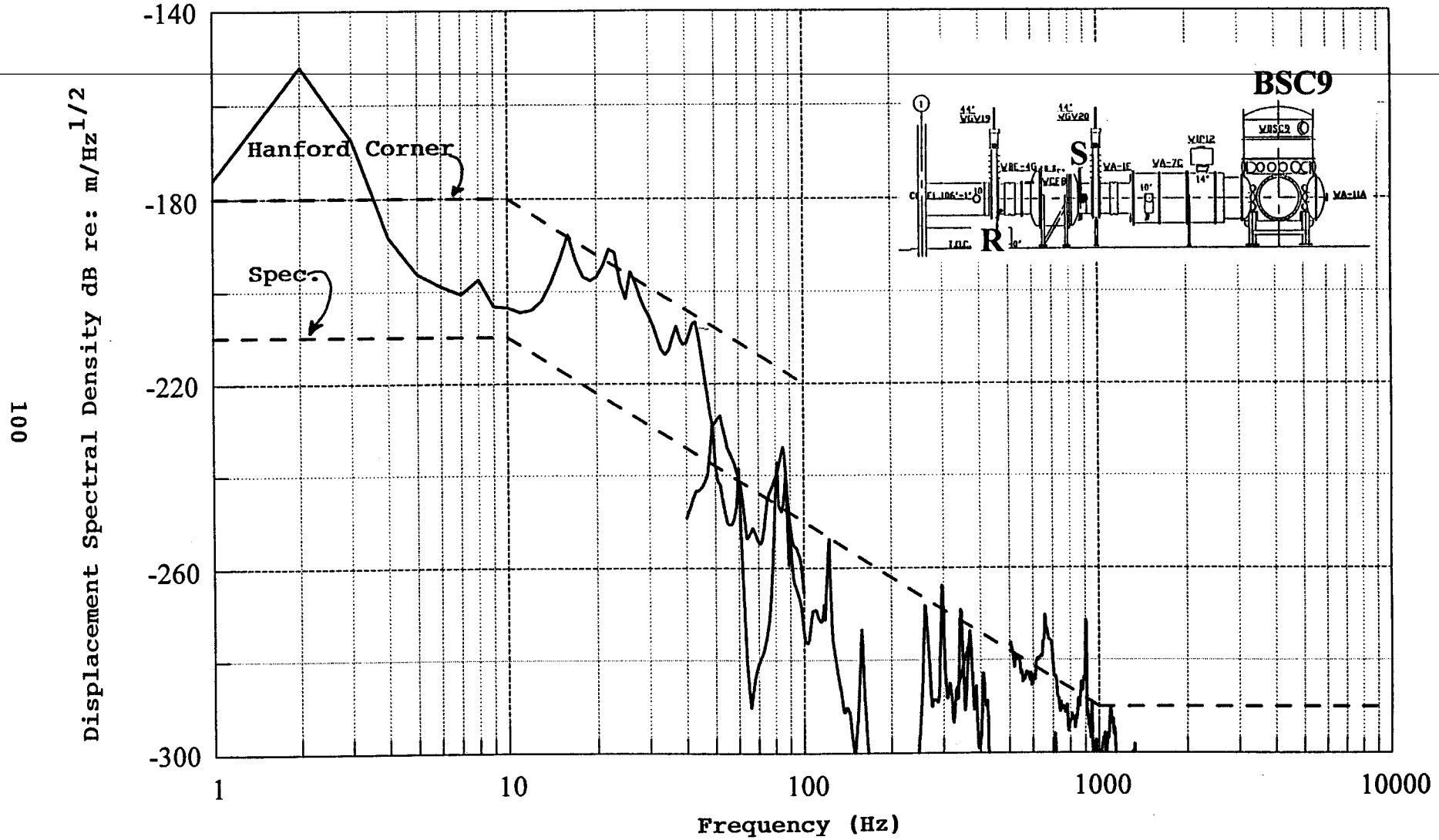

Fig. 23i – Predicted displacement spectra near Right End Station receiver location 3b, near gate valve GV19 caused by operation of the roughing turbo-pump on cryo-pump CP8.

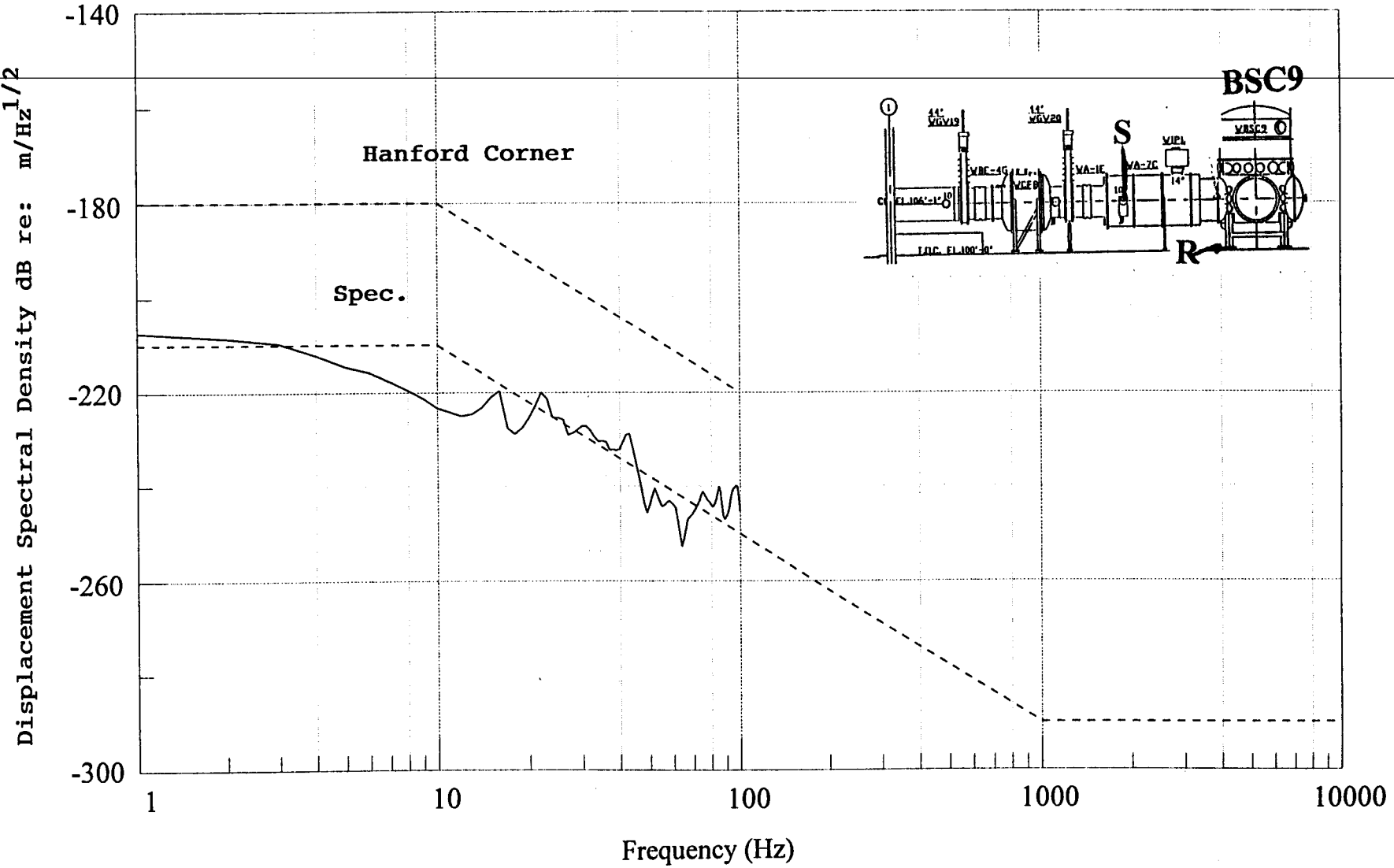

Fig. 23j - Predicted displacement spectra near Right End Station receiver location 1a, on the floor near beam splitter BSC caused by operation of turbo-pump TC6.

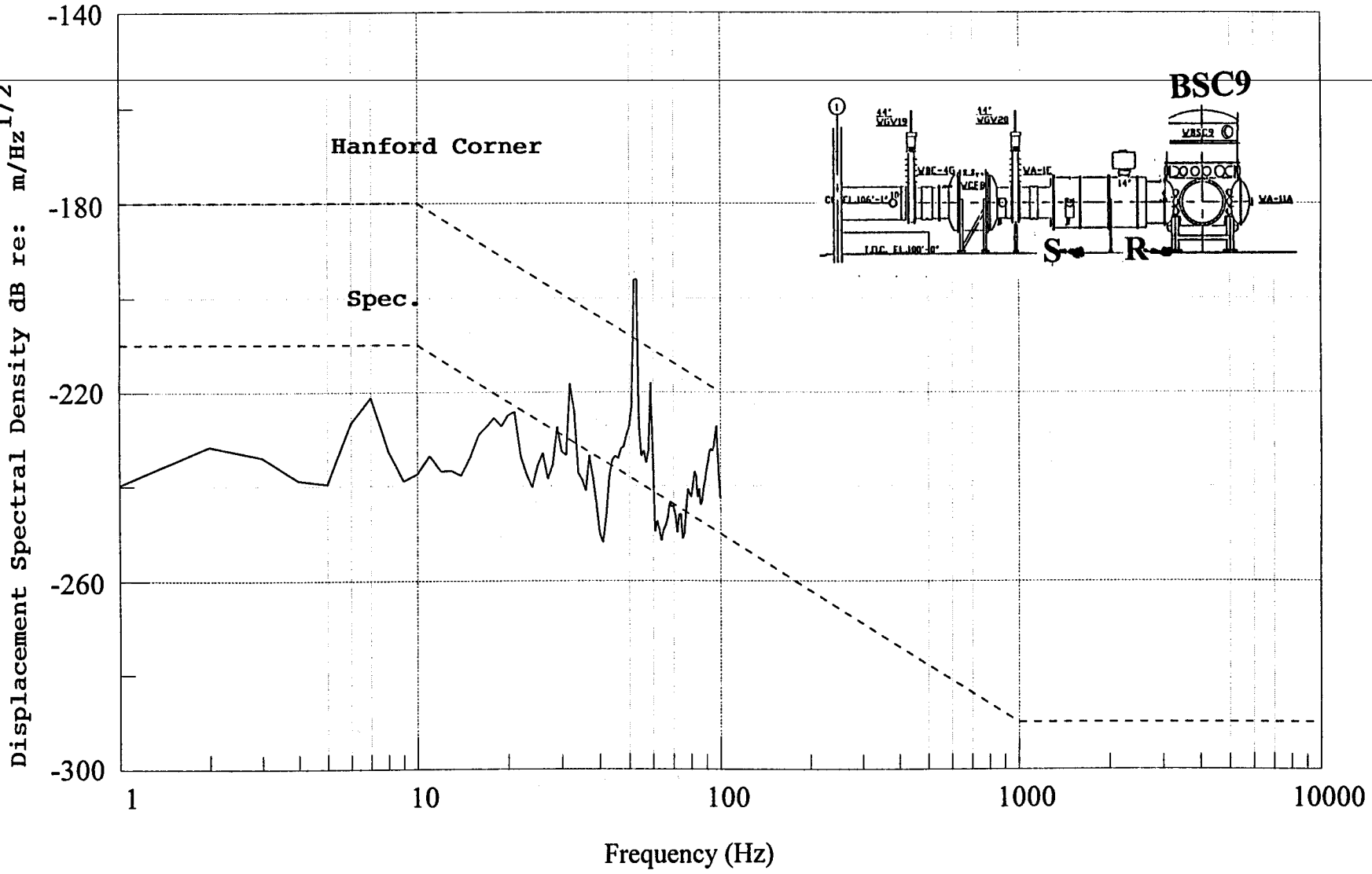

Fig. 23k - Predicted displacement spectra near Right End Station receiver location 1a, on the floor near beam splitter BSC9 caused by operation of turbo-pump cart TC6.

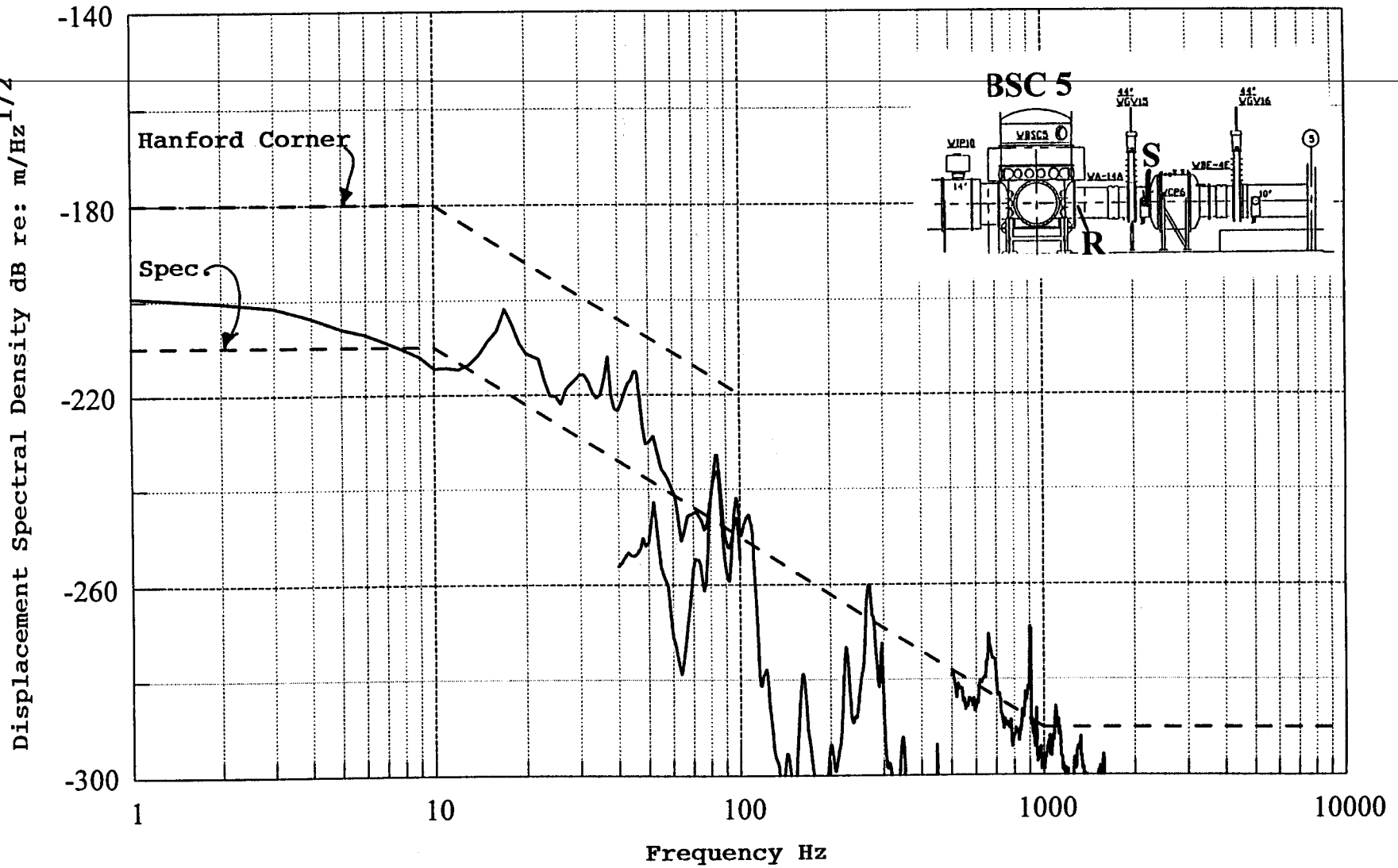

Fig. 24a – Predicted displacement spectra near Right Mid Station receiver location 1a, on the tube near beam splitter BSC5 caused by operation of the roughing turbo-pump on cryo-pump CP6.

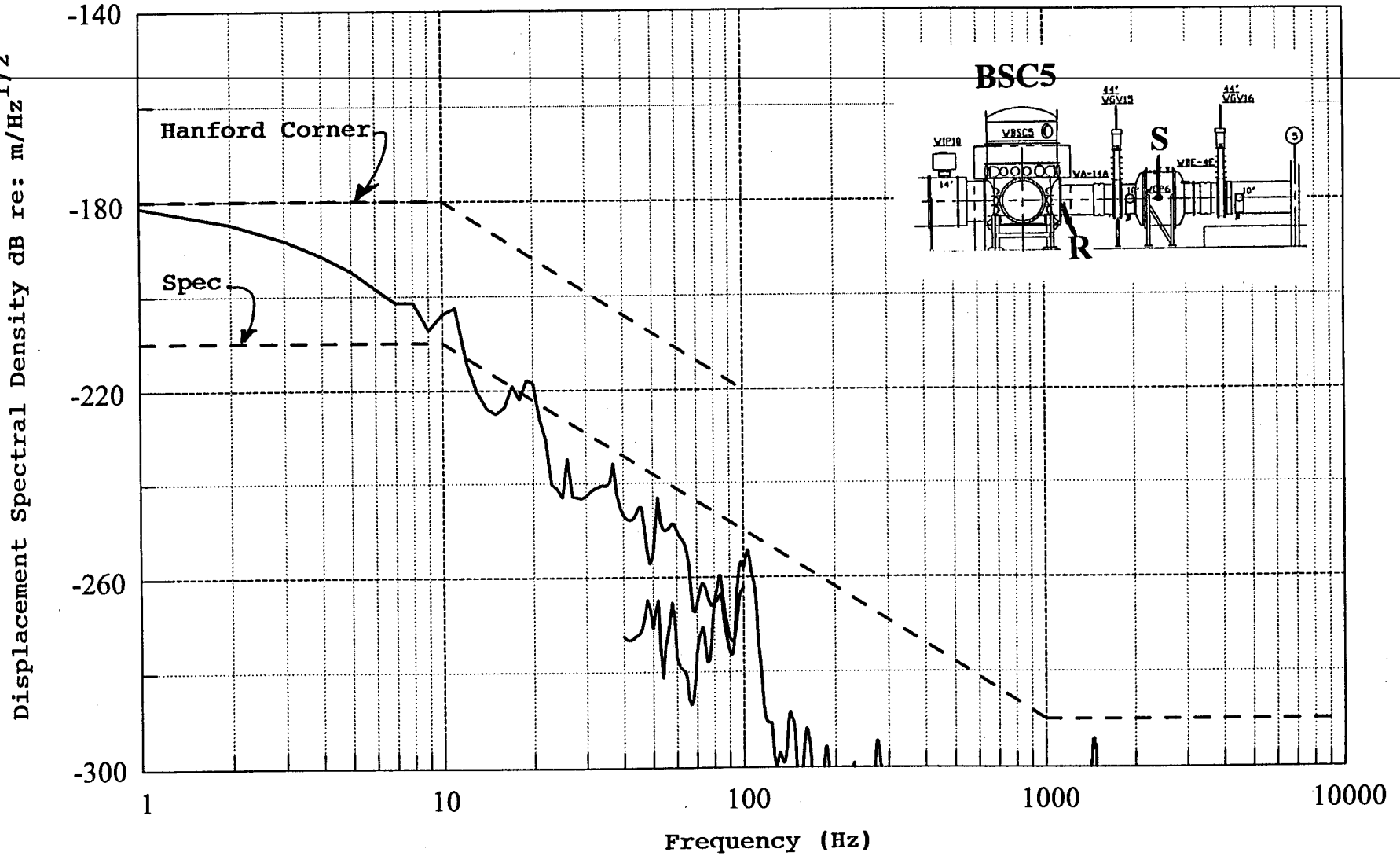

Fig. 24b – Predicted displacement spectra near Right Mid Station receiver location 1a, on the tube near beam splitter BSC5 caused by operation of cryo-pump CP6.

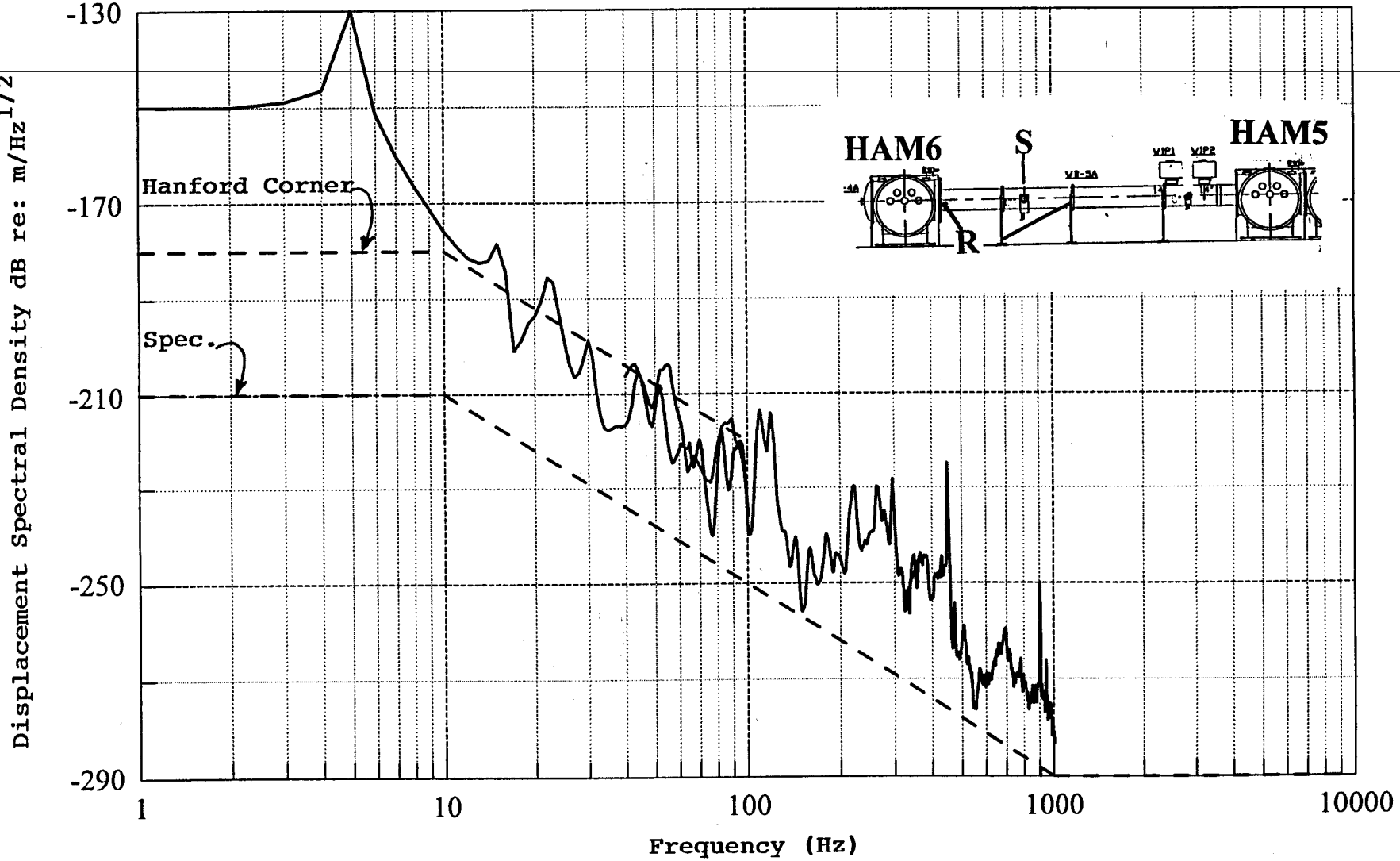

Fig. 25a – Predicted displacement spectra near Corner Station receiver location 2a, on the tube near HAM6 caused by operation of the turbo-pump on B-5A (10 in. port). (Note source-receiver is mirror image of that for location 2a, near HAM1.)

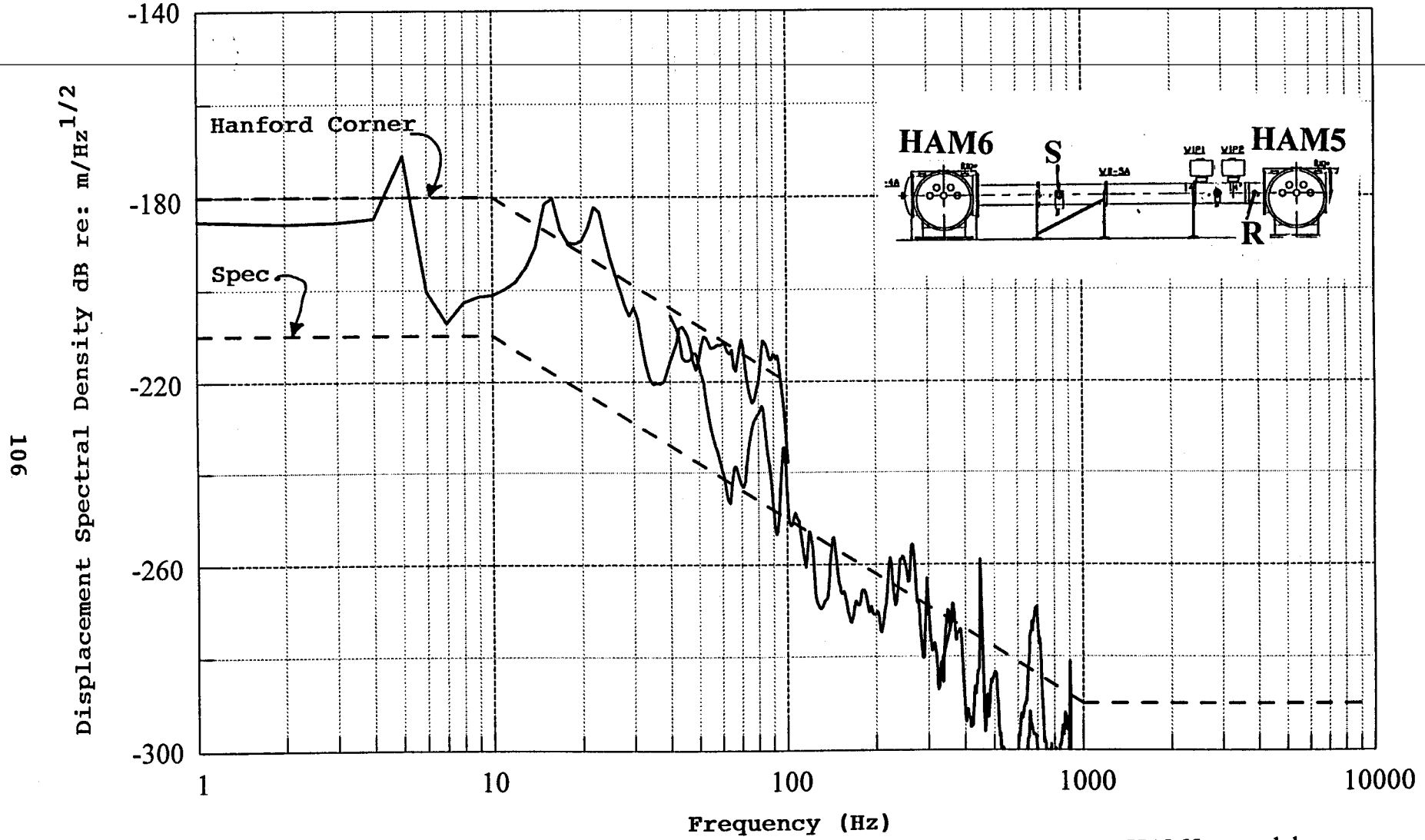

Fig. 25b – Predicted displacement spectra near Corner Station receiver location 2c on the tube near HAM5 caused by operation of the turbo-pump on B-5A (10 in. port). (Note source-receiver is mirror image of that for location 2b, HAM2.)

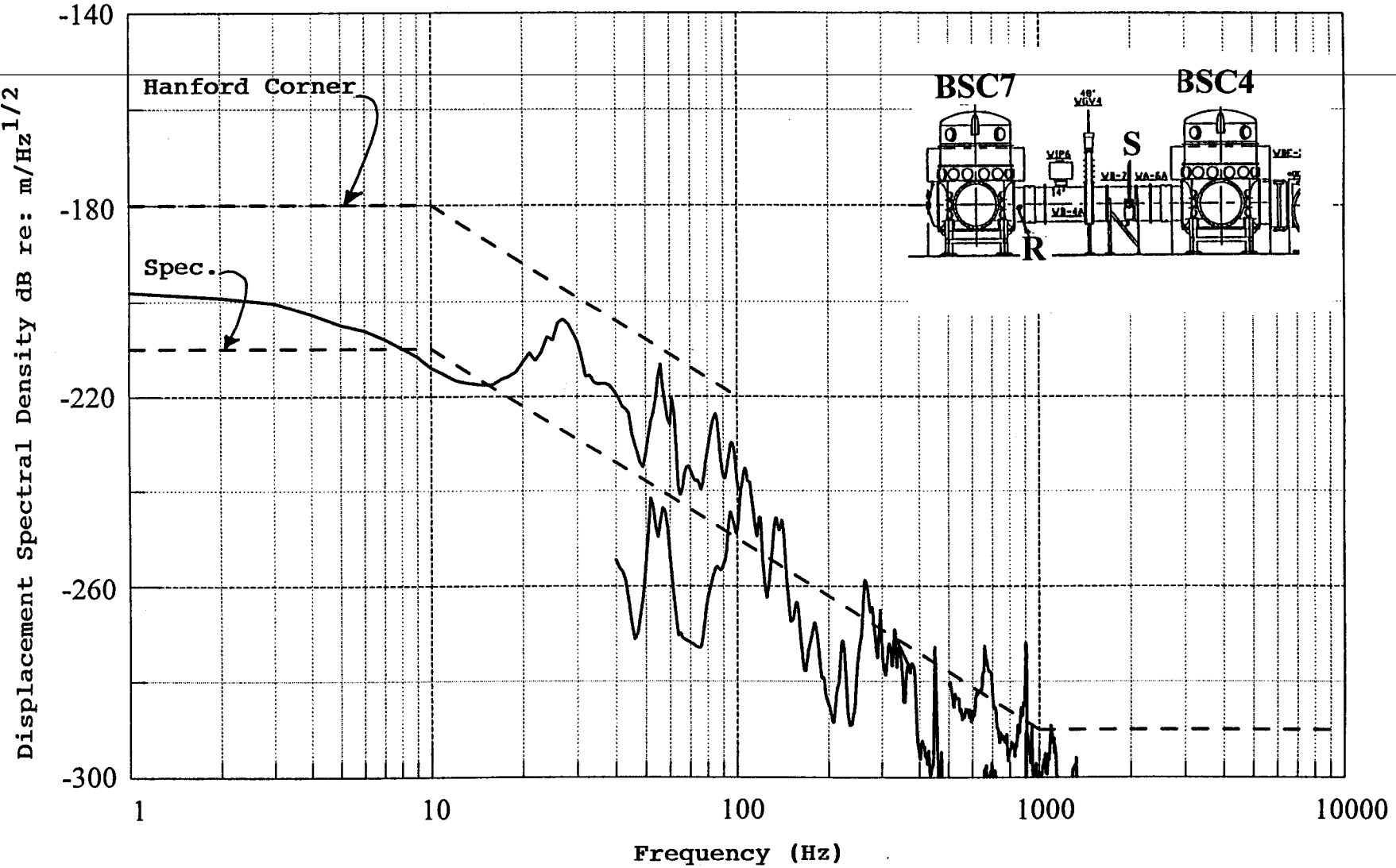

Fig. 26a – Predicted displacement spectra near Corner Station receiver location 1e, the tube near BSC7 caused by operation of the turbo pump on B-7 (between BSC4 and BSC7).

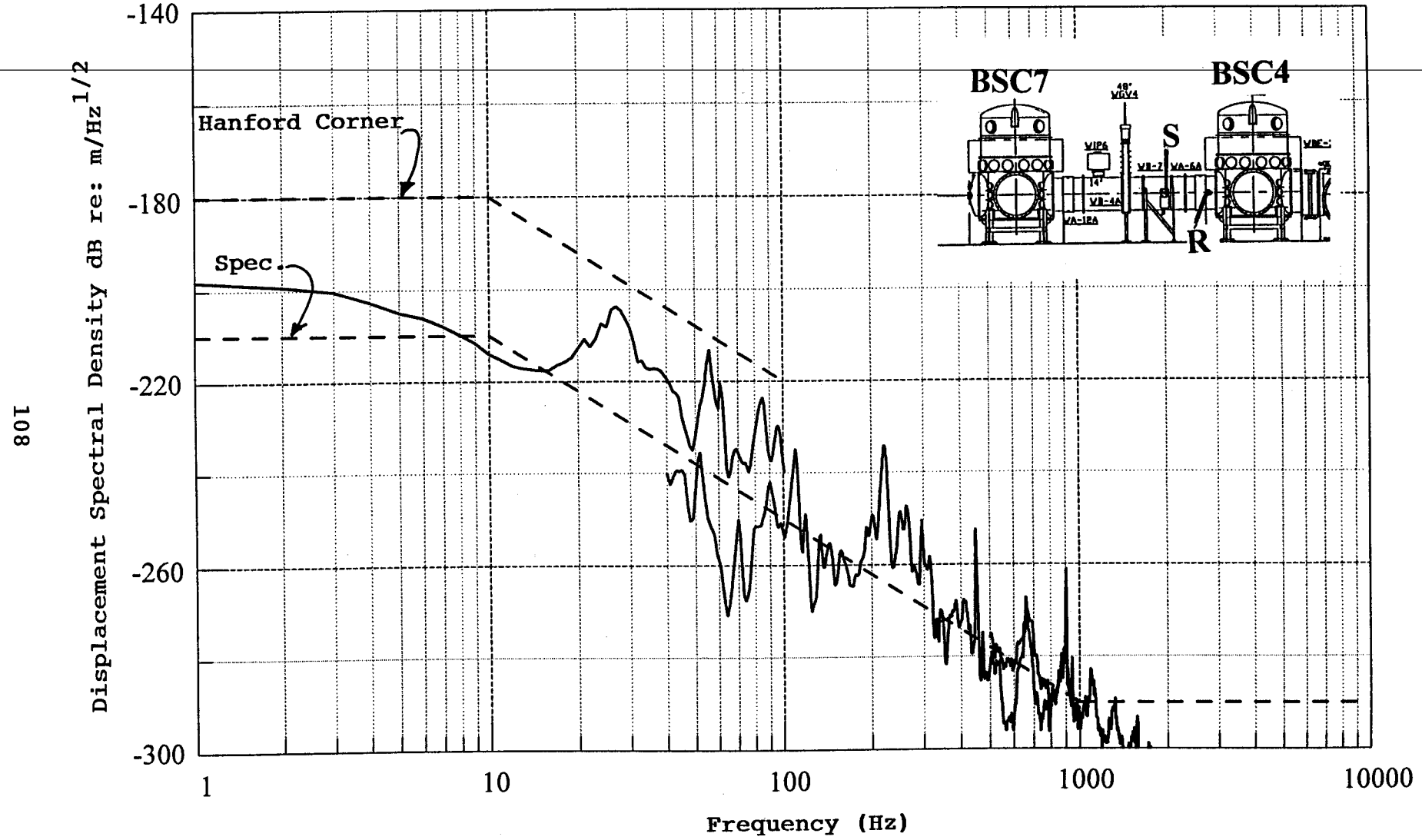

108

Fig. 26b –Predicted displacement spectra near Corner Station receiver location 1d, the tube near BSC4 caused by operation of the turbo pump on B-7 (between BSC4 and BSC7).

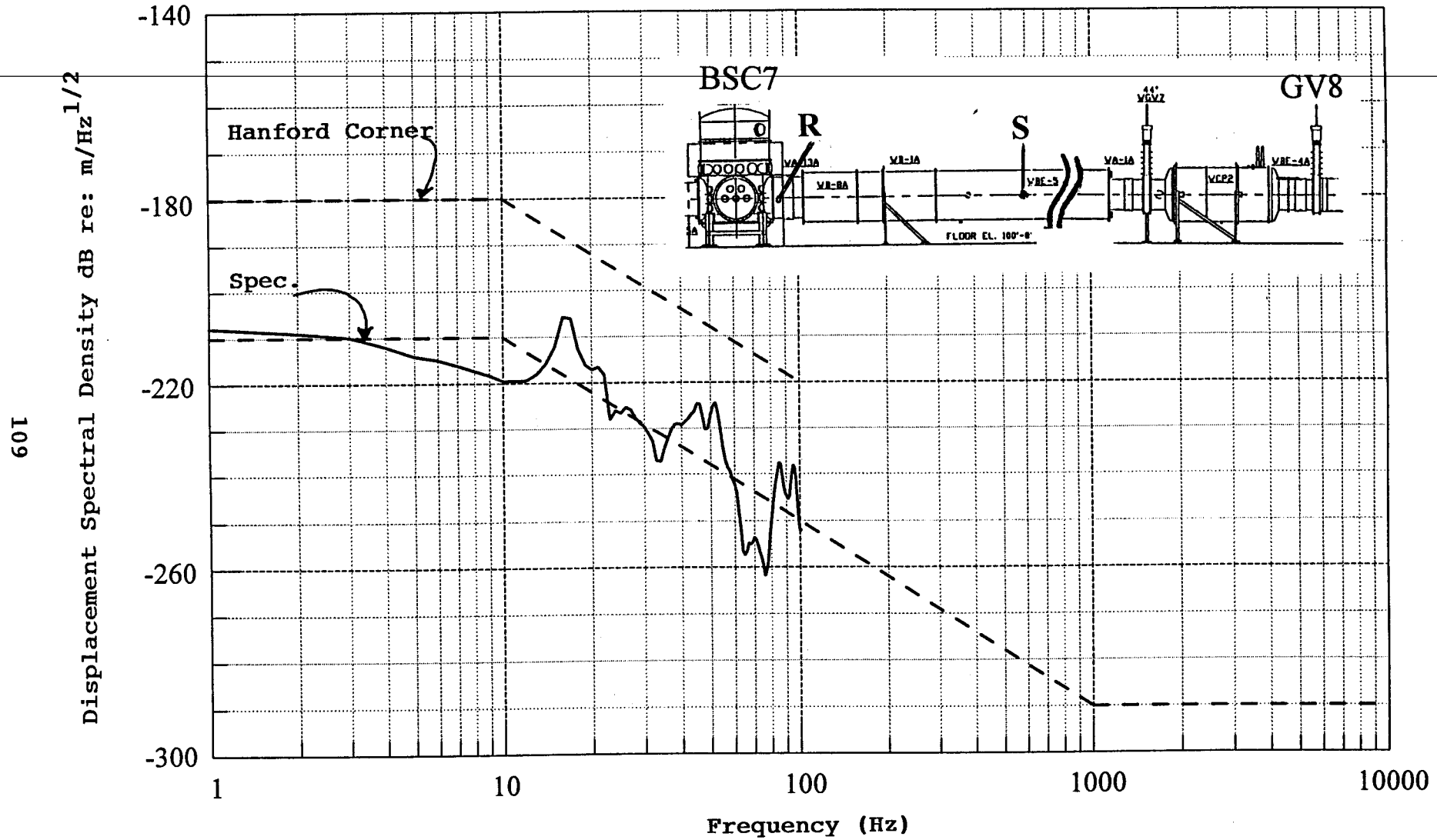

Fig. 27a – Predicted displacement spectra near Corner Station receiver location 1e, the tube near BSC7 caused by operation of turbo pump TC2.

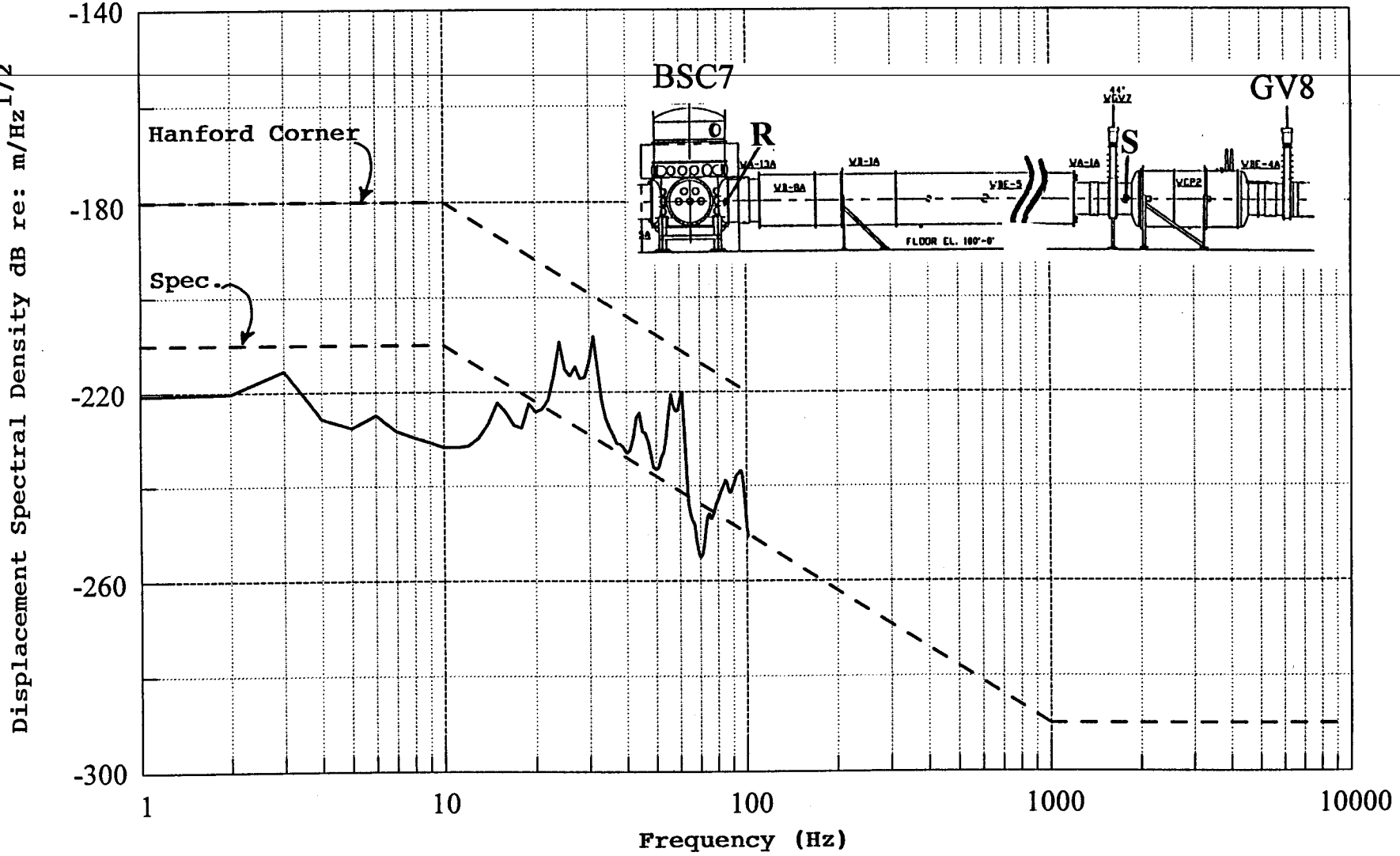

Fig. 27b – Predicted displacement spectra near Corner Station receiver location 1e, the tube near BSC7 caused by operation of the roughing turbo pump for cryo-pump CP2.

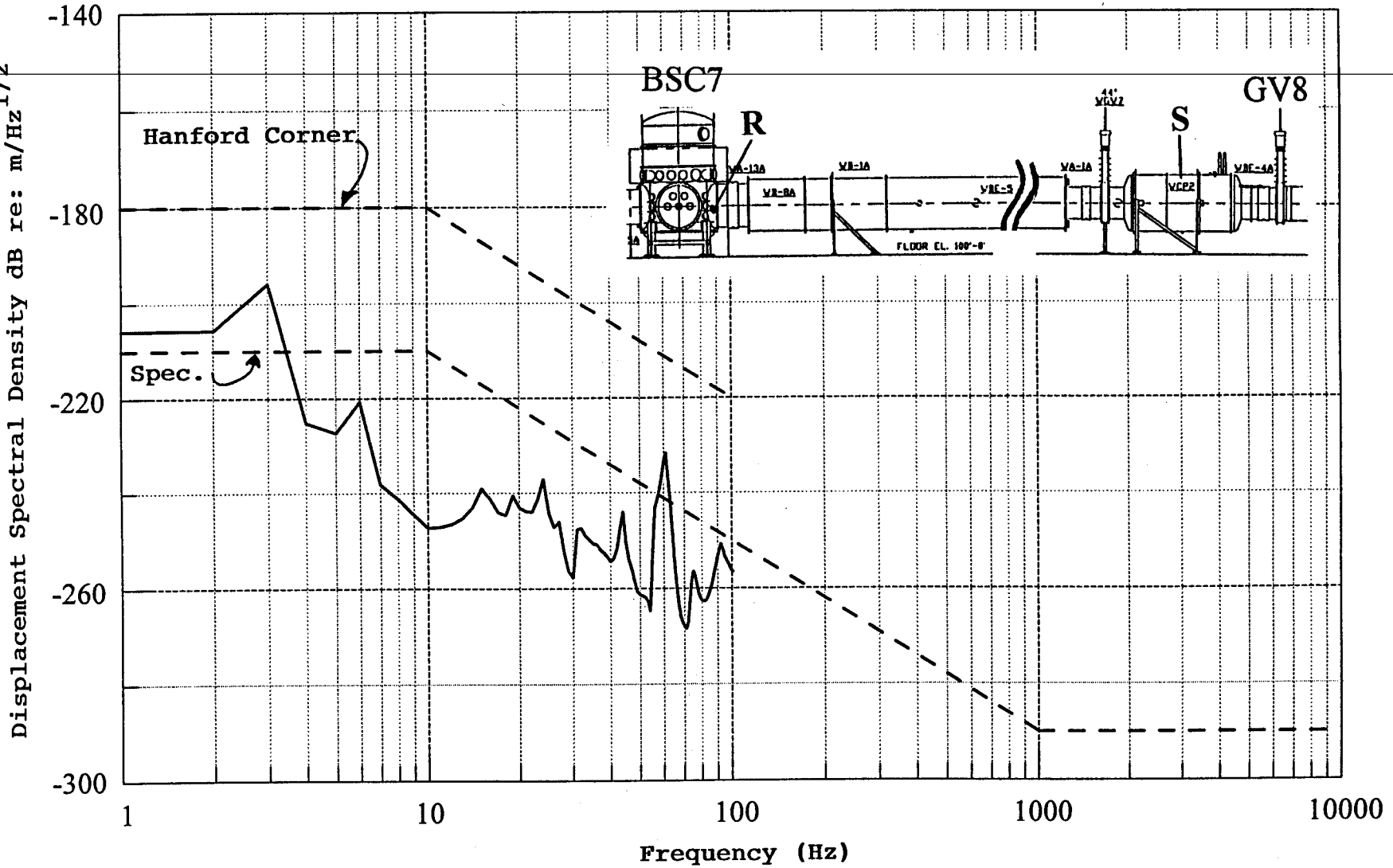

Fig. 27c – Predicted displacement spectra near Corner Station receiver location 1e, the tube near BSC7 caused by operation of cryo-pump CP2.

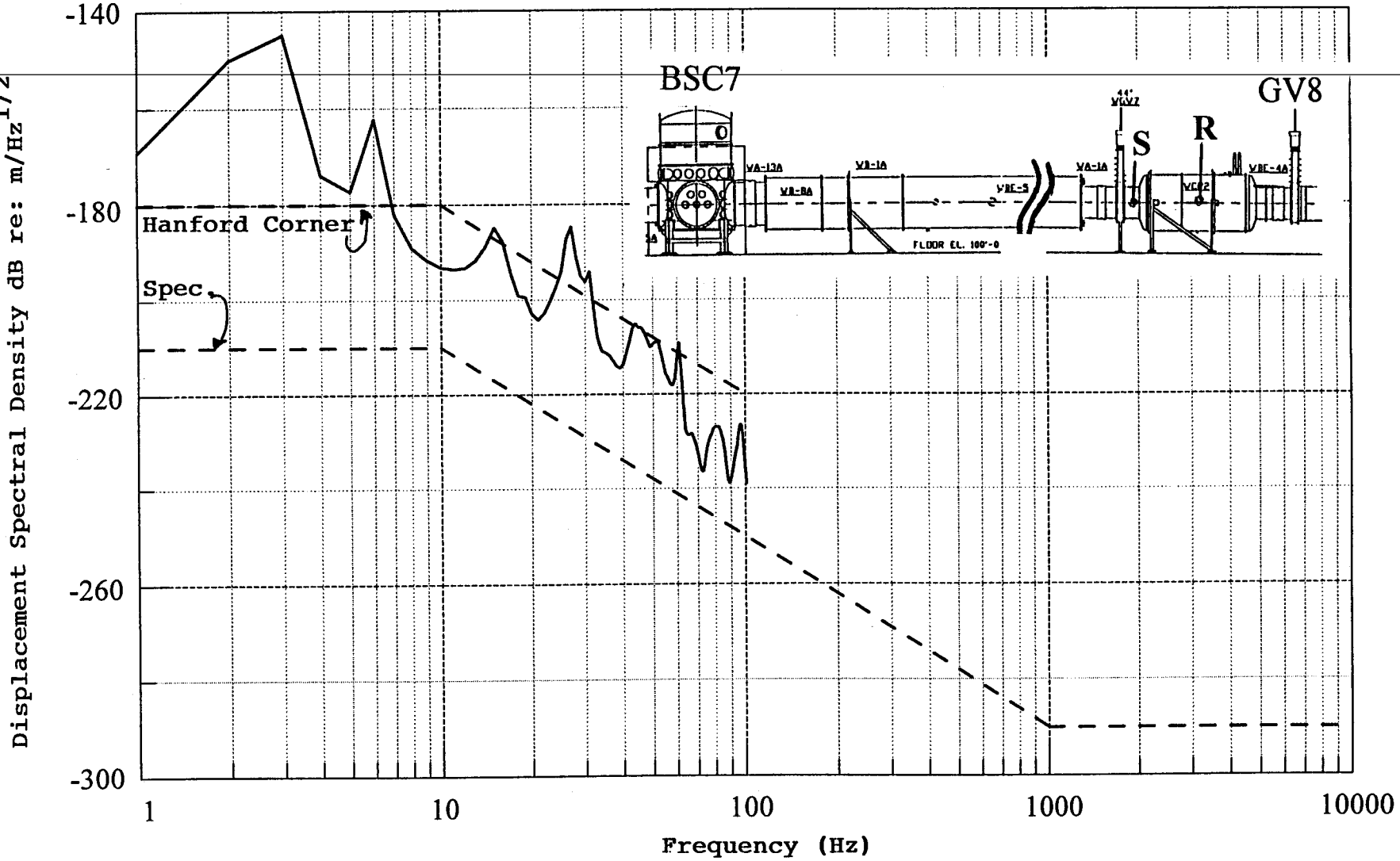

Fig. 27d – Predicted displacement spectra near Corner Station receiver location 3d, on cryo-pump CP2 housing caused by operation of the roughing turbo pump for cryo-pump CP2.

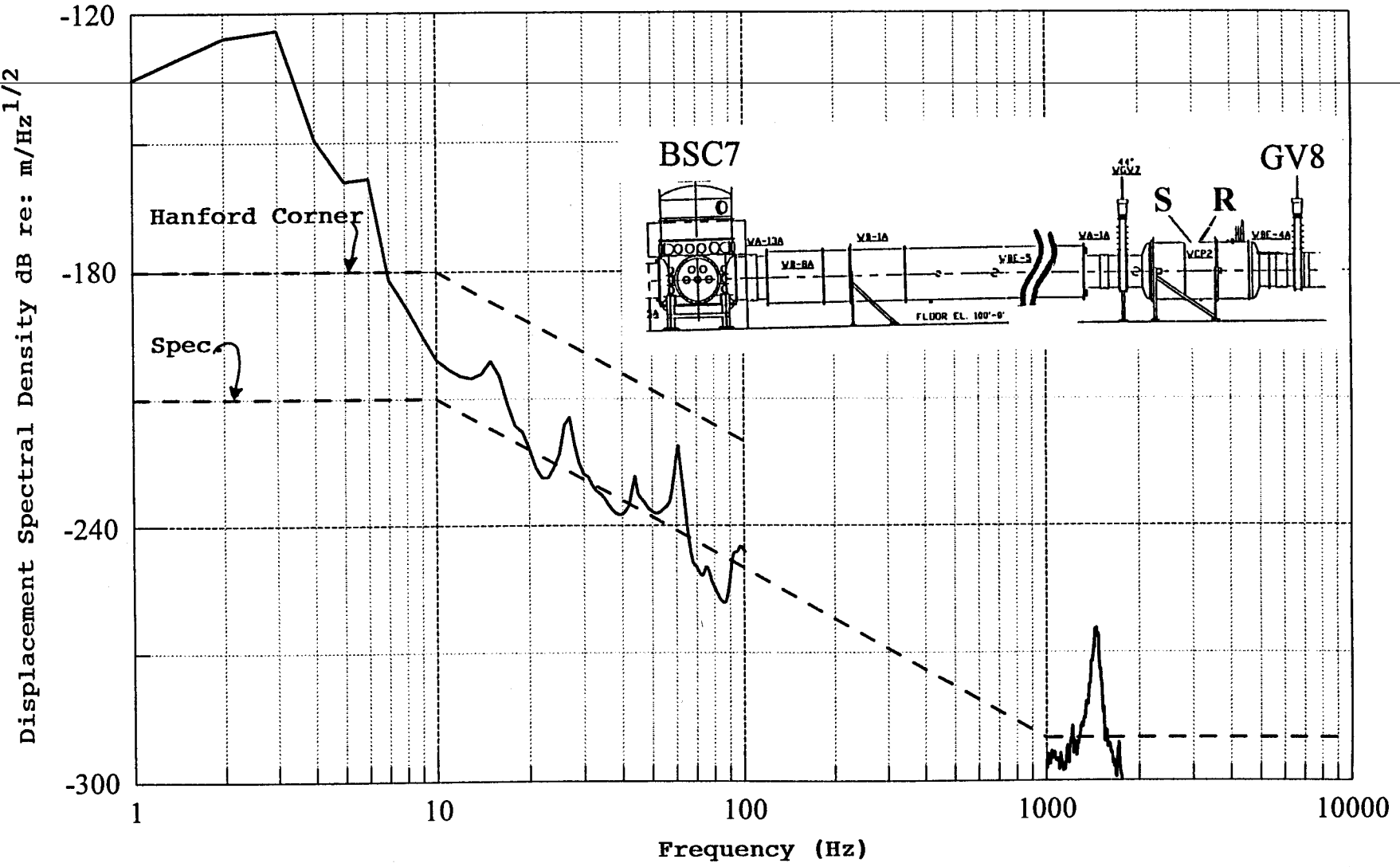

Fig. 27e – Predicted displacement spectra near Corner Station receiver location 3d, on cryo-pump CP2 housing caused by operation of cryo-pump CP2.

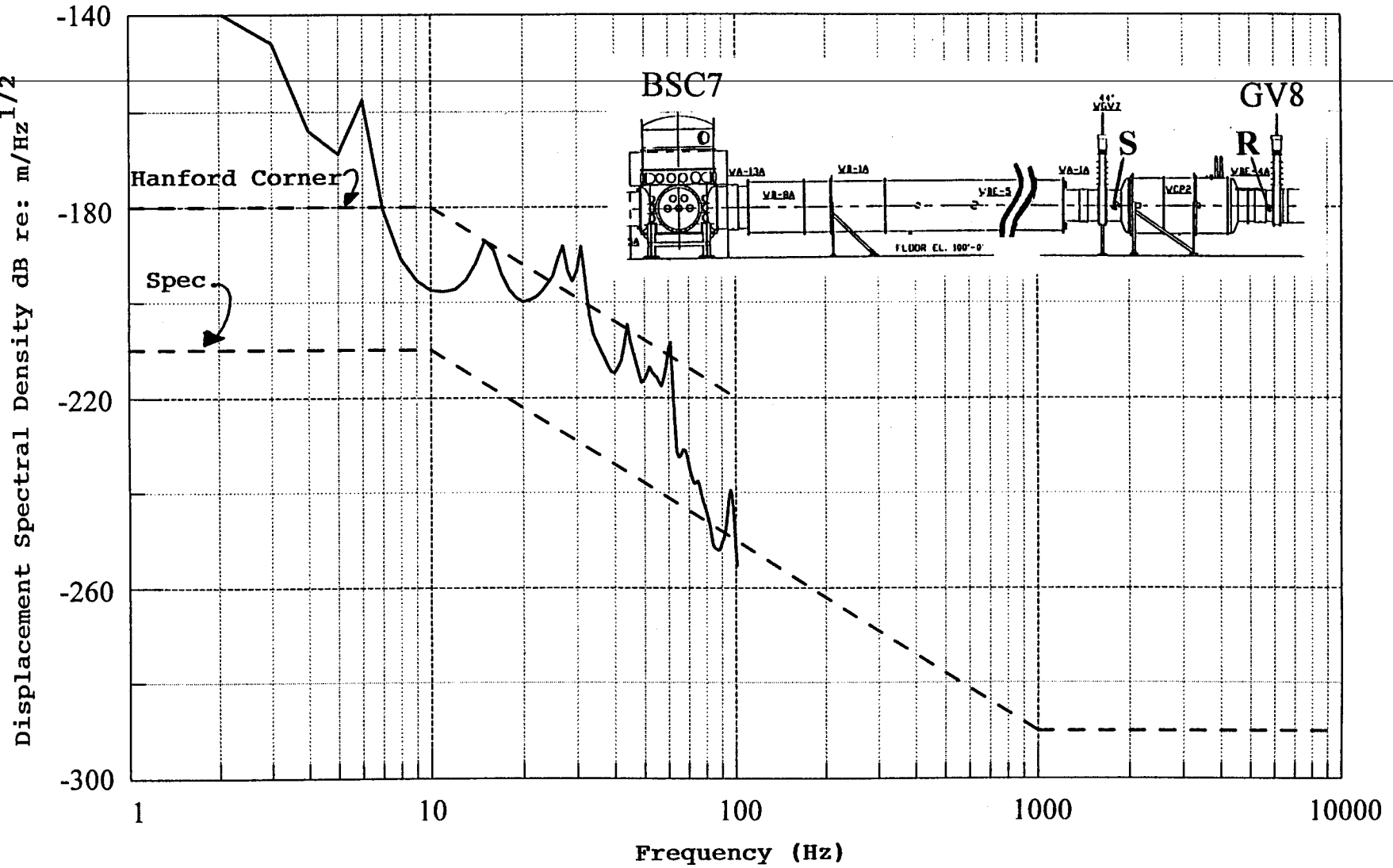

Fig. 27f – Predicted displacement spectra near Corner Station receiver location 3e, at gate valve GV6 caused by operation of the roughing turbo pump for cryo-pump CP2.

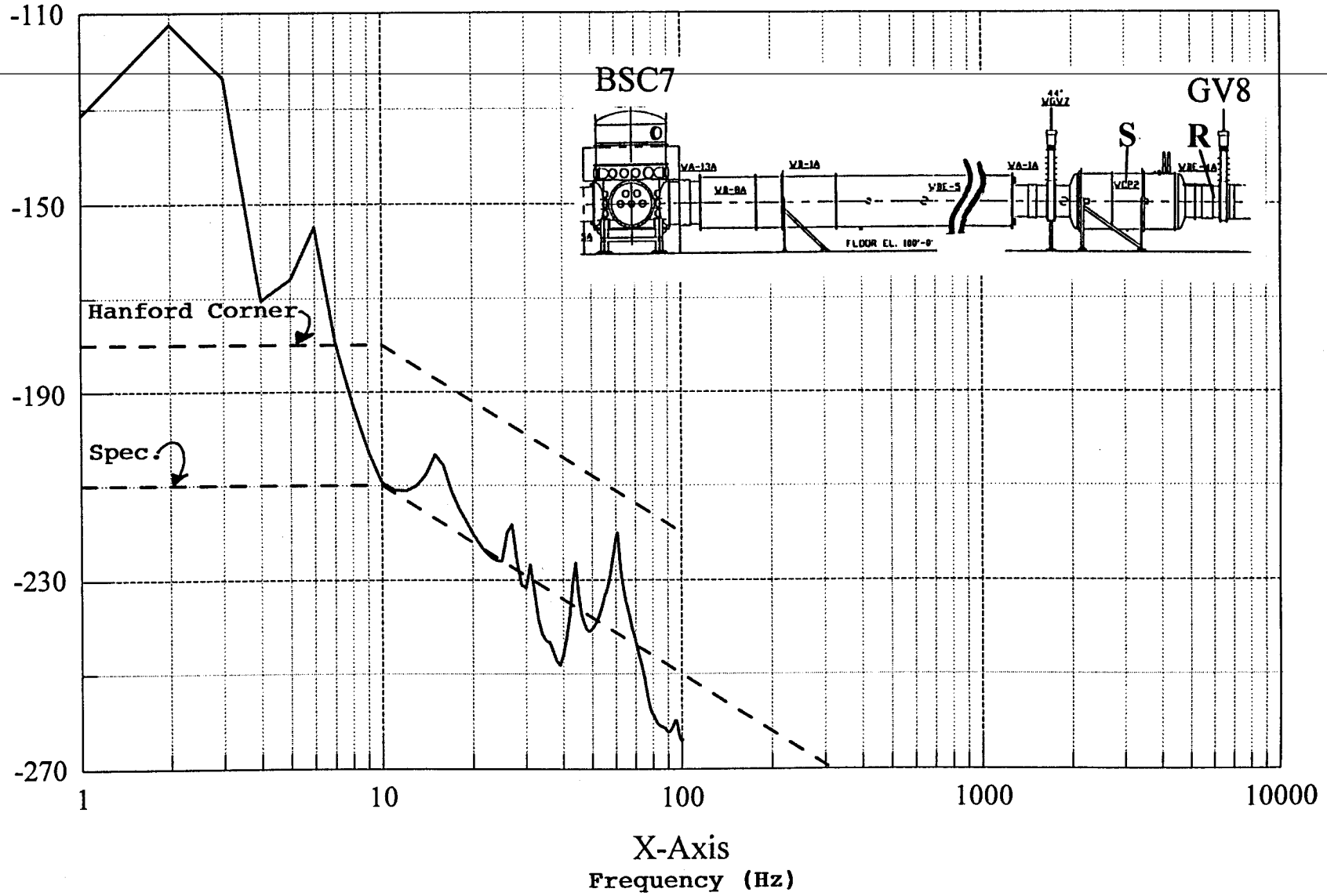

Fig. 27g - Predicted displacement spectra near Corner Station receiver location 3e, at gate valve GV6 caused by operation of cryo-pump CP2.

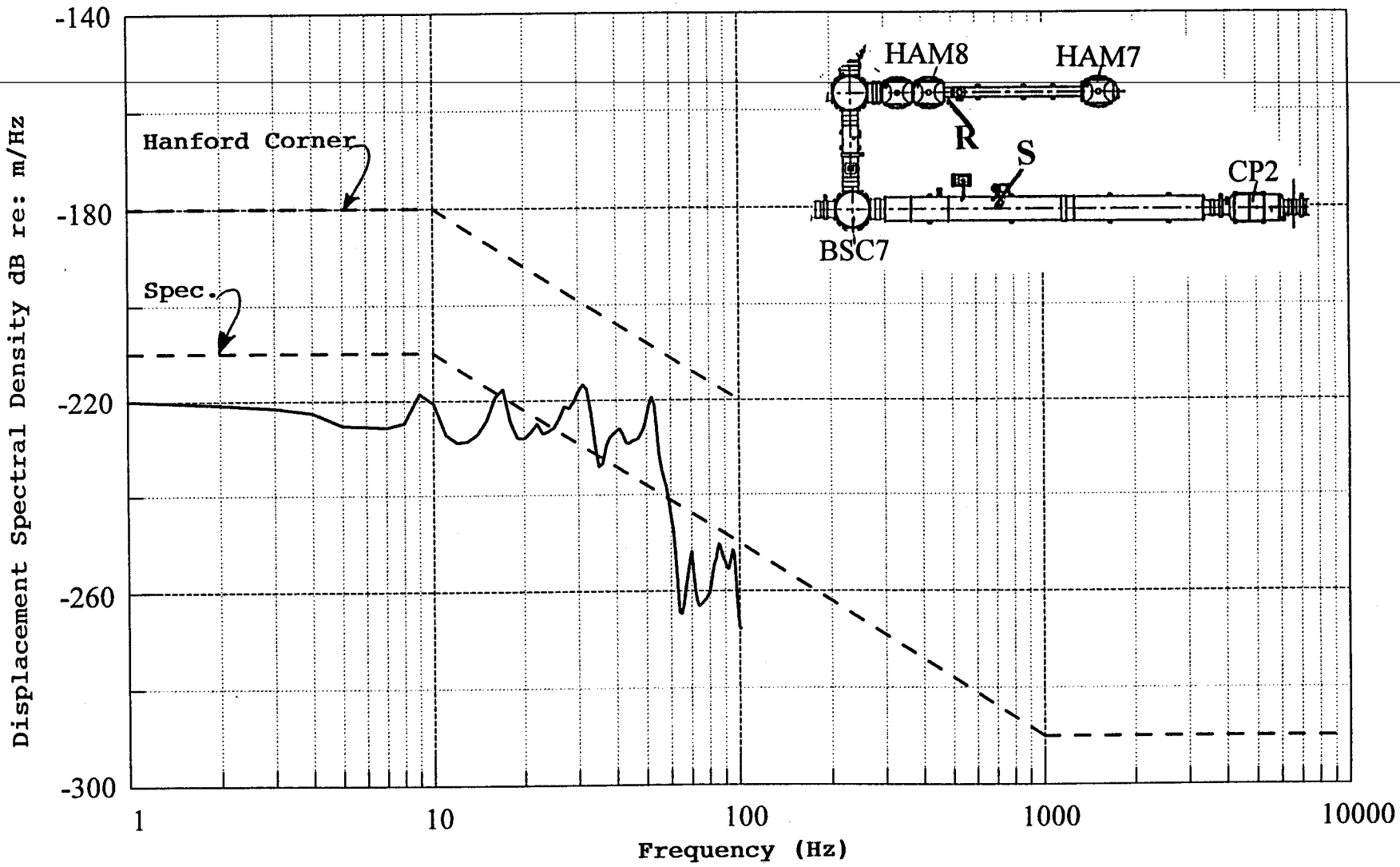

Fig. 28a – Predicted displacement spectra near Corner Station receiver location 2e, near HAM8 caused by operation of the turbo pump on BE-5 (between CP2 and BSC7).

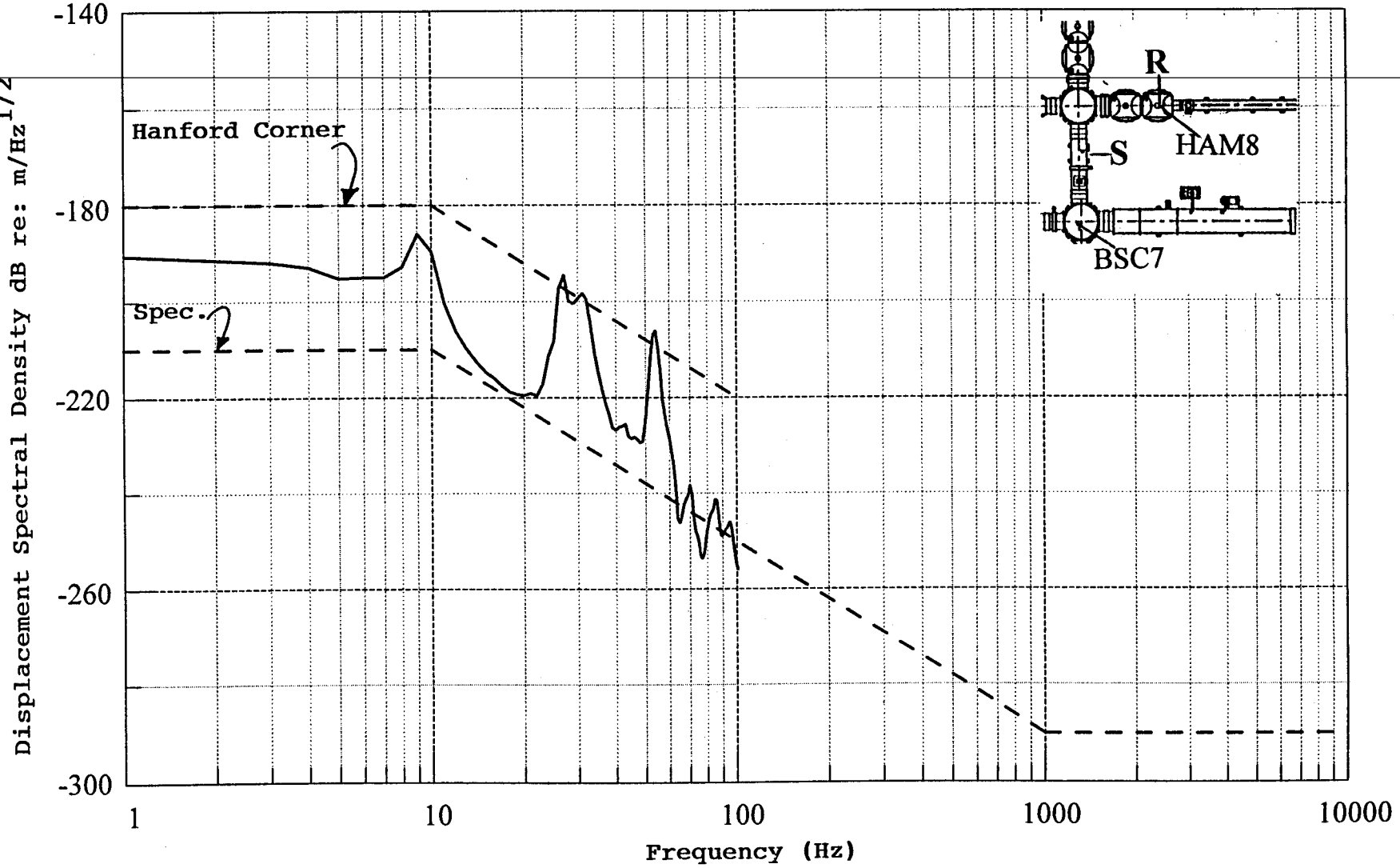

Fig. 28b – Predicted displacement spectra near Corner Station receiver location 2e, near HAM8 caused by operation of the turbo pump on B-7 (between BSC4 and BSC7).

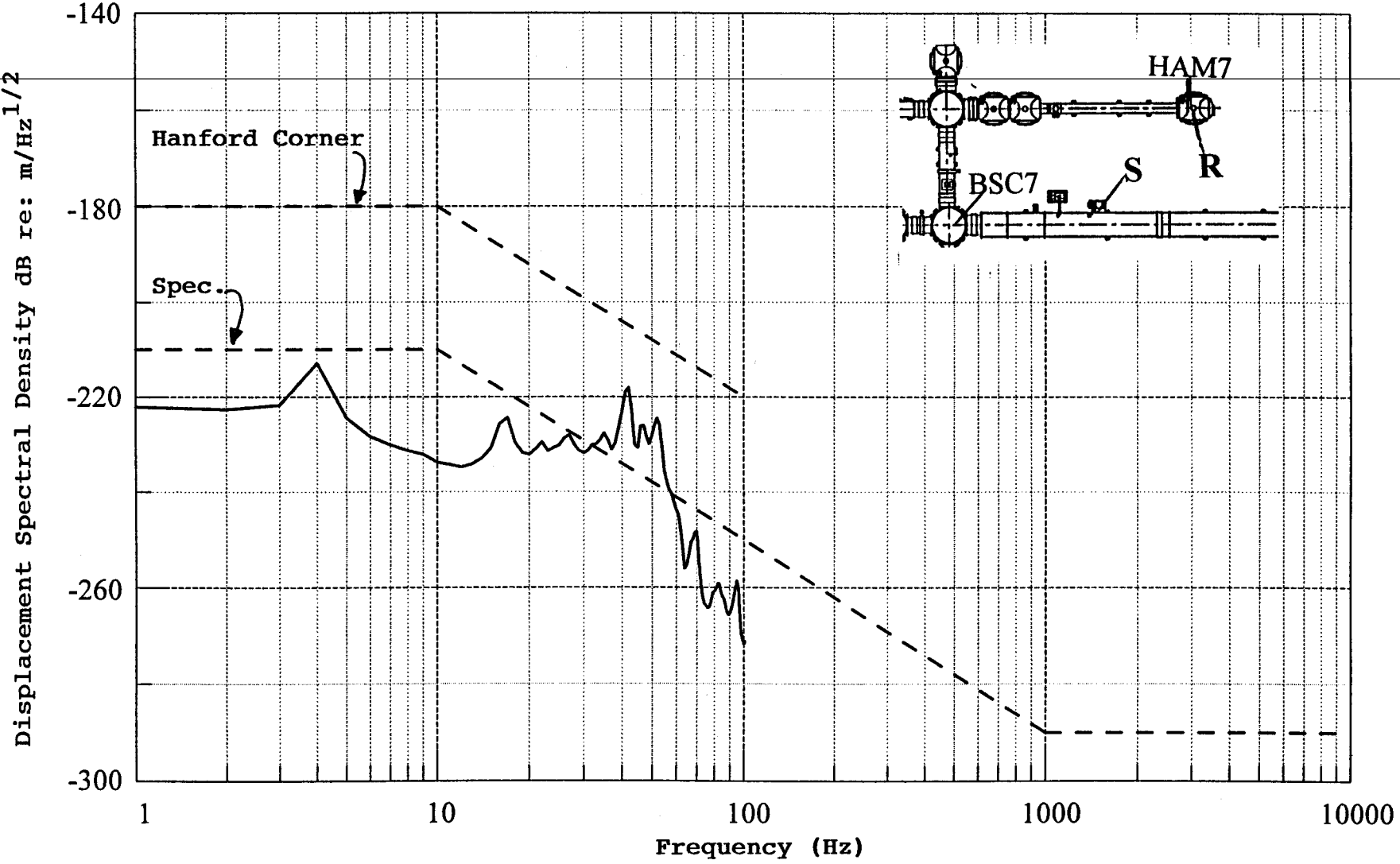

Fig. 28c – Predicted displacement spectra near Corner Station receiver location 2d, near HAM7 caused by operation of the turbo pump on BE-5 (between CP2 and BSC7).

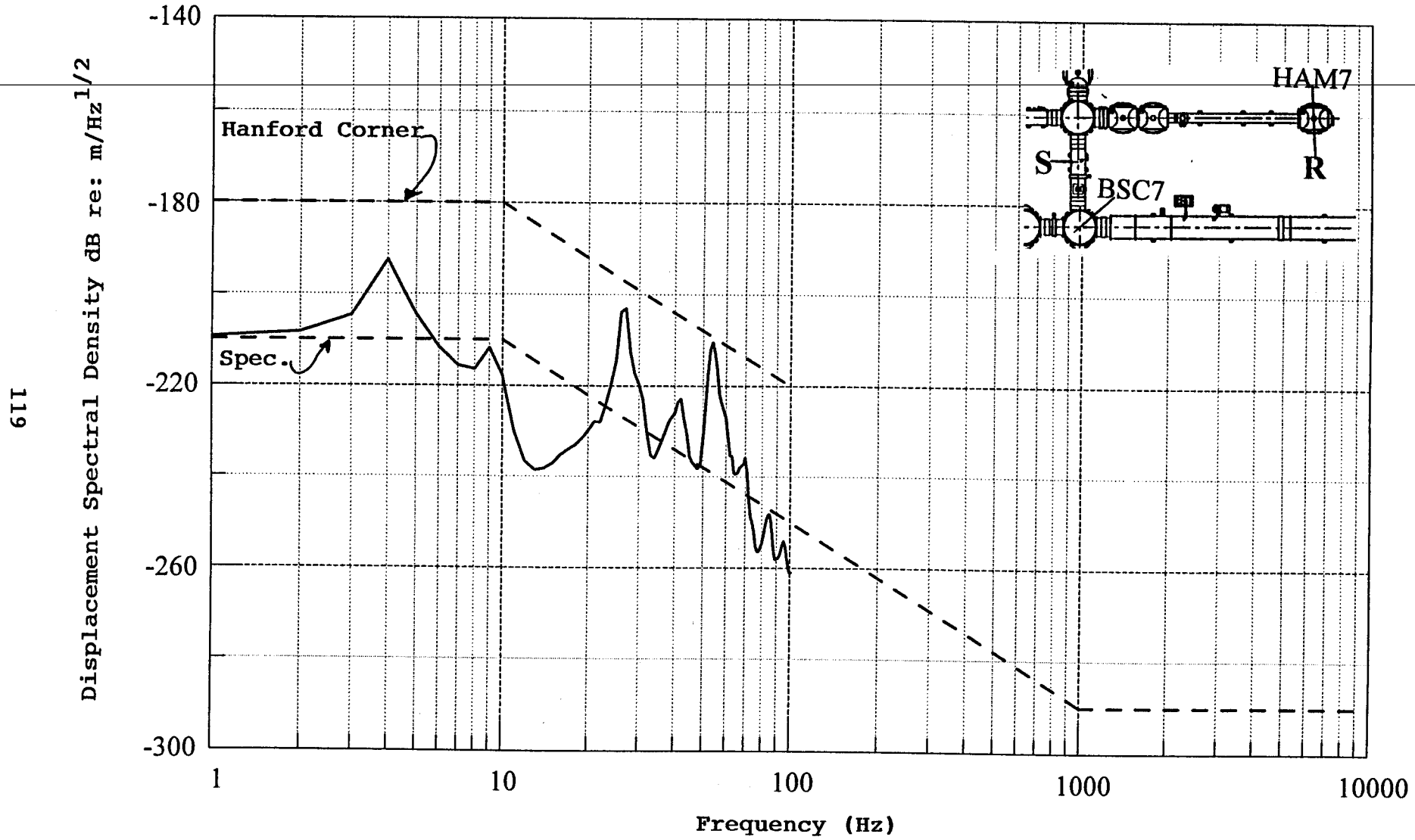

Fig. 28d – Predicted displacement spectra near Corner Station receiver location 2d, near HAM7 caused by operation of the turbo pump on B-7 (between BSC4 and BSC7).

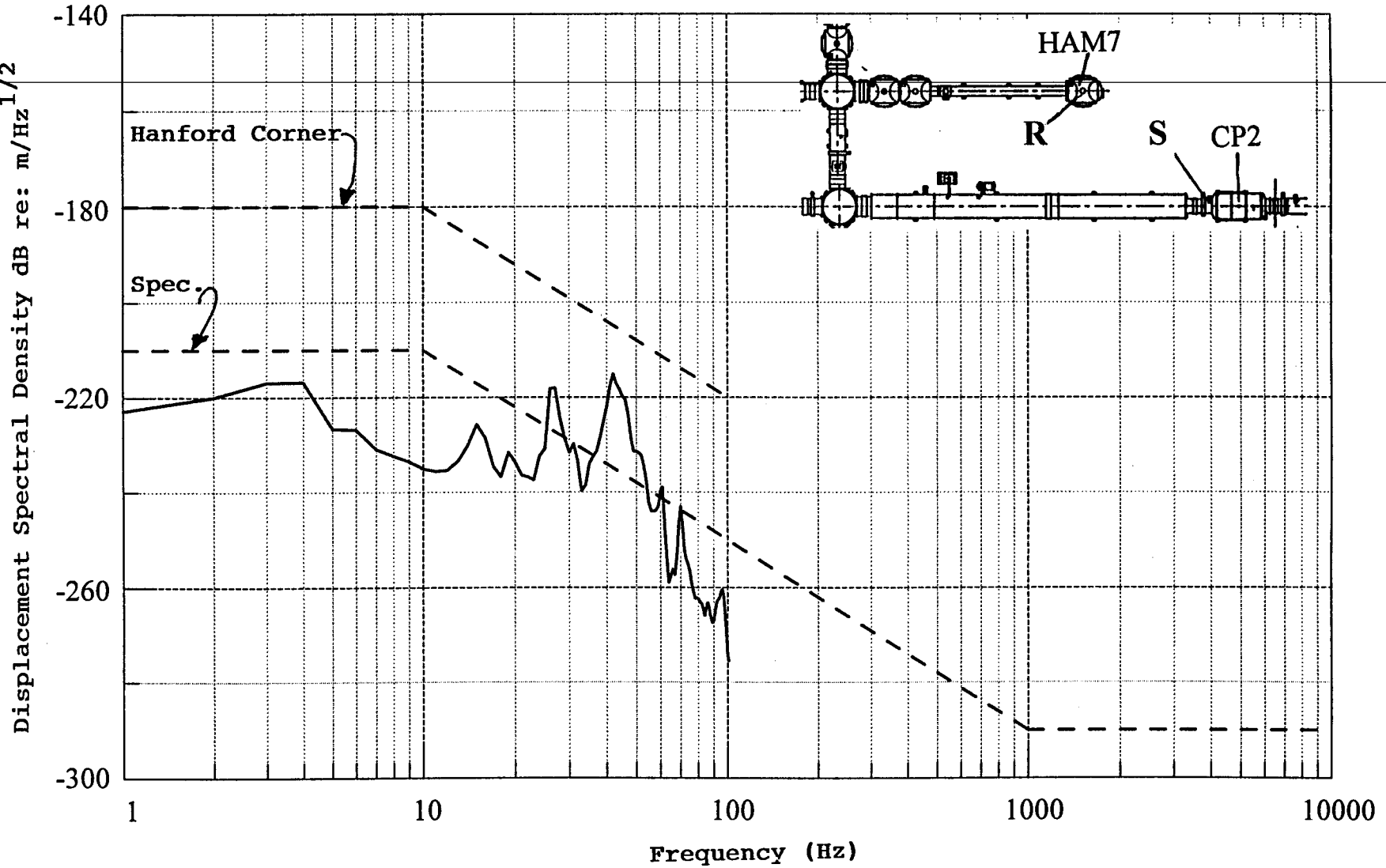

Fig. 28e – Predicted displacement spectra near Corner Station receiver location 2d, near HAM7 caused by operation the roughing turbo pump for cryo-pump CP2.

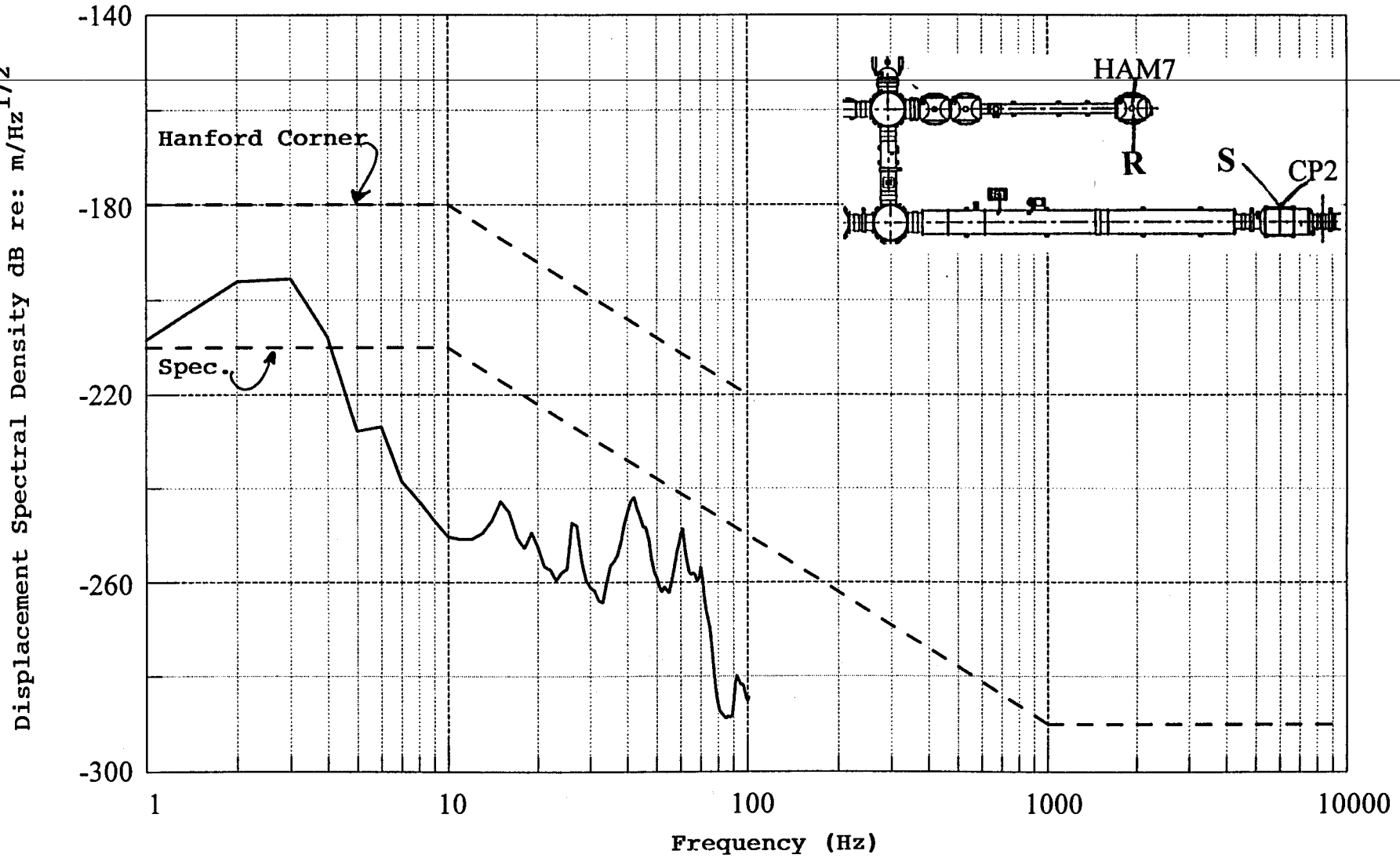

Fig. 28f - Predicted displacement spectra near Corner Station receiver location 2d, near HAM7 caused by operation of cryo-pump CP2.

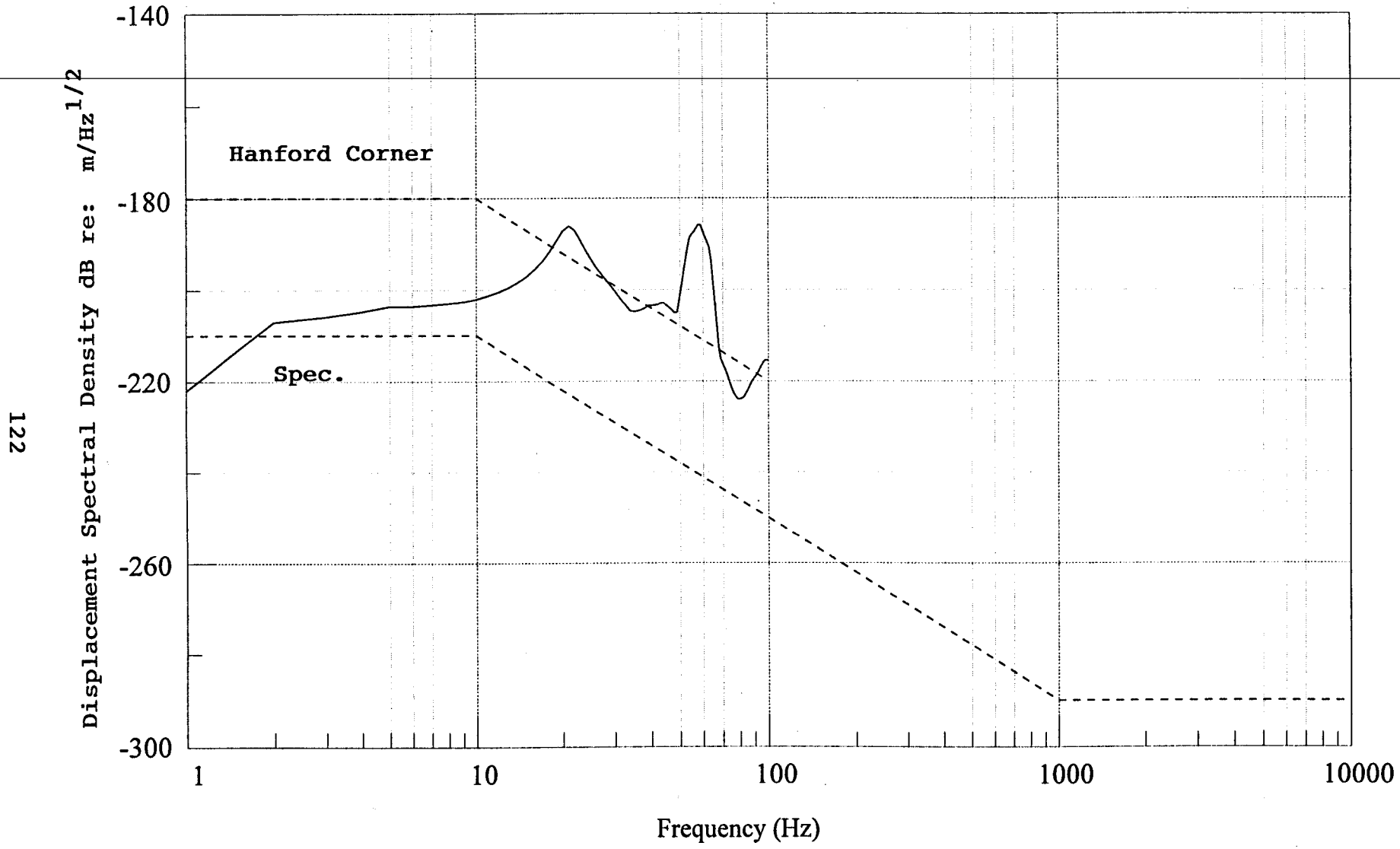

Fig. 29a - Estimated vacuum area floor response due to turbomolecular backing pump in Mechanical Room.

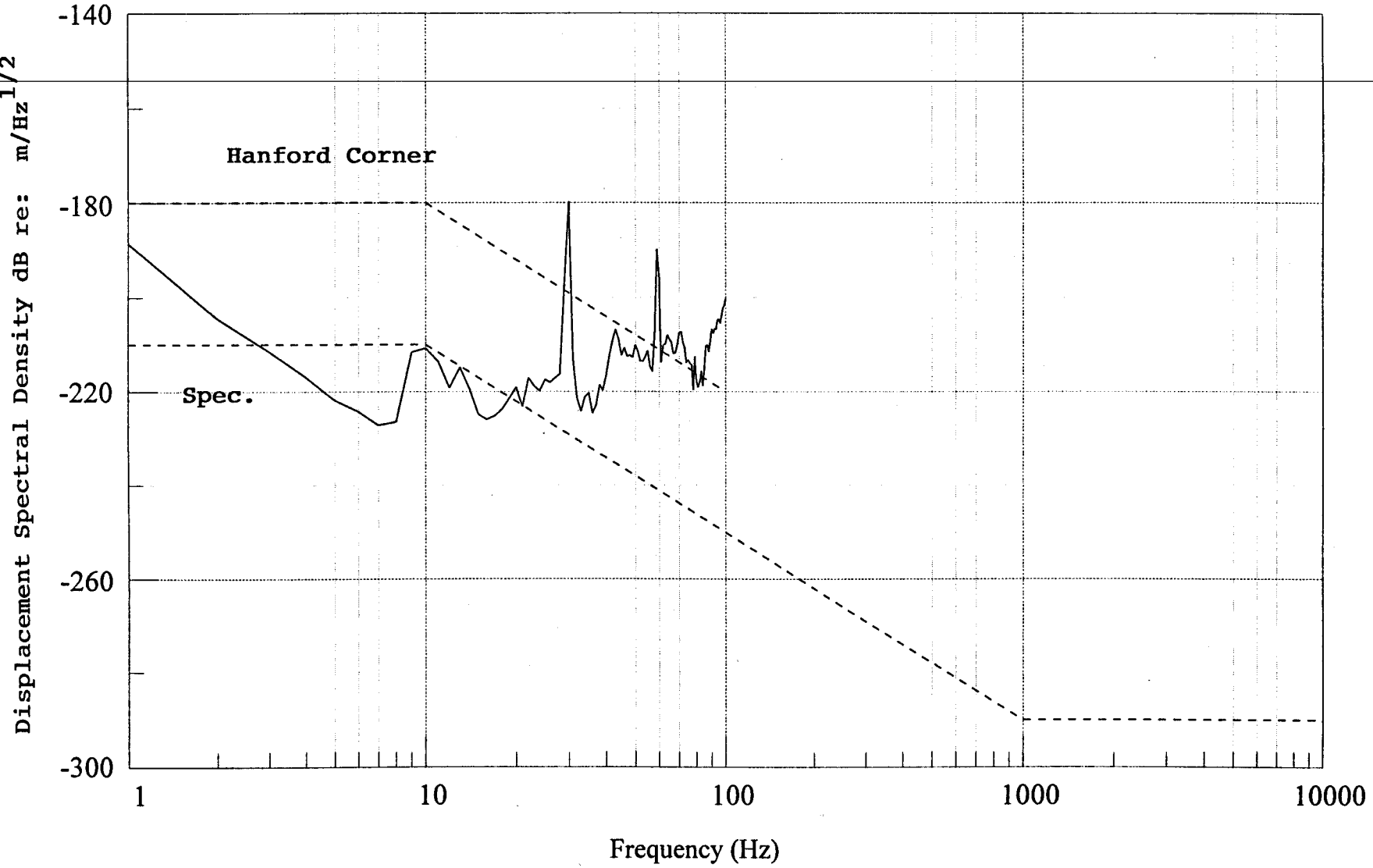

Fig. 29b - Estimated vacuum area floor response due to vent and purge system in Mechanical Room.

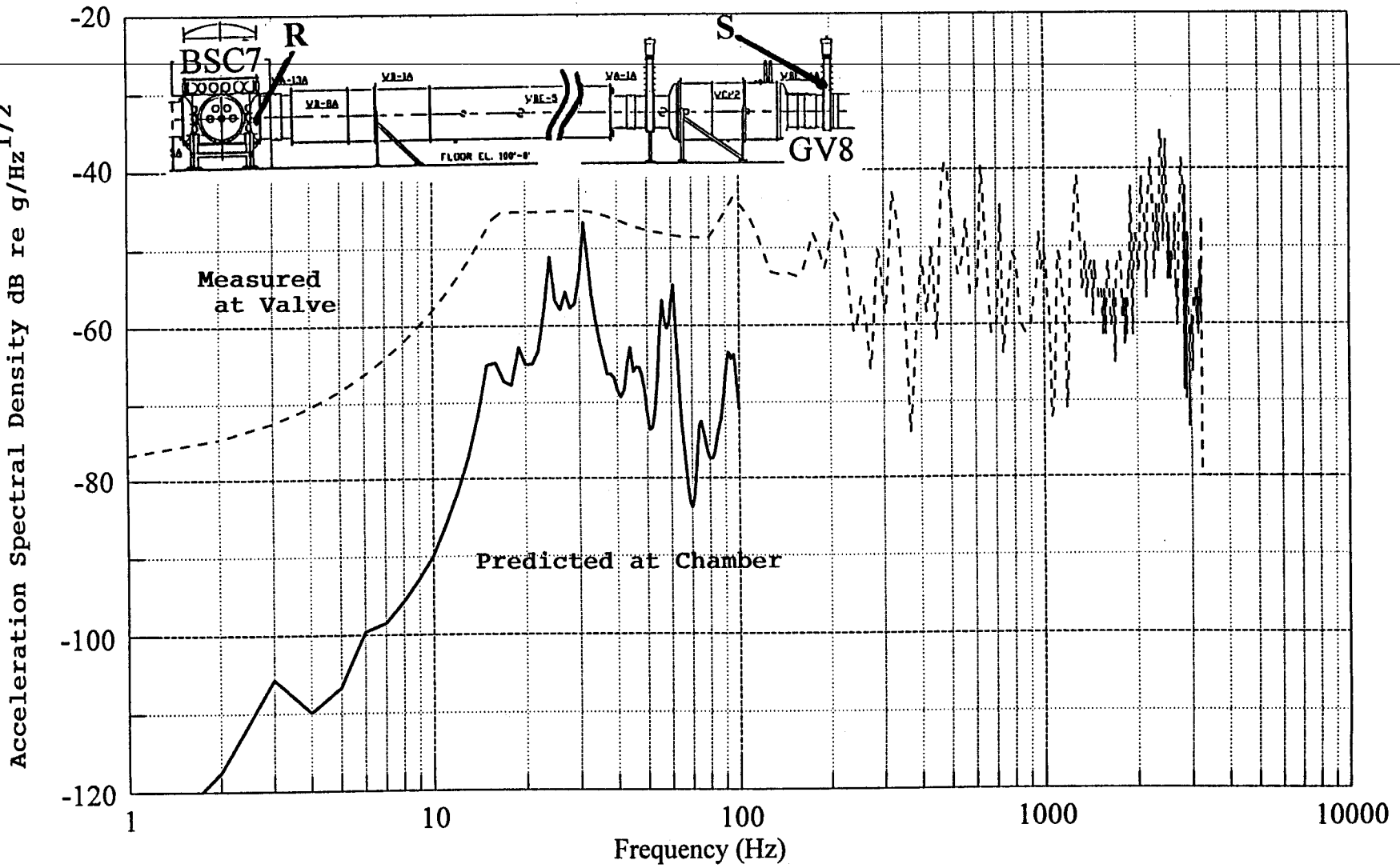

Fig. 30a - Estimated response at BSC7 due to pneumatic actuated gate valve GV8 shock input (Corner Station).

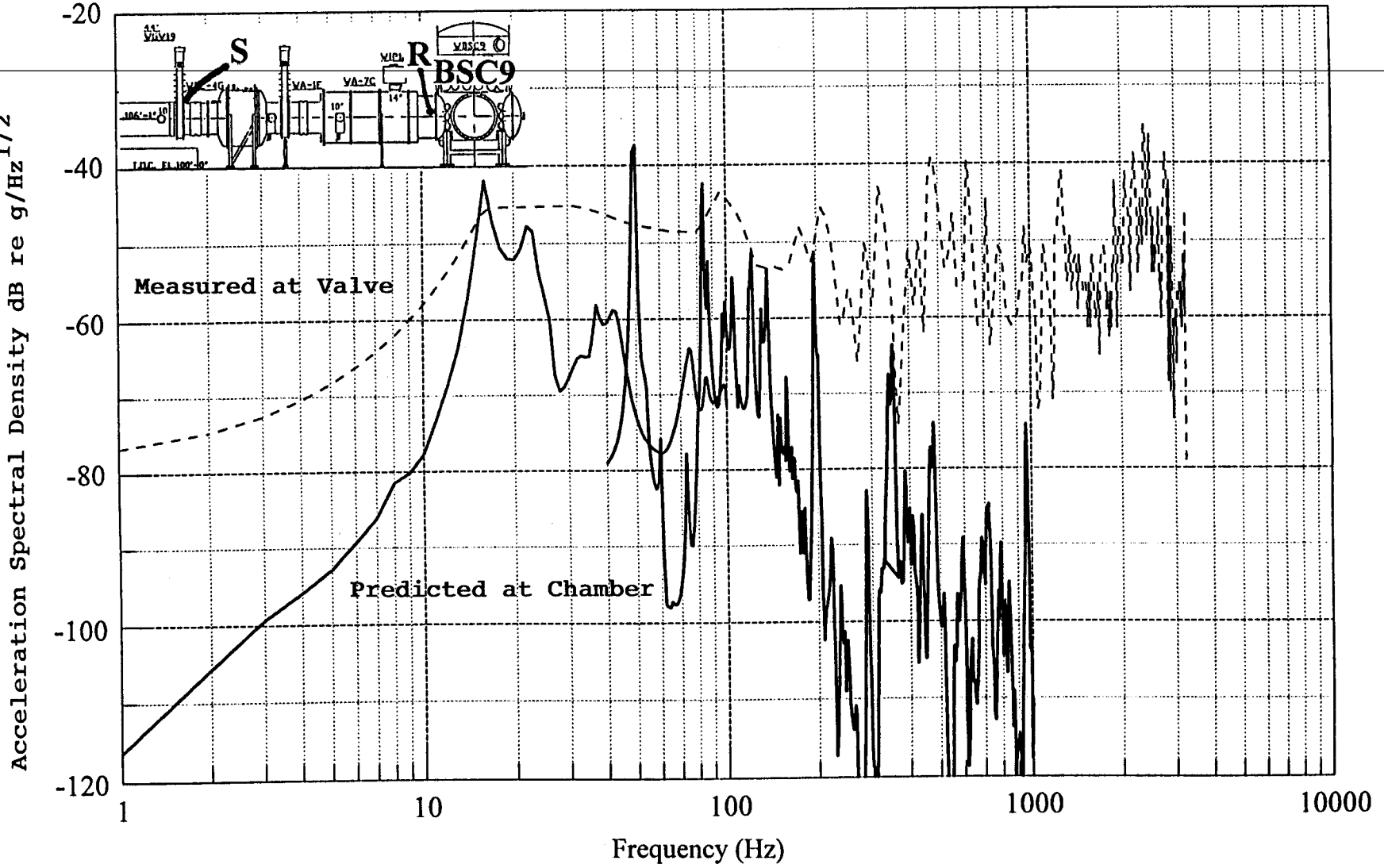

Fig. 30b - Estimated response at BSC9 due to shock levels caused by a pneumatic gate valve (GV19) if it was located in the End Station.

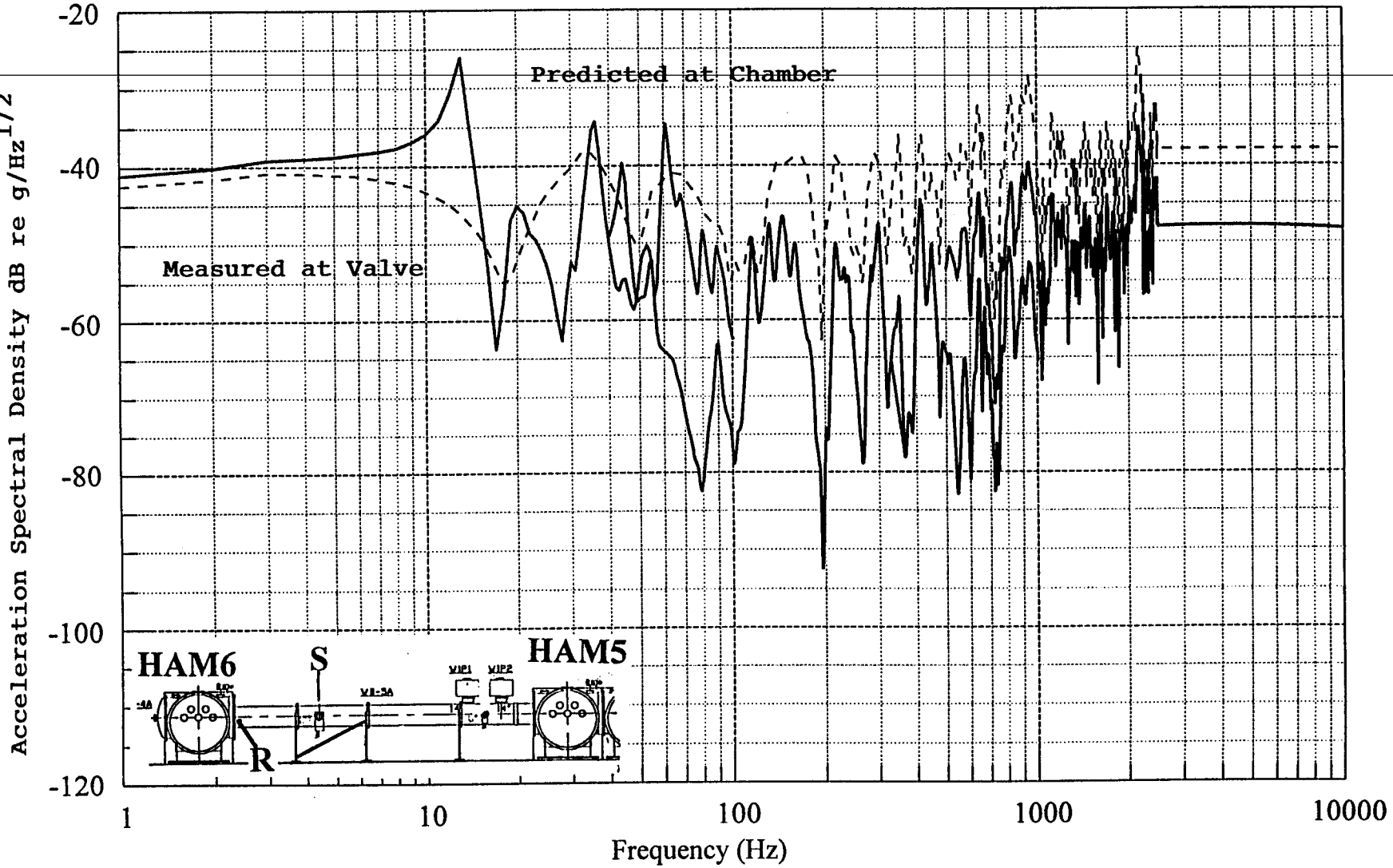

Fig. 30c - Estimated response at HAM6 due to 10" manual valve shock input at turbo-pump (Corner Station).

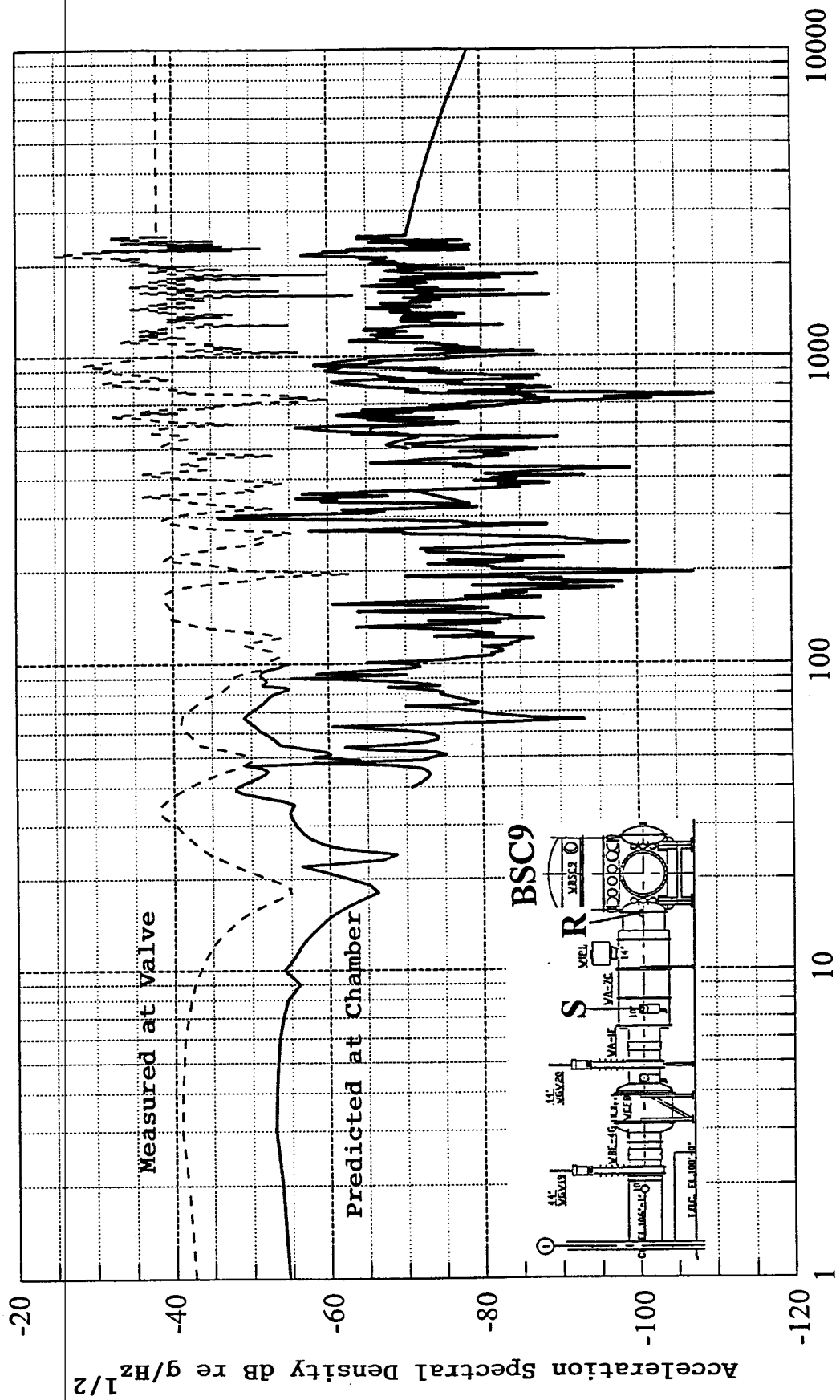

Fig. 30d - Estimated response at BSC9 due to 10" manual valve shock input at turbo-pump (End Station).

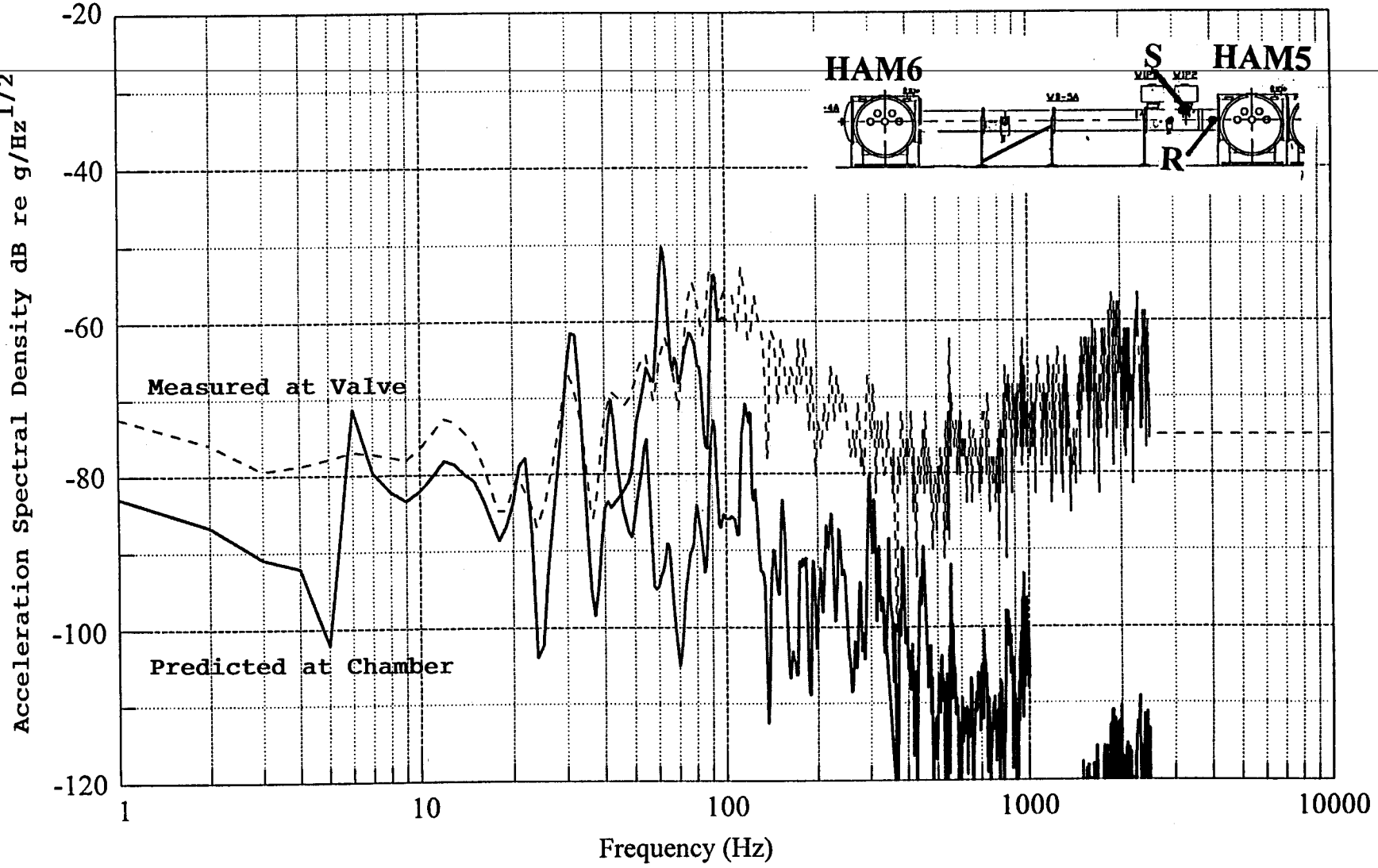

Fig. 30e - Estimated response at HAM5 due to 10" manual valve shock input at Ion pump (Corner Station).

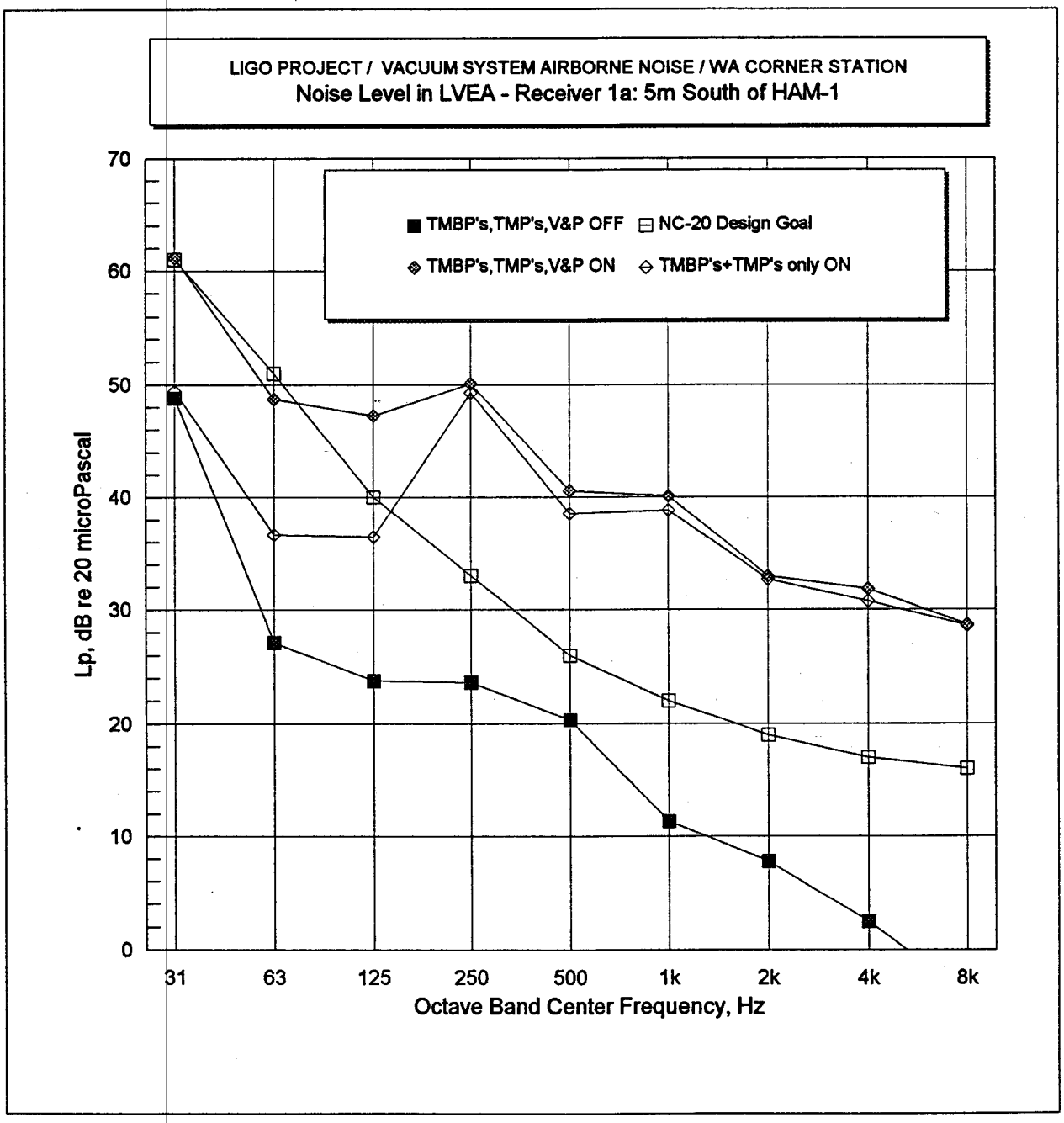
LIGO PROJECT / VACUUM SYSTEM AIRBORNE NOISE / WA CORNER STATION
Noise Level in LVEA - Receiver 1a: 5m South of HAM-1
TMBP's,TMP's,V&P OFF
NC-20 Design Goal
TMBP's,TMP's,V&P ON
TMBP's+TMP's only ON
Lp, dB re 20 microPascal
70
60
50
40
30
20
10
0
31
63
125
250
500
1k
2k
4k
8k
Octave Band Center Frequency, Hz

Fig. 31a

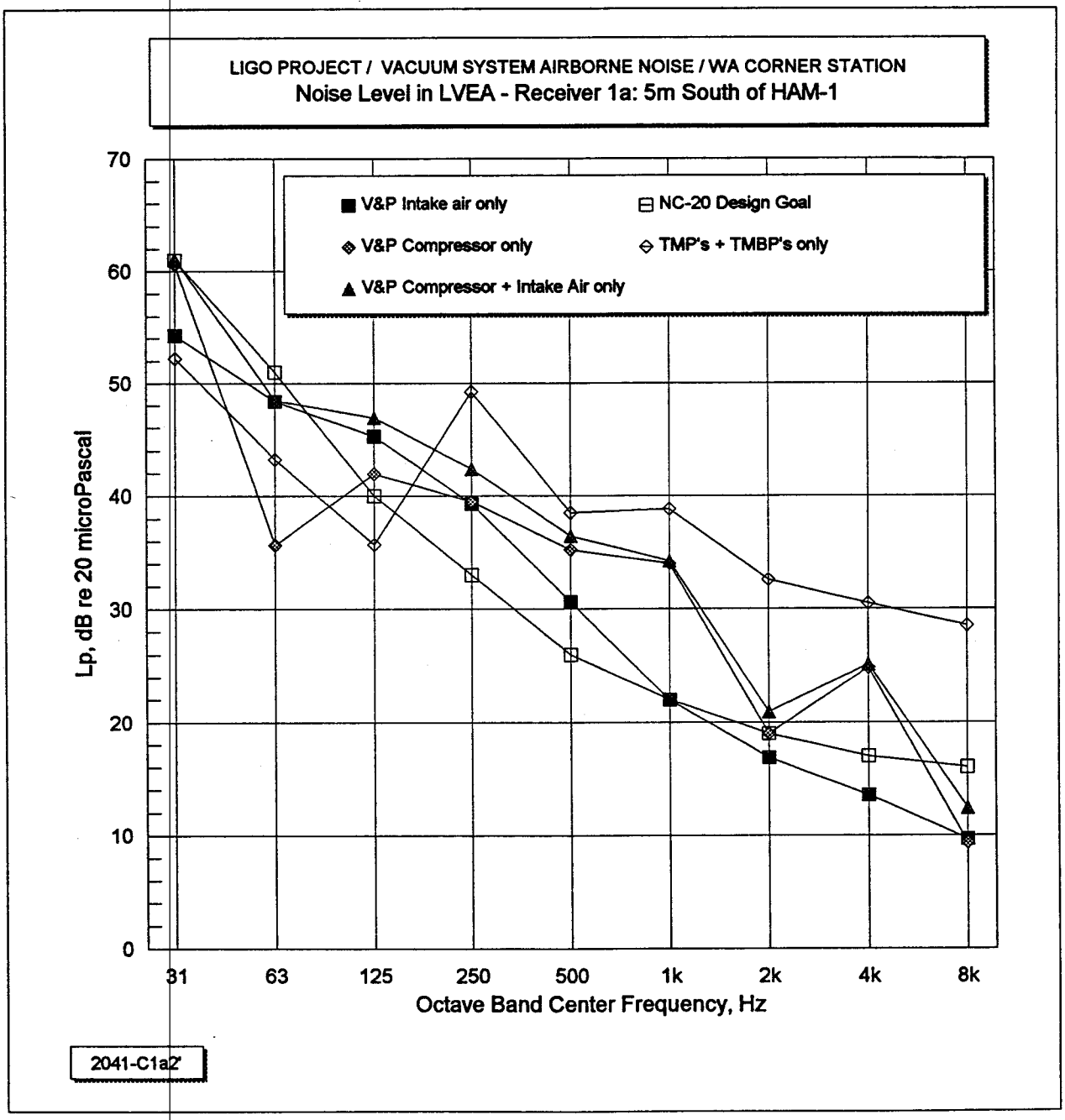
LIGO PROJECT / VACUUM SYSTEM AIRBORNE NOISE / WA CORNER STATION
Noise Level in LVEA - Receiver 1a: 5m South of HAM-1
V&P Intake air only
NC-20 Design Goal
V&P Compressor only
TMP's + TMBP's only
V&P Compressor + Intake Air only
Lp, dB re 20 microPascal
70
60
50
40
30
20
10
0
31
63
125
250
500
1k
2k
4k
8k
Octave Band Center Frequency, Hz
2041-C1a2'

Fig. 31b

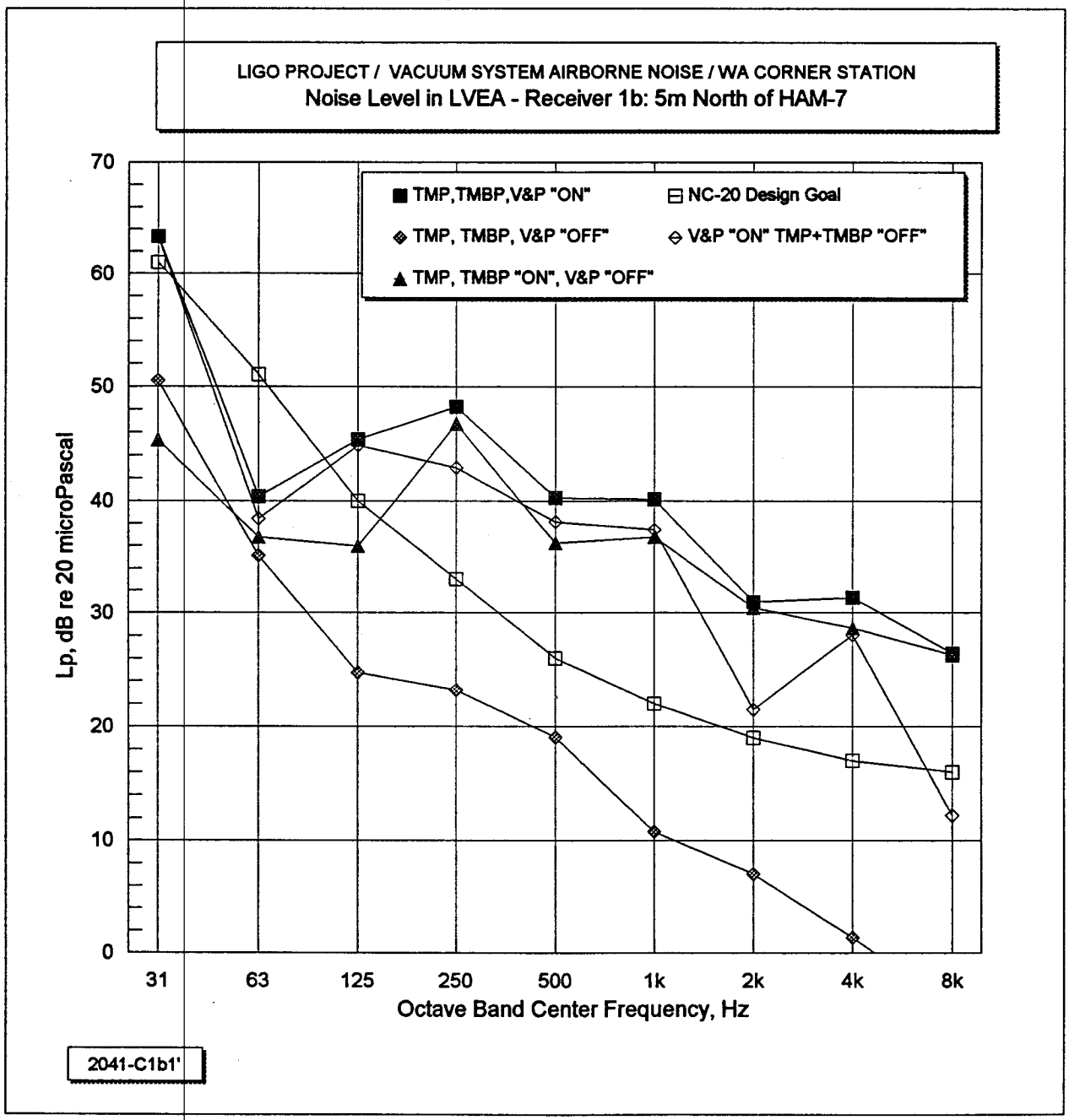
LIGO PROJECT / VACUUM SYSTEM AIRBORNE NOISE / WA CORNER STATION
Noise Level in LVEA - Receiver 1b: 5m North of HAM-7
TMP,TMBP,V&P "ON"
NC-20 Design Goal
TMP, TMBP, V&P "OFF"
V&P "ON" TMP+TMBP "OFF"
TMP, TMBP "ON", V&P "OFF"
Lp, dB re 20 microPascal
70
60
50
40
30
20
10
0
31
63
125
250
500
1k
2k
4k
8k
Octave Band Center Frequency, Hz
2041-C1b1'

Fig. 31c

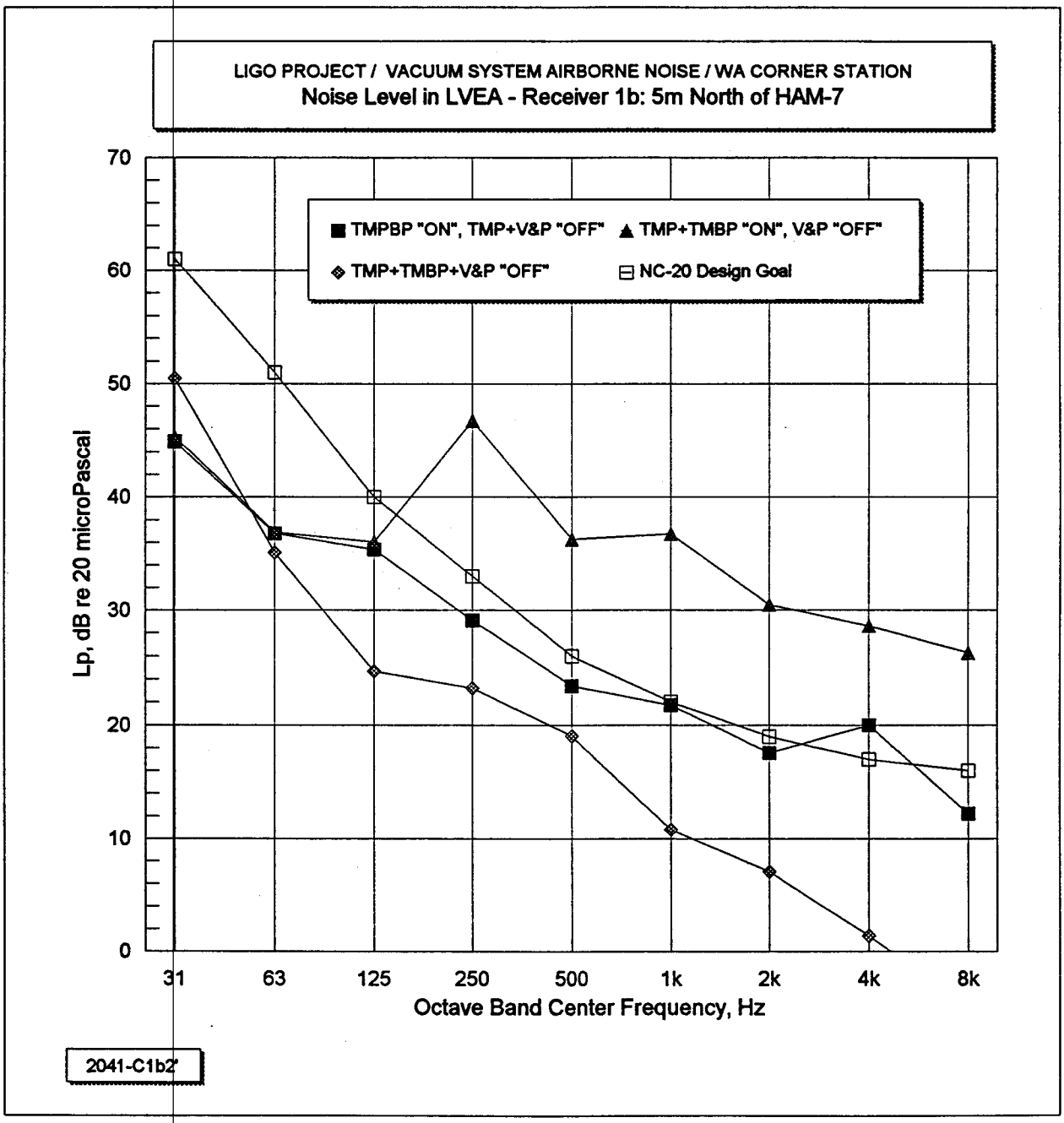
LIGO PROJECT / VACUUM SYSTEM AIRBORNE NOISE / WA CORNER STATION
Noise Level in LVEA - Receiver 1b: 5m North of HAM-7
TMPBP "ON", TMP+V&P "OFF"
TMP+TMBP "ON", V&P "OFF"
TMP+TMBP+V&P "OFF"
NC-20 Design Goal
Lp, dB re 20 microPascal
70
60
50
40
30
20
10
0
31
63
125
250
500
1k
2k
4k
8k
Octave Band Center Frequency, Hz
2041-C1b2

Fig. 31d

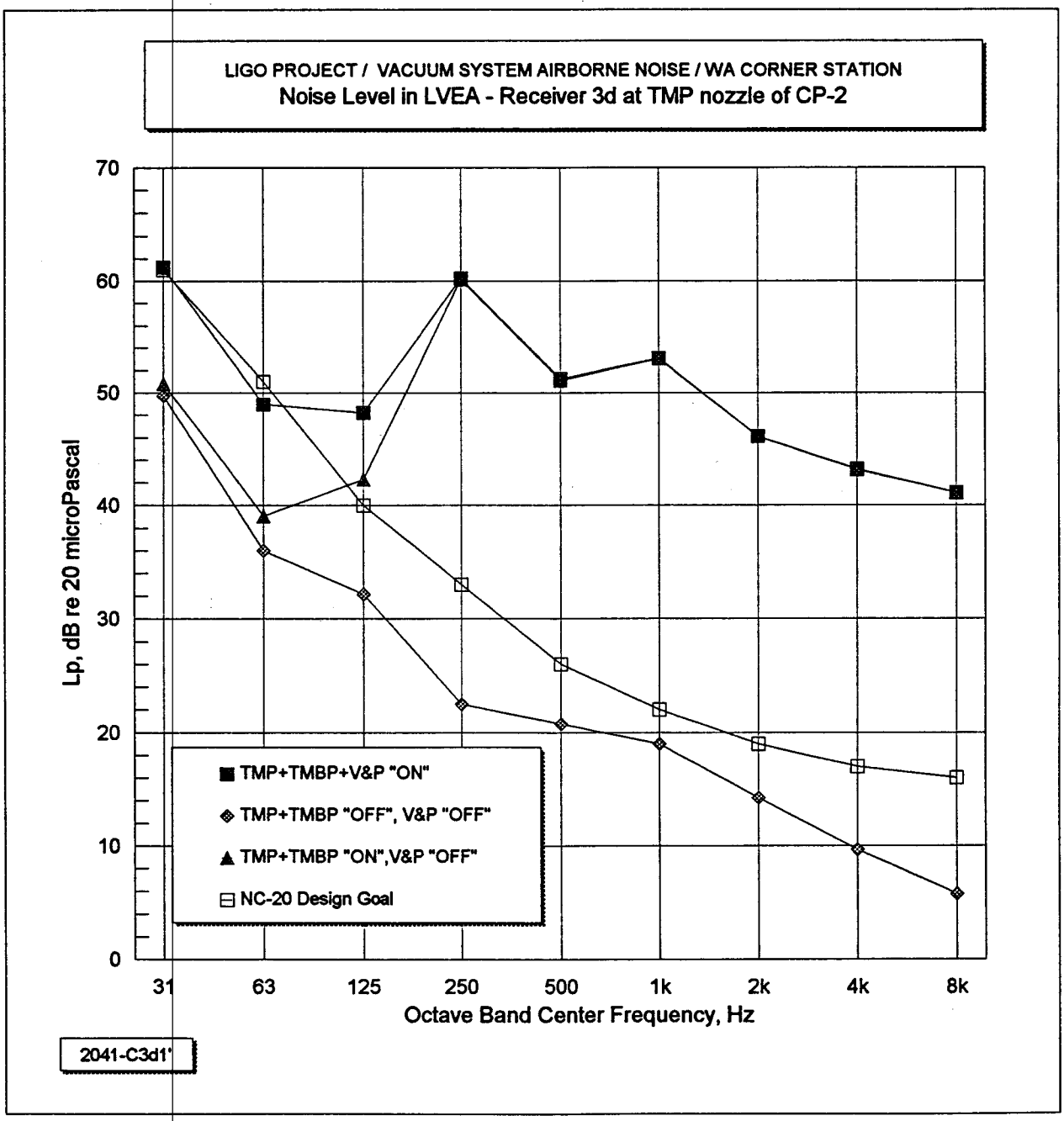
LIGO PROJECT / VACUUM SYSTEM AIRBORNE NOISE / WA CORNER STATION
Noise Level in LVEA - Receiver 3d at TMP nozzle of CP-2
Lp, dB re 20 microPascal
70
60
50
40
30
20
10
0
31
63
125
250
500
1k
2k
4k
8k
Octave Band Center Frequency, Hz
TMP+TMBP+V&P "ON"
TMP+TMBP "OFF", V&P "OFF"
TMP+TMBP "ON",V&P "OFF"
NC-20 Design Goal
2041-C3d1'

Fig. 31e

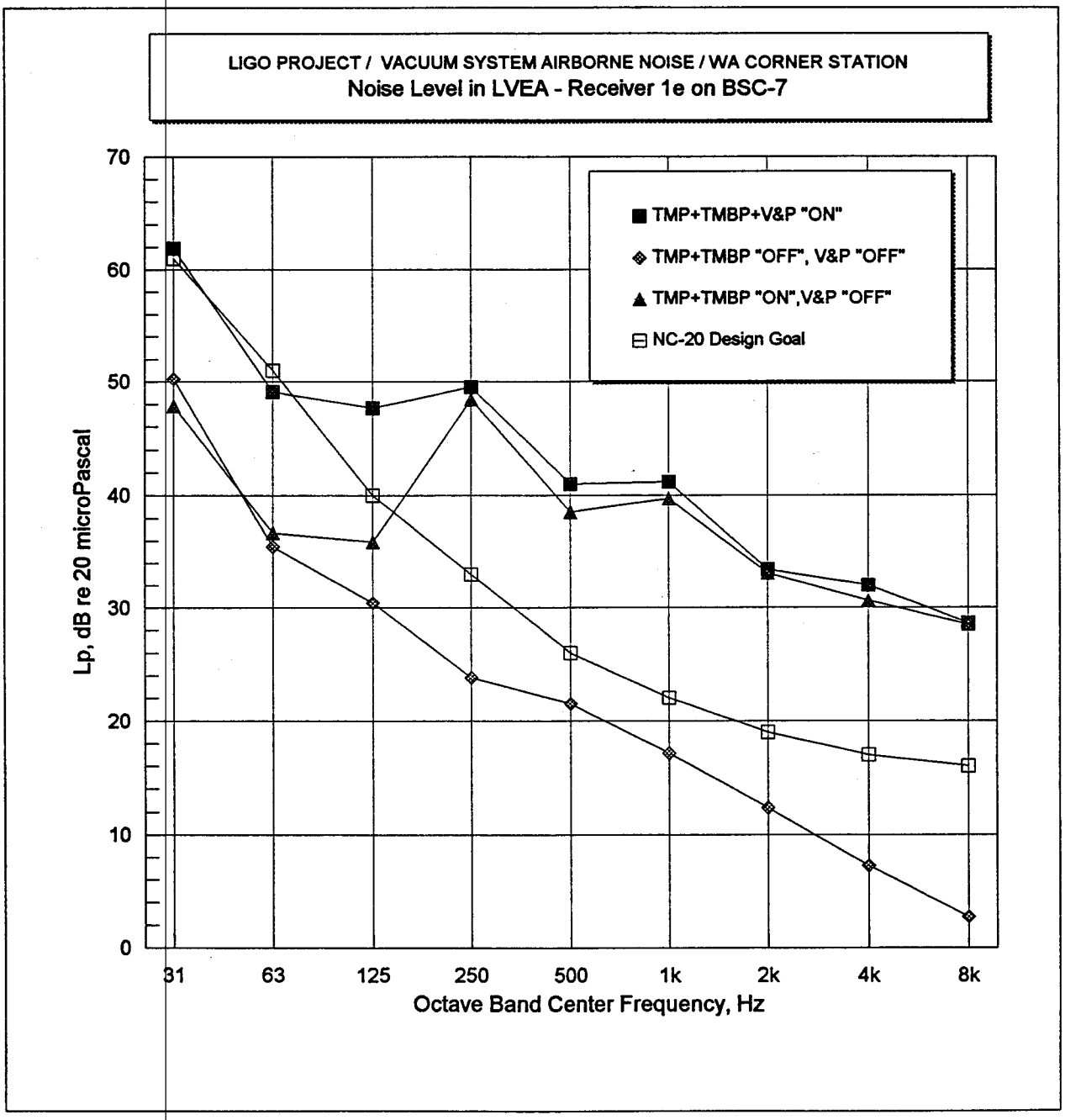
LIGO PROJECT / VACUUM SYSTEM AIRBORNE NOISE / WA CORNER STATION
Noise Level in LVEA - Receiver 1e on BSC-7
TMP+TMBP+V&P "ON"
TMP+TMBP "OFF", V&P "OFF"
TMP+TMBP "ON",V&P "OFF"
NC-20 Design Goal
Lp, dB re 20 microPascal
70
60
50
40
30
20
10
0
31
63
125
250
500
1k
2k
4k
8k
Octave Band Center Frequency, Hz

Fig. 31f

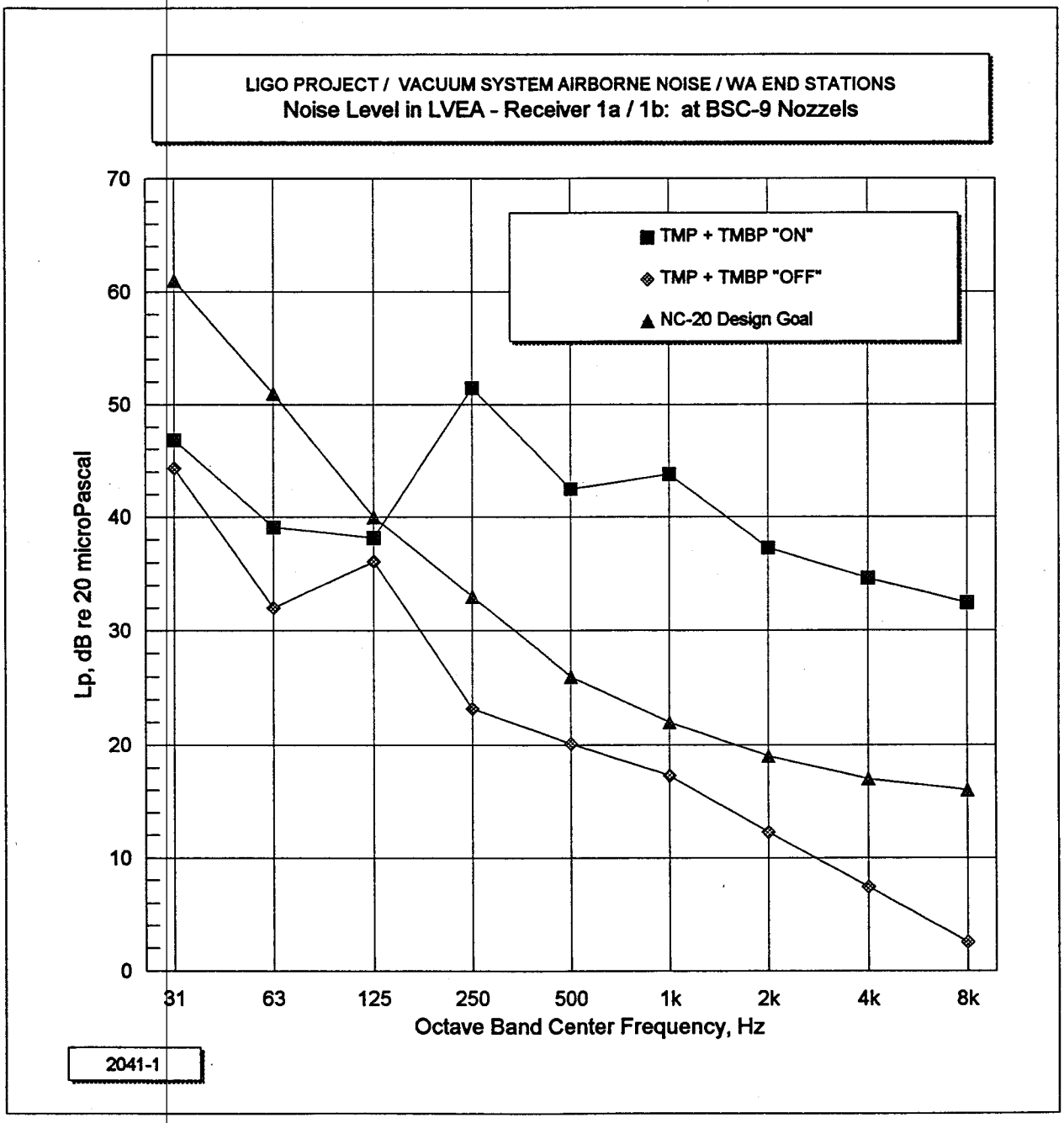
LIGO PROJECT / VACUUM SYSTEM AIRBORNE NOISE / WA END STATIONS
Noise Level in LVEA - Receiver 1a / 1b: at BSC-9 Nozzels
TMP + TMBP "ON"
TMP + TMBP "OFF"
NC-20 Design Goal
Lp, dB re 20 microPascal
70
60
50
40
30
20
10
0
31
63
125
250
500
1k
2k
4k
8k
Octave Band Center Frequency, Hz
2041-1

Fig. 32a

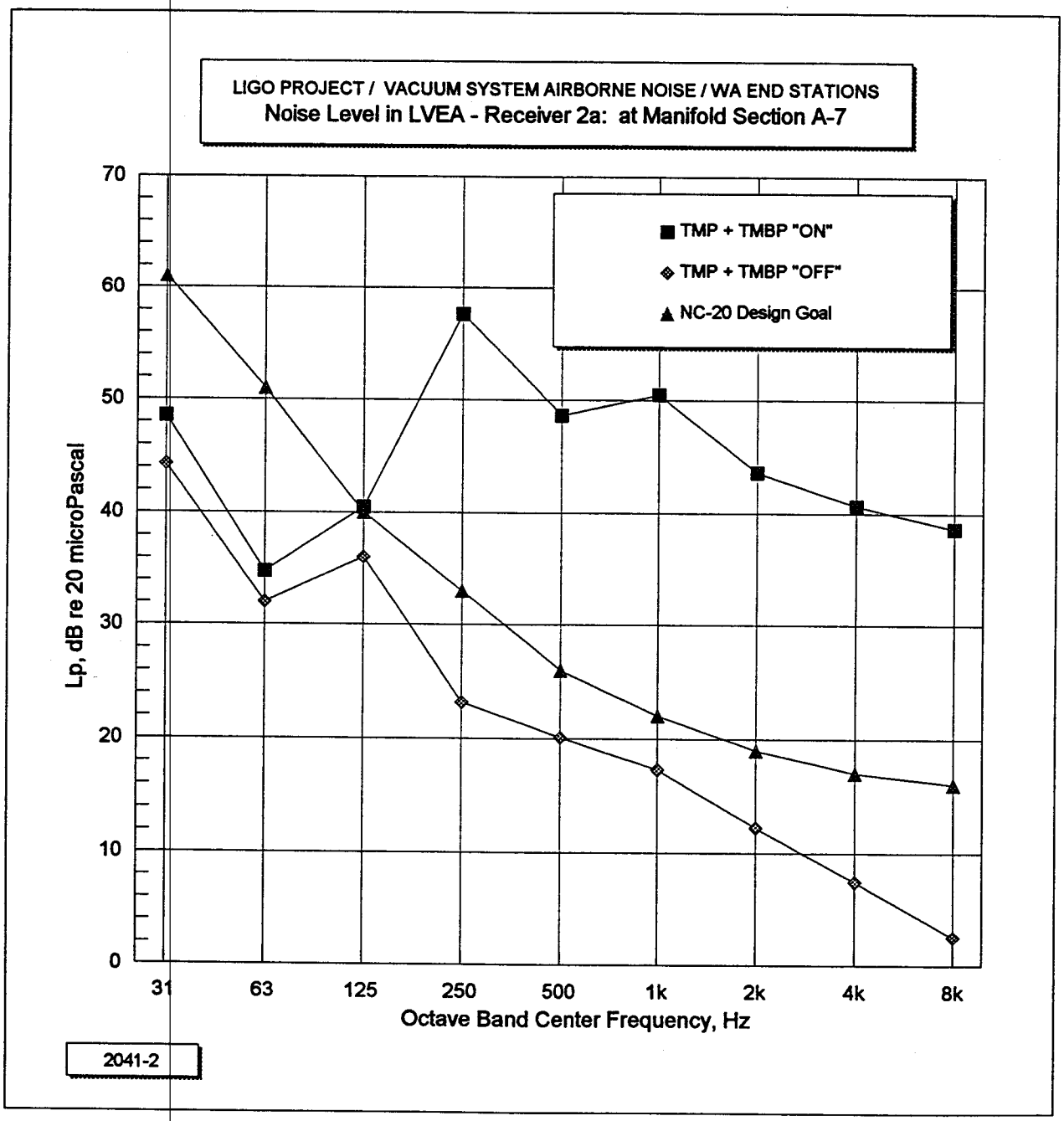
LIGO PROJECT / VACUUM SYSTEM AIRBORNE NOISE / WA END STATIONS
Noise Level in LVEA - Receiver 2a: at Manifold Section A-7
TMP + TMBP "ON"
TMP + TMBP "OFF"
NC-20 Design Goal
Lp, dB re 20 microPascal
70
60
50
40
30
20
10
0
31
63
125
250
500
1k
2k
4k
8k
Octave Band Center Frequency, Hz
2041-2

Fig. 32b